Final Report

NASA Grant NSG-7417

Velocity Model of the Shallow Lunar Crust

(NASA-CR-162573) VELOCITY MODEL OF THE SHALLOW LUNAR CRUST Final Report (Texas A&M Univ.) 159 p HC A08/MF A01 CSCL 03B

N80-16014

Unclas
G3/91 46692

Prepared by

Anthony F. Gangi, Principal Investigator
Department of Geophysics
Texas A&M University
College Station, Texas 77843

for

National Aeronautics and Space Administration
Lunar Programs Office
NASA Headquarters, Code SM
Washington, D.C. 20546

1 Jan., 1980

Grant Period: 1 Mar., 1978 to 31 Dec., 1979

FINAL REPORT, NASA GRANT NSG-7417

Abstract

Velocity Model of the Shallow Lunar Crust

Anthony F. Gangi
Department of Geophysics
Texas A&M University

The travel times of the seismic waves obtained for the Apollo-14 and -16 Active Seismic Experiments and the Apollo-16 grenade launches are shown to be consistent with a powder-layer model of the shallow lunar crust. The velocity variation with depth determined from these data is: $v(z) \approx 110\ z^{1/6}$ m/sec for z less than 10 meters and $v(z) \approx 250$ m/sec for z greater than 10 meters. The velocity values found for the 10 meter depth are similar to those found by Kovach, et al. (1972). The $z^{1/6}$ depth dependence for the velocity of the topmost layer is that predicted on the basis of a powder layer (Gangi, 1972). The Amplitude variation of the direct waves as a function of source-to-receiver separation, x, is $A(x) = A_o x^{-n} \exp(-ax)$ where $1.5 < n < 2.2$ and $a \approx 0.047$ neper/m.

Velocity-spectra analyses of the direct, surface-reflected, bottom-reflected and refracted waves give results that are consistent with the velocity model inferred from the traveltime data.

Table of Contents

Introduction. The data from the Apollo-14 and Apollo-16 Active Seismic Experiments (ASE) as well as the Apollo-16 grenade launches and the Apollo-17 Lunar Seismic Profiling Experiment (LSPE) were used to study the velocity structure of the shallow Lunar crust.

We found that the powder-layer model – which has a theoretical depth dependence for its velocity given by (Gangi, 1972): $v(z) \simeq 110\ z^{1/6}$ m/sec, for z in meters – is consistent with the traveltime data for depths of the order of 9 to 11 meters. Beneath this depth, there is a discontinuous increase in the velocity to approximately 250 m/sec for the Apollo-14 site and to approximately 300 m/sec for the Apollo-16 site. The latter value is not as accurate as the Apollo-14 site value because of the data quality. The velocity of 250 m/sec at a depth of about 10 meters is consistent with the results found by Kovach, et al., (1972) for the Apollo-16 site. However, the velocity jump found in this study for that depth is from about 161 m/sec to 250 m/sec rather than the 114 m/sec to 250 m/sec found by Kovach, et al., (1972).

Results obtained. The results of the investigations performed under this grant have been presented in two publications (copies are attached as Appendicies): "Velocity Structure of the Shallow Lunar Crust", A. F. Gangi and T. E. Yen, The Moon and the Planets, v. 20, 1979, pp. 439-468 which is given in Appendix 1 and Velocity Determination of the Very Shallow Lunar Crust, Tzuhua E. Yen, M.S. Thesis, Department of Geophysics, Texas A&M University, August, 1979, 107 pp + xiii which is in Appendix 2.

In these publications, the velocity model for the shallow lunar crust was determined and refined using the traveltimes and amplitude data from the Apollo-14 and -16 ASEs as well as the Apollo-16 grenade launches. Various data-processing techniques were used to improve the quality of the original data: 1) the original data were deglitched by hand, 2) they were frequency-bandpass

filtered, 3) traces with the same shot/receiver separation were stacked and 4) variation on the velocity-spectra method of Taner and Koehler (1969) were performed on direct arrivals, surface-reflected arrivals, bottom-reflected arrivals and the refracted arrivals. The velocity-spectra technique is a beam-steering or array-focusing method which gives a maximum response for the output of a receiving array when the proper time delays are inserted in each element of the array.

Velocity-Spectra Analyses. In the velocity-spectra analyses, it was assumed that the velocity in the top layer of the lunar crust varied as $z^{1/6}$ and the purpose of the analyses was to determine: 1) the reference velocity (taken as the velocity at 1 km depth in Yen's thesis and as the velocity at 1 meter in this report – the difference between the two values is a factor of $\sqrt{10}$ or 3.162), 2) the depth to the discontinuous velocity change and 3) the value of the velocity at or below the velocity discontinuity. From the velocity spectrum for the direct waves, the reference velocity was found to be 101 m/sec (for the 1-meter reference depth; for the 1-km reference depth, the value becomes 320 m/sec, see p. 84f., Appendix 2). This value was also obtained using the surface-reflected waves (ibid). From the velocity spectra of the reflected waves (i.e., those reflected from the velocity discontinuity) the reference velocity was found to be 100 m/sec (318 m/sec) and the depth to the reflector was found to be 8.4 meters (see p. 86f., Appendix 2). The velocity spectra of the refracted waves gave 9.4 $\pm$ 0.3 meters for the depth to the velocity discontinuity and 230 $\pm$ 16 m/sec for the velocity of the refractor (see p. 90f., Appendix 2). These values are to be compared with the values 109 m/sec (345 m/sec) for the reference velocity, 11 meters for the depth to the velocity discontinuity, and 254 m/sec for the underlying refractor found using the traveltime data (see p. 53f., Appendix 2, especially, Fig.26, p.64).

Apollo-17 LSPE Data. We found that it was not possible to incorporate the Apollo-17 LSPE data into the program to obtain traveltimes for the larger distances. This was due to the fact that the signal-to-noise ratio was too small to allow these data to be used. The same was true for the Apollo-16 grenades.

Apollo-16 Grenade Launches. The Apollo-16 grenade launches did provide useable data even though only two of the geophones (geophones 1 and 2) had useable amplitudes for all three launches and even though the launch times of the grenades were not known accurately. We found arrivaltimes at geophone 1 for the launching of grenades 2,3 and 4 to be 177, 151 and 121 milliseconds, respectively, despite the fact that all the grenade launches were from the same location (see Table 14, p. 67, Appendix 2). Nevertheless, the time differences between the arrivals at geophones 1 and 2 (which were approximately the same for all three launches, see Table 14, ibid) were used to test the velocity model as was one (low-quality) determination of the arrivaltime at geophone 3. This latter reading was used to determine the velocity of the high-velocity layer (the refractor) which underlies the powder layer at about 10 m depth. These data showed that a powder-layer depth of 9 meters, a reference velocity of 110 m/sec (350 m/sec), and a refractor velocity of 250 m/sec were consistent with the data (see p.66f, Appendix 2).

Deconvolution. The data on the Apollo-14 and the Apollo-16 ASEs were deconvolved to try to improve the determinations of the arrivaltimes of both the first and later arrivals. This procedure is used to both narrow the waveform of the seismic events in time and to decrease the rise time of the onset of the pulses. Narrowing the pulses would decrease the overlap and interference of different arrivals while decreasing the rise times would allow more accurate

determination of the arrival times. We found that there was little or no benefit to the procedure because the signal-to-noise ratio of the original data were so low. While it was possible to decrease the rise time and decrease the pulse widths, the concommitant increase in the noise prevented any improvement in the determinations of the arrivaltimes of the various events. This could be predicted from the spectral analyses made of the signal traces which showed that the signal-to-noise ratio of the traces was low.

Amplitude Analyses. The amplitudes of the direct waves were reanalyzed assuming that there was exponential attenuation of the amplitudes with distance due to absorption (or scattering) in the powder layer. It had been previously predicted that the amplitudes of the direct waves should decrease as $x^{-(13-m)/12}$ for the 1/6-th power velocity variation and as x^{-2} for the constant-velocity model. The measured variation with the source-to-receiver separation, x, was found to be $x^{-1.5}$ to $x^{-2.2}$ (see Appendix 1, Abstract and p. 453 f.) when no exponential attenuation term is included. When the assumed amplitude variation was taken to be:

$$A(x) = A_o x^{-n} \exp(-ax)$$

(where x is the source-to-receiver separation, A_o is a reference amplitude, n is the exponent that measures the spreading of the wave surface as it propagates away from the source and a is the attenuation coefficient) the measured parameters, which were obtained by a least-squares fit to the data, were found to be: n=1.46, A_o=71.7 and a=0.047 nepers/meter (see p. 68f., Appendix 2, especially p. 74).

This large decrease in amplitude with distance due to the "absorption" term (i.e., a=0.047 nepers/m) is not consistent with the high Q values (low attenuation coefficients) found by Latham, et al. (1970). It is not proposed that the exponential term — exp(-ax) — is due to absorption in the powder

layer, but rather is due to the change in waveform that can be expected for waves propagating in an inhomogeneous medium; in particular, the powder layer with its 1/6th-power variation in the velocity with depth.

Scattering and Full-wave Analysis. No progress was made on the scattering or the full-wave analysis part of the proposed program. We encountered difficulties in reading the data tapes on our computer system which held up progress and took more time that anticipated. Also, those parts of the program that were completed took more effort that anticipated, leaving no time to work on these two tasks. We feel these are important tasks and should be completed, if not now, at least some time in the future.

Errata. Two errors exist in publication in Appendix 1. The date of receipt of the manuscript is given as 3 January, 1973 and this should read 3 January, 1979 instead. Also, the acknowledgement that the work was performed under NASA Grant NSG-7417 was deleted from the manuscript.

Summary. The results on the analysis of the Apollo-14 and Apollo-16 ASE data, the Apollo-16 Grenades and their launches, and the Apollo-17 LSPE data show that the velocity structure of the shallow lunar crust is: 1) there is a powder layer about 10 meters thick which has a velocity variation given by $v(z)=110(z)^{1/6}$ m/sec for z in meters and 2) there is a discontinuous increase in the velocity from about 161 m/sec to about 250 m/sec at a depth of 10 meters. These results were obtained by using the traveltimes of direct and refracted waves and by using the velocity spectra of direct waves, waves reflected from the surface, waves reflected from the discontinuous velocity jump at 10 meters depth and the waves refracted along the velocity discontinuity.

References

Gangi, A.F., 1972, The lunar seismogram: Moon, v. 4, pp. 40-48.

Kovach, R.L., J.S. Watkins and P. Talwani, 1972, Active seismic experiment: Section 10 of the Apollo-16 Preliminary Science Report, NASA SP-315.

Latham, G.V., M. Ewing, F. Press, G. Sutton, J. Dorman, Y. Nakamura, N. Toksoz, R. Wiggins, J. Derr and F. Duennebier, 1970, Passive seismic experiment: Science, v. 167, pp. 455f.

Taner, M.T. and F. Koehler, 1969, Velocity spectra-Digital computer derivation and application of velocity functions: Geophysics, v. 34, pp. 859-881.

APPENDIX I

VELOCITY STRUCTURE OF THE SHALLOW LUNAR CRUST

ANTHONY F. GANGI and TZUHUA E. YEN
Department of Geophysics, Texas A & M University, College Station, Texas, U.S.A.

(Received 3 January, 1978)

Abstract. The data from the Apollo-14 and Apollo-16 Active Seismic Experiments have been reanalyzed and show that a power-law velocity variation with depth, $v(z) \cong 110 z^{1/6}\,\mathrm{m\,s^{-1}}$ $(0 < z < 10\,\mathrm{m})$, is consistent with both the travel times and amplitudes of the first arrivals for source-to-geophone separations up to 32 m. The data were improved by removing spurious glitches, by filtering and stacking. While this improved the signal-to-noise ratios, it was not possible to measure the arrival times or amplitudes of the first arrivals beyond 32 m. The data quality precludes a definitive distinction between the power-law velocity variation and the layered-velocity model proposed previously. However, the physical evidence that the shallow lunar regolith is made up of fine particles adds weight to the 1/6-power velocity model because this is the variation predicted theoretically for self-compacting spheres.

The 1/6-power law predicts the travel time, $t(x)$, varies with separation, x, as $t(x) = t_0(x/x_0)^{5/6}$ and, using a first-order theory, the amplitude, $A(x)$, varies as $A(x) = A_0(x/x_0)^{-(13-m)/12}$, $m > 1$; the layer-velocity model predicts $t(x) = t_0(x/x_0)$ and $A(x) = A_0(x/x_0)^{-2}$, respectively. The measured exponents for the arrival times were between 0.63 and 0.84 while those for the amplitudes were between -1.5 and -2.2. The large variability in the amplitude exponent is due, in part, to the coarseness with which the amplitudes are measured (only five bits are used per amplitude measurement) and the variability in geophone sensitivity and thumper-shot strengths.

A least-squares analysis was devised which uses redundancy in the amplitude data to extract the geophone sensitivities, shot strengths and amplitude exponent. The method was used on the Apollo-16 ASE data and it indicates there may be as much as 30 to 40% variation in geophone sensitivities (due to siting and coupling effects) and 15 to 20% variability in the thumper-shot strengths. However, because of the low signal-to-noise ratios in the data, there is not sufficient accuracy or redundancy in the data to allow high confidence in these results.

1. Introduction

The first lunar seismograms recorded by the Apollo-11 seismometers (Latham *et al.*, 1970a, b) surprised many seismologists. Their unusually long durations (see Figure 1) gave rise to numerous theoretical speculations. Proposed mechanisms ranged from secondary-ejecta effects (Latham *et al.*, 1970a; Chang *et al.*, 1970; Mukhamedzhanov, 1970) to scattering of the waves by shallow internal fractures and inhomogeneities (Latham *et al.*, 1970a, b) or by topographic irregularities (Gold and Soter, 1970). It soon became clear that the secondary-ejecta mechanisms were not viable ones because the same long duration occurred for seismograms from moonquakes with foci in the lunar interior.

Early data indicated that the compressional-wave velocity was very low near the lunar surface ($\sim 0.1\,\mathrm{km\,s^{-1}}$; Latham *et al.*, 1970c, Sutton and Duennebier, 1970) and increased to approximately $6\,\mathrm{km\,s^{-1}}$ at a depth of 20 km (Latham *et al.*, 1970d). Latham *et al.* (1970a, b) showed that the variation of the amplitude envelope with time and distance was consistent with a diffusive-scattering mechanism provided the Q of the medium was greater than 3000.

The Moon and the Planets 20 (1979) 439–468. 0165–0807/79/0204–0439$04.50

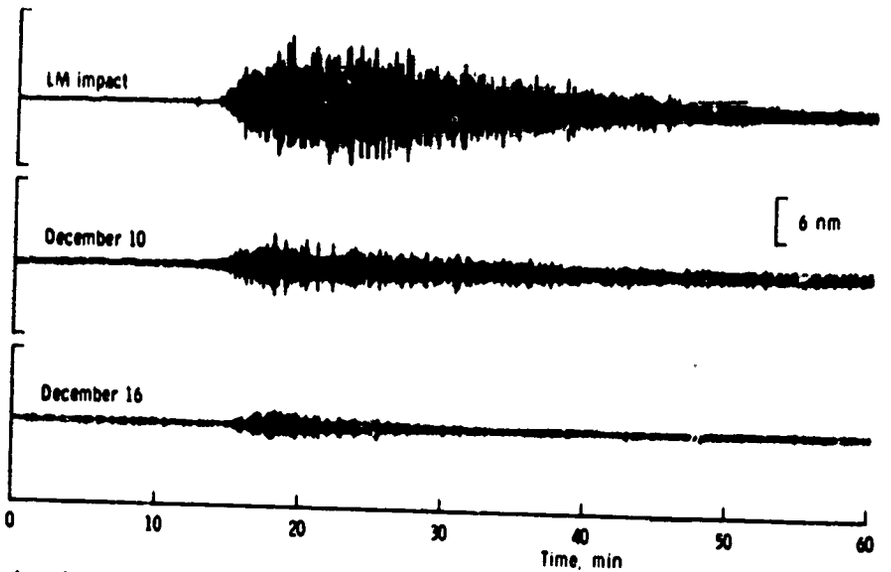

Fig. 1. Long-period, vertical component (LPZ) lunar seismograms, Apollo-11 Passive Seismic Experiment, 1969. (From Latham *et al.*, 1970a).

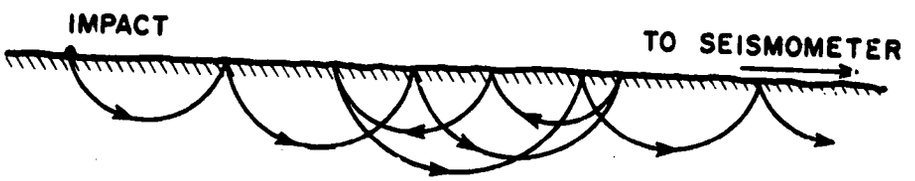

Fig. 2. Seismic ray paths for a linearly increasing velocity variation with depth and topographic irregularities. (From Gold and Soter, 1970).

Gold and Soter (1970) interpreted the Apollo-12 data to imply that the shallow lunar crust consisted of a deep layer of powder. They assumed a linear velocity variation with depth and, through computer simulation using ray acoustics, they were able to approximate the actual signal very well. They showed that the long duration could be explained by scattering of the nearly vertically-incident waves by topographic irregularities (Figure 2). They also showed that the seismic amplitudes are greatly enhanced in such a medium, so that it required less power to transmit seismic waves than previously believed.

Kovach *et al.* (1971) proposed a layered model with a stepwise-increasing velocity variation based on the data of the Active Seismic Experiment (ASE) at the Apollo-14 landing site. They obtained a *p*-wave velocity (V_p) of $104\,m\,s^{-1}$ for a top layer of 8.5 m thickness and a $V_p = 299\,m\,s^{-1}$ for an underlying layer (the Fra Mauro formation) of 38 to 76 m thickness. A similar model was used to interpret the Apollo-16 ASE data and gave a $V_p = 114\,m\,s^{-1}$ for a 12.2 m thick top layer and a $V_p = 250\,m\,s^{-1}$ for an underlying layer 70 m thick (Kovach *et al.*, 1972).

Gangi (1972) proposed a self-compacting-powder model which gives a velocity varying

as the sixth root of the depth; in this model the velocity at the lunar surface goes to zero. This, in turn, gives a long duration to the signal by scattering from topographic irregularities, very low correlation between horizontal and vertical displacements, a changing signal envelope that varies with source-to-receiver separation and a varying spectrum over the signal duration. These effects have been noted by Latham *et al.* (1970c, d) and they also are explained by the diffusive scattering model (Latham *et al.*, 1970c) and the surface-irregularity scattering model (Gold and Soter, 1970).

Kovach and Watkins (1973) extended and refined the layered model by incorporating the traveltime of the Apollo-14 Lunar-Module ascent. However, they pointed out that: "the exact details of the velocity variation in the upper 5–10 km of the Moon cannot yet be resolved (i.e., whether it is smooth as depicted or a stepwise increase) but one simple observation can be made. Self-compression of any rock powder such as the Apollo 11 or 12 soils or terrestrial sands cannot duplicate the observed magnitude of the lunar velocity change and the steep velocity-depth gradient ($\sim 2\,\mathrm{km\,s^{-1}\,km^{-1}}$)". However, it is not expected that a self-compacting-powder layer of 5 km thick would exist on the Moon; if such a layer exists, it would be, most likely, thinner than 1 km and probably thinner than 100 m.

Dainty *et al.* (1974) performed a detailed analysis of the diffusive-scattering mechanism and compared their theoretical results both with lunar data and seismic-modelling data. They showed they could match the envelopes of the lunar seismograms using this theory if, for a frequency of 0.45 Hz, the apparent thickness of the scattering layer is 25 km, the mean distance between scatterers at the base of the layer is ~ 5 km and the Q of the medium is 5000. The corresponding values for a frequency of 1.0 Hz are: 14 km scattering-layer thickness, ~ 2 km between scatterers and a Q of 5000. The thickness of the scattering layer (and its variability with frequency) seem to be inordinately large and may indicate that the model used is not appropriate for the lunar crust. A similar analysis should hold for body-wave scattering by topographic irregularities; in this case, the scattering-layer thickness would correspond to the surface area over which the nearly vertically-incident waves are efficiently scattered and the spacing between scatterers in the layer would correspond to the spacing between surface scatterers (of wave-length size).

Cooper *et al.* (1974) used the data of the Active Seismic Experiments of Apollo 14 and 16 along with the Lunar Seismic Profiling Experiment (LSPE) data of Apollo 17 and other man-made impacts to obtain a model of the velocity structure of the shallow lunar crust. They assumed a layered model and assumed that the first arrivals (beyond about 10 m) were seismic refractions. They found their travel time data were consistent with a five-layer model in which the velocity is: (1) $100\,\mathrm{m\,s^{-1}}$ in the top layer of 4 m thickness, (2) $327\,\mathrm{m\,s^{-1}}$ in the next layer to a depth of 32 m (thickness of 28 m), (3) $495\,\mathrm{m\,s^{-1}}$ to a depth of 390 m, (4) $960\,\mathrm{m\,s^{-1}}$ to a depth of 1385 m and (5) $4700\,\mathrm{m\,s^{-1}}$ for a depth down to at least 1800 m. However, this last velocity is determined from a single source (the LM impact) at distances of the order of 8.7 km from the geophone array (four geophones). The shallower structure is obtained from the traveltime data resulting from the

eight explosive-package detonations and the LM ascent; all these sources are within 3 km of the geophone array. Cooper *et al.* (1974) show these data can be fitted well with a continuous, linearly-increasing velocity with depth, z; namely, $V = 395 + 778z$ (m s^{-1}) for z in meters. They also state that "Various power law velocity models can be made to fit the observed data . . ." when only the explosive-package and LM-ascent data are used.

It is clear there is still some question regarding the velocity variation with depth in the shallow lunar crust ($z \lesssim 1$ km). Since the shallow lunar crust severely modifies the received signals, even those from large distances, it is important to know this shallow velocity variation well. Therefore, it is worthwhile to reanalyze the data to determine which velocity variation with depth is the most probable. The data from the Apollo-14 and Apollo-16 ASE's have been reanalyzed and the results are given below.

2. Apollo-14 and -16 ASE Data

The data used in this analysis are from the astronaut-activated thumper device of the Apollo-14 and Apollo-16 ASE's. In both experiments, three geophones were sited on the surface in a linear array with 45.72 m (150 ft) spacing between geophones (Lauderdale and Eichelman, 1974). The thumper device was fired at 4.57 m (15 ft) intervals between the ends of the arrays (see Figure 3). Firings (shots) 5, 6, 8, 9, 10, 14, 15 and 16 of the Apollo-14 ASE misfired and no data are available for them. For the Apollo-16 ASE, two shots were omitted between geophones 1 and 2; namely, those at the 4.57 m spacing from the two geophones.

The signals from the geophones are sampled every 1.887 ms, corresponding to a Nyquist frequency of about 265 Hz. Because of data transmission limitations, a trade-off between sampling rate and the number of bits per sample had to be made. The result was that only five bits were available for each sample. In order to cover the maximum possible dynamic range with only 32 possible binary numbers, the seismic signals were log compressed for large signal levels. The correspondence of the binary-data values (0–31) and the voltage from geophone 1, Apollo 16 is shown in Table I. The other geophone voltages have similar correspondence with the binary data. With only 32 levels possible for the geophone output voltage, the resulting traces will have a coarse character. This makes it difficult to obtain accurate amplitude information if no processing of filtering is performed on the data. Fortunately, it is possible to process the data to obtain reasonably accurate amplitude values.

In order to achieve meaningful results from the analysis, it was necessary to improve the original ASE data. Figure 4 shows three representative traces of the raw data from the Apollo-16 ASE. These data are from the tenth thumper shot and the source-to-receiver separations are 50.29 m (165 ft), 4.57 m (15 ft) and 41.14 m (135 ft) for geophones 1, 2 and 3 respectively. The thumper-firing time is 1.2 s after the beginning of the traces. While a high signal-to-noise ratio (S/N) exists for the shortest separation, the S/N for the other two traces is so low that it is difficult, if not impossible, to pick the first arrivals or to measure their amplitudes. In addition, geophone 1 shows severe

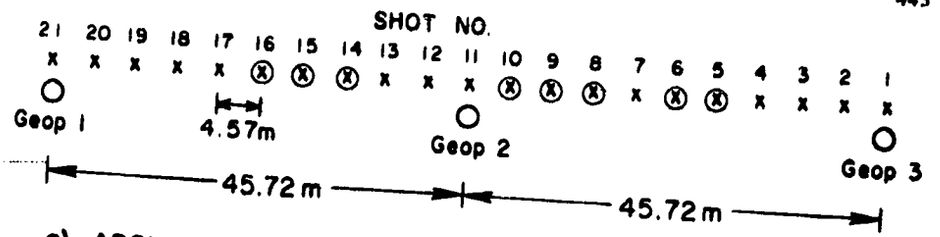

a) APOLLO-14 ACTIVE SEISMIC EXPERIMENT. (21 shots) Shots 5, 6, 8, 9, 10, 14, 15 and 16 misfired.

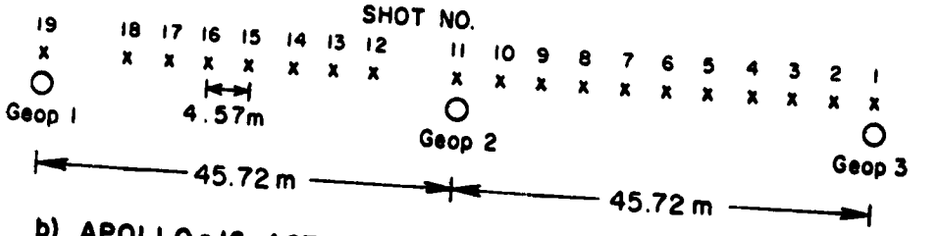

b) APOLLO-16 ACTIVE SEISMIC EXPERIMENT. (19 shots)

Fig. 3. Plan view of the geophone siting and thumper-shot locations for the Apollo-14 and Apollo-16 Active Seismic Experiments. (Geophones: o; shots: x; misfired shots: ⊗).

Table I

Correspondence of binary data values (B.D.) with the geophone voltage (V) (Geophone 1, Apollo 16)

B.D.	V	B.D.	V.	B.D.	V
0	− 2.299	11	− 0.00363	22	0.02101
1	− 1.279	12	− 0.00202	23	0.03783
2	− 0.7115	13	− 0.00112	24	0.06813
3	− 0.3958	14	− 0.00047	25	0.1227
4	− 0.2202	15	− 0.00000	26	0.2209
5	− 0.1225	16	+ 0.00048	27	0.3978
6	− 0.06817	17	0.00111	28	0.7164
7	− 0.03793	18	0.00200	29	1.290
8	− 0.02110	19	0.00360	30	2.323
9	− 0.001174	20	0.00648	31	4.183
10	− 0.000653	21	0.01167		

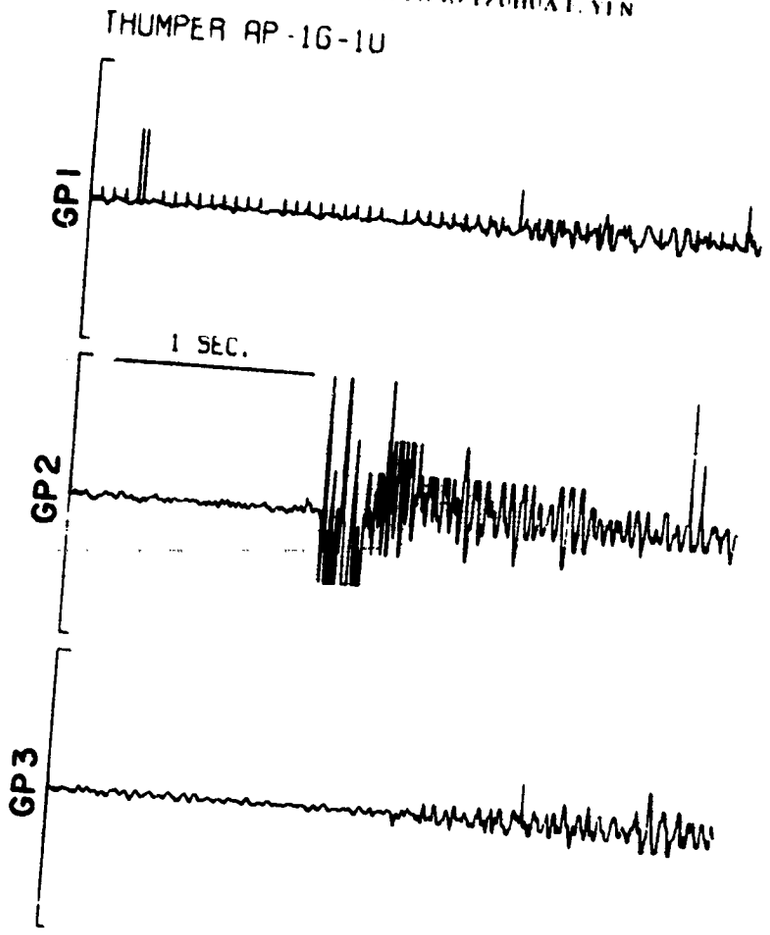

Fig. 4. Representative raw-data traces from the Apollo-16 ASI. (Thumper shot 10).

"glitches", most of which are almost uniformly spaced in time and of uniform amplitude but there are others of varying amplitude and times of occurance. Similar large glitches are seen on the other two traces. A close look at the data showed that there are smaller glitches throughout the records; these are recognized by the fact that they are of short duration – generally, only one or two samples – and had values which were inconsistent with preceeding and following sample values.

The first data-improving operation performed was to go through the data *by hand* and remove the extraneous values and replace them by values interpolated from neighboring values. A computer program was not used in this process because: (1) there are relatively few glitches (excluding the regular, periodic ones in geophone 1, there are fewer than 1%), (2) the coarseness of the amplitude values precludes automatic, computer interpolation

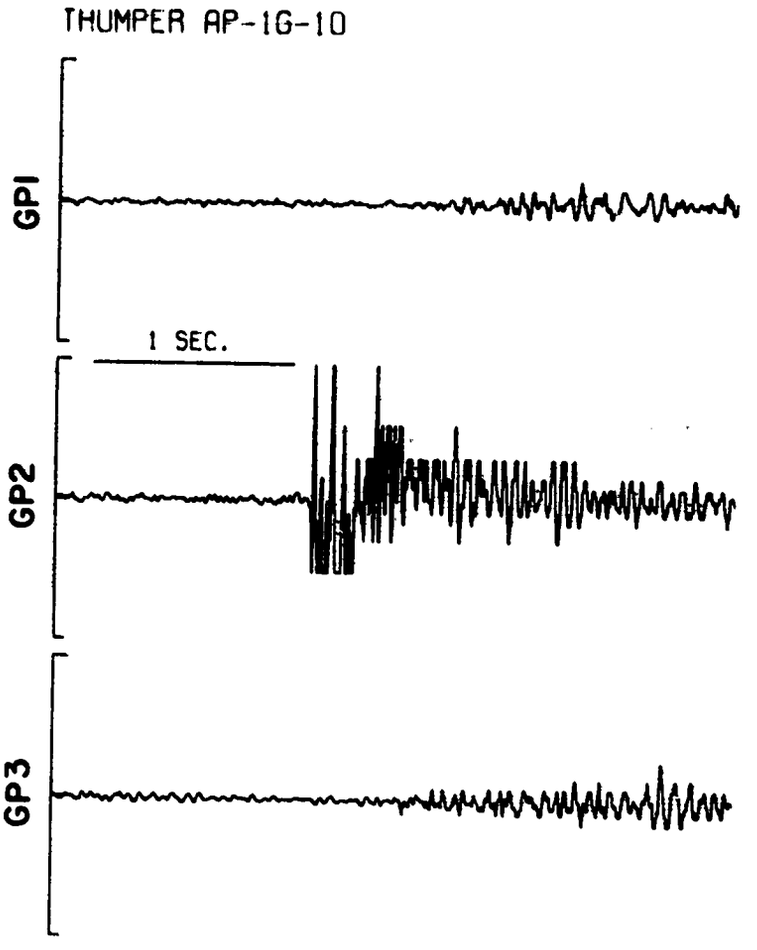

Fig. 5. "Deglitched" versions of the traces in Figure 4.

and (3) a number of different criteria were used simultaneously to identify and correct the bad sample values. The result of the 'deglitching' process is shown in Figure 5 for the same traces shown in Figure 4. While this improved the records considerably, it is clear the S/N ratios for the geophone-1 and -3 traces are still too low to allow positive identification of the first arrivals.

To imporve the S/N and smooth out the traces, the data were bandpass filtered with a four-pole, anti-aliased, Butterworth filter (~ 12 dB/octave slopes at both low and high frequencies) which had 3 dB frequencies at 10.5 Hz and 66.25 Hz. The result, for the same three traces, are shown in Figure 6. While this improved the S/N significantly and improved the character of the traces (compare Figures 5 and 6), the S/N for separations larger than 9.14 m (30 ft) was still low because of the decrease in the direct arrival's amplitude.

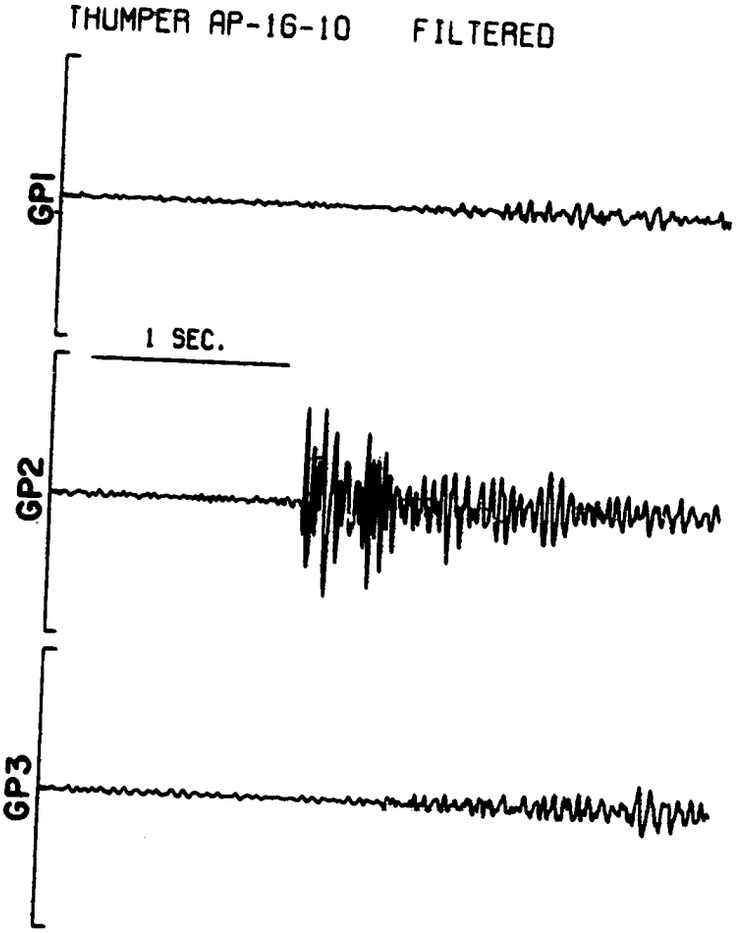

Fig. 6. Bandpass-filtered versions of the traces in Figure 4. (3 dB frequencies: 10.5 and 66.25 Hz).

Spectral analyses of the seismic traces were made to determine the frequency band of the seismic energy and to see if there was significant aliasing of the data. The amplitude spectrum (for geophone 2, shot 10, Apollo-16 ASE) of the first two seconds (1024 samples) is shown in Figure 7. While only half of the full amplitude spectrum (0 to 265 Hz) is shown there, it is clear that there is little, if any, aliasing because most of the signal energy is contained between 10 and 90 Hz with the major part between 10 and 40 Hz. This is the spectrum of the middle trace shown in Figures 4, 5 and 6.

To further improve the data, the traces with the same source-to-receiver separation for both ASE's were summed (or "stacked") together. The implicit assumptions being made here are: (1) the velocity variation with depth is the same at both the Apollo-14 and -16 sites and (2) there is lateral homogeneity for the direct waves at both sites. The first

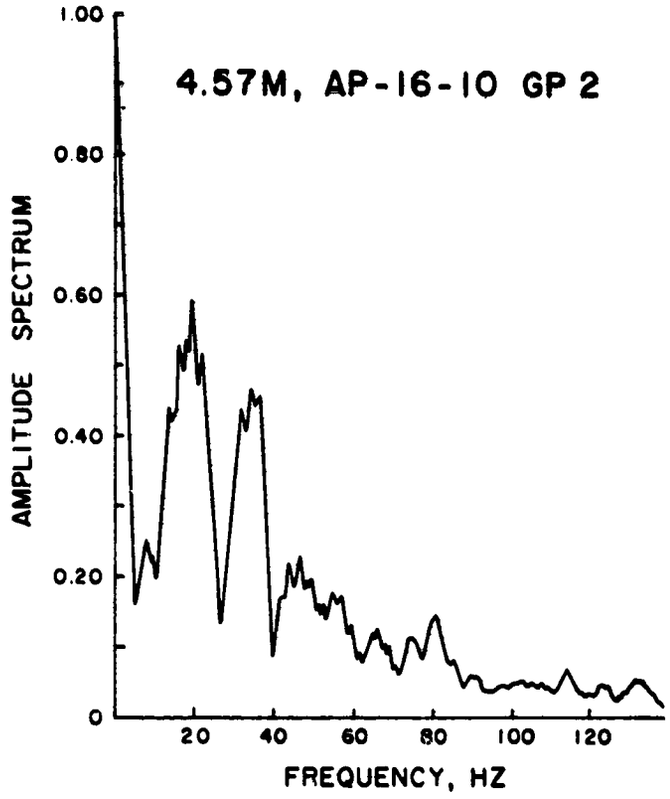

Fig. 7. Amplitude spectrum of the first two seconds of the signal from geophone 2, thumper shot 10, Apollo-16 ASE. (Separation: 4.57 m).

Table II

Shot-to-geophone separations

Separation		No. of	Apollo-14 Shot Nos.*			Apollo-16 Shot Nos.*		
(ft)	(m)	traces	GP-1	GP-2	GP-3	GP-1	GP-2	GP-3
0	0.00	6	21	11	1	19	11	1
15	4.57	5	20	12	2	–	10	2
30	9.14	7	19	13	3	18	9,12	3
45	13.71	6	18	–	4	17	8,13	4
60	18.29	6	17	7	–	16	7,14	5
75	22.86	4	–	–	–	15	6,15	6
90	27.43	6	–	17	7	14	5,16	7
105	32.00	6	–	4,18	–	13	4,17	8
120	36.58	7	13	3,19	–	12	3,18	9

* Thumper-shot numbers which had the proper separation from the three geophones.

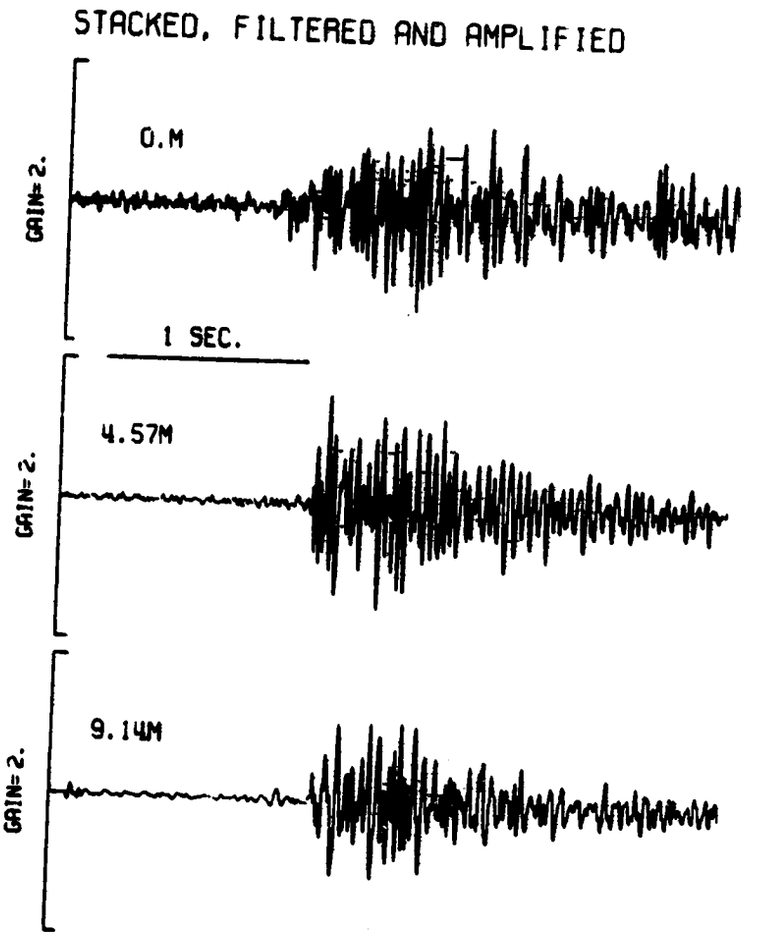

Fig. 8. Stacked, filtered and amplified traces for shot-to-geophone separations of 0, 4.57 and 9.14 m. (Apollo-14 and Apollo-16 signals combined; Bandpass: 10.5 to 66 Hz).

assumption is reasonably consistent with the results found by Kovach *et al.* (1971) for the two sites; the second assumption is consistent with the equivalent assumption made by Kovach *et al.* (1971) in their interpretation of the data at each site.

The traces that had the same source-to-receiver separation are listed in Table II for both the Apollo-14 and -16 ASE's. The thumper-shot numbers, corresponding to the given shot-to-geophone separations, are listed in the right half of the table. Among the two experiments, there were between 4 and 7 traces with the same separation. If the background noise is random and the assumptions cited hold, the stacking should give improvements in S/N between 2 and $\sqrt{7}$. The resulting sum signals were amplified so that the peak excursions would be plotted almost full scale for each trace. A representative

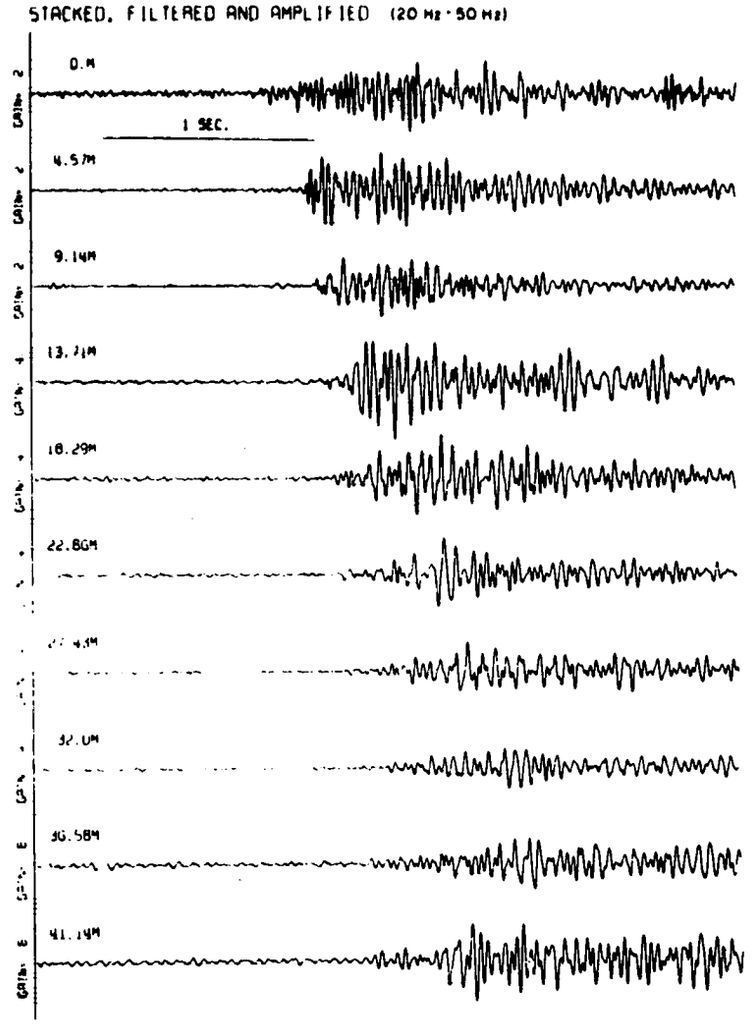

Fig. 9. Stacked, filtered and amplified ASE profile (Apollo-14 and Apollo-16 signals combined; Bandpass: 20 to 50 Hz).

result is shown in Figure 8. The second trace in Figure 8 is at the same separation as the middle traces in Figures 4, 5 and 6 (i.e., the geophone-2 trace for the 10th thumper shot of the Apollo-16 ASE). For this trace, the S/N improvement should be better than a factor of 2; however, this degree of improvement was not achieved. Nevertheless, improvements in S/N were achieved for this trace, and for the other traces at larger separations, by the stacking technique.

The result of summing the deglitched traces is shown in Figure 9. These signals were

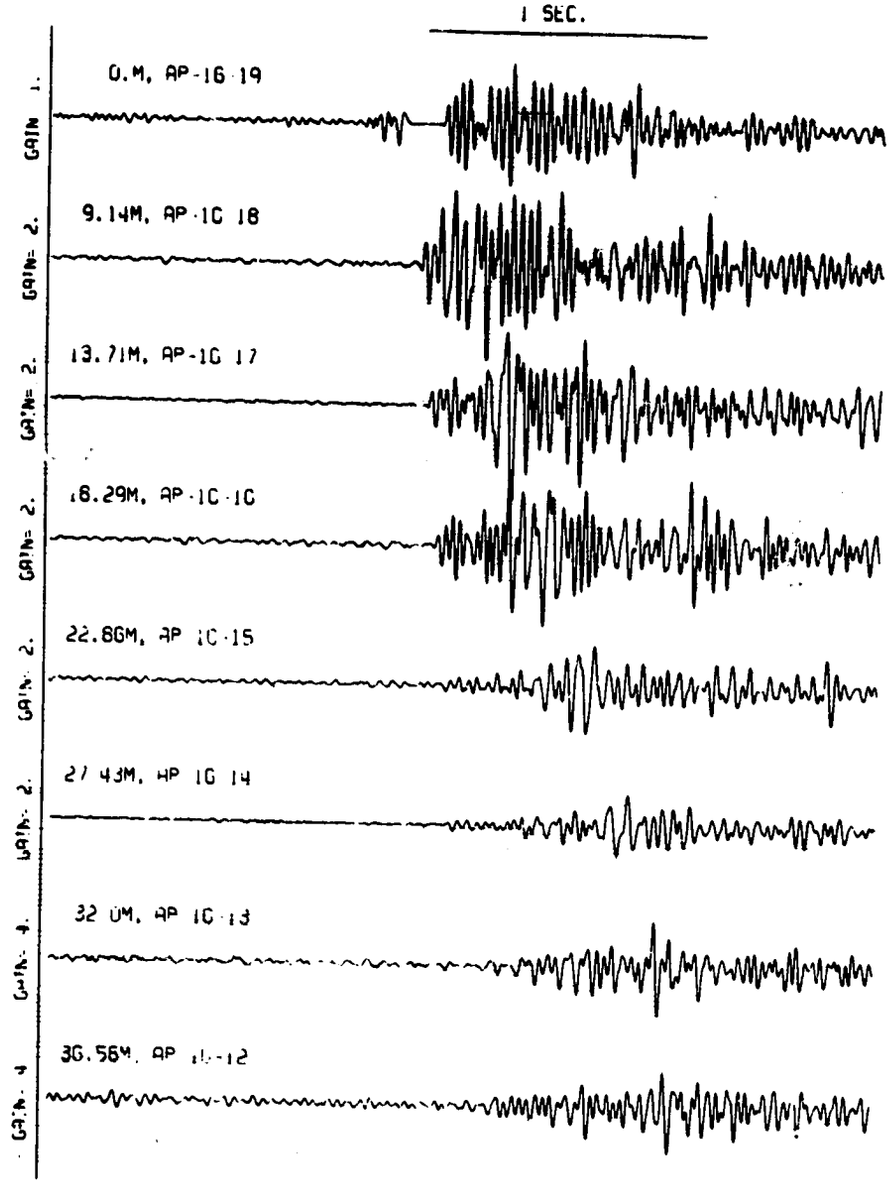

Fig. 10. Single-geophone profile, filtered and amplified. (Geophone 1, Apollo-16 ASE; Bandpass: 20 to 50 Hz).

filtered, before summing, with a 4-pole, anti-aliased, bandpass, Butterworth filter with 3 dB frequencies at 20 and 50 Hz. Arrival times can be determined with some certainty for separations up to 32.00 m (105 ft); it is difficult, if not impossible, to pick arrivals beyond that distance.

One of the single-geophone profiles (geophone 1, Apollo 16) is shown in Figure 10. Arrival times can be easily picked for separations up to 18.29 m (60 ft) and, with difficulty, for 22.86 m (75 ft) and 27.43 m (90 ft). At 32.00 m separation (105 ft), the first arrival is buried in the noise. We were not able to determine a first arrival with any degree of certainty for separations greater than 32.00 m (105 ft). This is consistent with the finding of Kovach and Watkins (1973) for the thumper shots.

3. Results

The travel times and amplitudes of the direct (first arriving) seismic signals of the Apollo-14 and -16 ASE's were analyzed. The travel times and amplitudes for separations up to 32.00 m (105 ft) were obtained both from the summed (stacked) traces and from individual traces. In one case, all the 'noise-free' traces from both ASE's were stacked in an attempt to improve the S/N ratio. In two other cases, only the 'noise-free' traces from each ASE were stacked to give Apollo-14-only and Apollo-16-only stacked profiles. If there are significant differences in the velocity structure at the two sites, these individual-site stacks would show the difference. Little difference was found, over the 32 m, in the travel times for these two stacks. The travel times for individual geophone profiles were also measured to test the assumption of lateral homogeneity at each site. The quality of the data precluded any positive conclusion regarding this assumption; however, the improvement in S/N ratio achieved by the various stacking indicate this is a reasonable assumption.

4. Travel Times

The travel times for five of the cases investigated are listed in Table III. In those cases where the S/N ratio was high (up to and including 18.29 m separation), the travel times could be determined to within 1/2 sample time (± 1 ms). However, systematic errors – such as those due to variations in the separations, elevation differences, shot-time, etc. – could be as high as one or two sample times.

Log/log plots of travel time versus separation were used to test the hypothesis of a power-law velocity variation. It can be shown, using Kaufman's (1953) work, that a velocity variation with depth, z, given by

$$v(z) = v_0(z/z_0)^n, \tag{1}$$

results in a direct-wave travel time $t(x)$ with separation x, given by (see also Gangi, 1972)

$$t(x) = t_0(x/x_0)^{1-n}, \tag{2}$$

where t_0 is the traveltime corresponding to the separation x_0 and v_0 is the velocity at depth z_0. This incorporates both the travel time/separation relationships for a constant-velocity medium ($n = 0$) and that for a self-compacting-powder medium ($n = 1/6$). Therefore, for the two power-law velocity models ($n = 0$ and $n = 1/6$), the travel time curve in

Table III
Travel times (milliseconds)

Separation x (m)	Measured travel times§ 1	2	3	4	5	Calculated travel times A	B	C
4.57	55	53	56	52	–	51.7	44.0	40.1
9.14	91	91	–	87	99	92.1	87.9	80.2
13.71	123	123	124	–	128	129.1	131.9	120.3
18.29	151	149	152	–	155	164.2	175.8	160.4
22.86	–	–	–	–	177?	197.7	219.8	200.5
27.43	206?	230	196?	229	199?	230.1	*245.0	240.6
32.00	255?	274?	264?	274?	–	261.7	*260.3	280.7
$1-n$	0.76	0.80	0.74	0.84	0.63	5/6	–	1
v_0 (m s^{-1})	590	430	630	340	1200	350	104	114

§ Times with question marks (?) indicate difficult time determinations.
* Traveltimes of the first refracted wave (earliest arrival).
1. Measured from Apollo-14 and -16 stacked data (3–66 Hz).
2. Measured from Apollo-14 (only) stacked data (3–66 Hz).
3. Measured from Apollo-16 (only) stacked data (3–66 Hz).
4. Measured from Apollo-14, geophone-2 profile (3–66 Hz).
5. Measured from Apollo-16, geophone-1 profile (3–66 Hz).
A. Self-compacting-powder model; $t = 14.57x^{5/6}$ (ms).
B. Apollo-14 layered model (Kovach and Watkins, 1973).
C. Apollo-16 layered model (Kovach and Watkins, 1973).

a log/log plot would be a straight line whose slope, m, would be determined by the power-law exponent ($m = 1 - n$).

The slopes of least-squares-fitted straight lines are given in Table III along with the velocity v_0 which corresponds to the velocity extrapolated to $z_0 = 1$ km. As indicated earlier, it is not expected that the powdered layer would extend to 1 km; therefore, v_0 is *not* an estimate of the velocity at that depth but is merely a constant used to characterize the velocity. The depth $z_0 = 1$ km is chosen only for convenience; the reference depth could have been chosen to be 1 m, in which case, the v_0's in Table III would be multiplied by $(0.001)^{1/6} = 0.3162$. While the measured slopes are variable, they are all consistently lower than $m = 1 - n = 1$, the value that would be obtained for the constant velocity model. The measured values tend to cluster near the value predicted by the self-compacting-powder model; namely, $m = 1 - 1/6 = 0.833$.

The variation in the reference velocity, v_0, is much greater than that of the slopes; its values vary between 340 and 630 m s^{-1}. The slope of 0.63 and reference velocity of 1200 m s^{-1} for the Apollo-16, geophone-1 profile (Column 5, Table III) are not very accurate because there are only three good data points (the traveltimes at 9.14, 13.71 and 18.29 m) for determining these values. It gave the least consistent values for n and v_0. In computing the least-squares lines, the questionable data were given a weight equal to one-quarter that of the high-S/N data.

Travel times were calculated from the Apollo-14 and Apollo-16 velocity models given

by Kovach and Watkins (1973). These are shown in columns B and C of Table III. In column A, the travel times for a powder-layer model with $v_0 = 350\,\mathrm{m\,s^{-1}}$ and $n = 1/6$ are tabulated. This latter model was an average model found from all the cases treated when the velocity exponent, n, was constrained to be 1/6. Overall, there are not large differences between the measured travel times and the calculated travel times using any of the models. However, the biggest differences between the Kovach and Watkins models and the measured values occur at the small separations, precisely where the S/N ratios are highest and where the travel times can be picked with the greatest certainty. Their models can be made to fit the close-in data simply by introducing a thin, lower velocity layer at the surface. But it should be recalled that they already have low velocities for the top layers (104 and $114\,\mathrm{m\,s^{-1}}$ for Apollo-14 and -16, respectively) which are relatively thin (8.5 and 12.2 m, respectively).

The travel time data for the combined Apollo-14 and -16 stacked traces (Column 1, Table III) are shown in Figure 11 along with the least-squares-fitted line. These data are from the deglitched traces which have been bandpass filtered with a fourth-order, Butterworth filter having 3 dB points at 3 and 66 Hz. It can be seen from Figure 11 that the straight line is an excellent fit to the data and that it would be difficult to change the slope from its given value (0.76) to 1.0, the latter value corresponding to the constant-velocity model. Equally good fits of data points to straight lines were found for the Apollo-14-only and Apollo-16-only stacked data.

5. Amplitudes

The travel times of the first arrivals over the 0–32 m range do not demonstrate a *clear* distinction between the powered-layer and the layered-velocity models. The data accuracy is

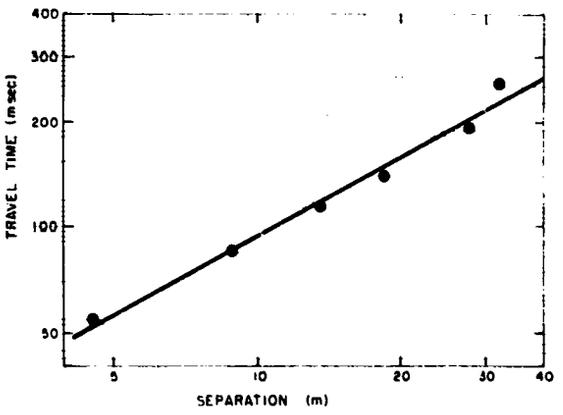

Fig. 11. Log–log plot of the travel times versus separations for the stacked and filtered traces. (Apollo-14 and Apollo-16 ASE signals combined; Bandpass: 3 to 66 Hz; measured slope: $m = 0.76$ and reference velocity: $v_0 = 590\,\mathrm{m\,s^{-1}}$).

such that either model can be accepted. To try to distinguish between the two models, the amplitudes of the first arrivals were measured and compared with the expected distance variation predicted by the two models.

Since the thumper shots give primarily vertical forces and the geophones are vertically oriented, the amplitude of the direct p-wave arrival in the layered model should vary as the inverse square of the separation - i.e.,

$$A(x) = A_0(x/x_0)^{-2}, \tag{3}$$

for small separations (see, for example, White, 1965; p. 215). On the other hand, for a power-law velocity model, the amplitude variation with separation is given by (see Appendix A)

$$A(x) = \left[-\frac{S(p)}{2\pi x}\frac{\mathrm{d}^2 t}{\mathrm{d}x^2}\right]^{1/2}, \tag{4}$$

where $S(p)\,\mathrm{d}p$ is the energy radiated in a bundle of rays having ray parameters lying between $p - \mathrm{d}p/2$ and $p + \mathrm{d}p/2$, the ray parameter is given by $p = \sin\theta(z)/v(z)$, $\theta(z)$ is the angle between the ray and the vertical (z) direction, $v(z)$ is the velocity variation with depth and t is the travel time for the ray (with ray parameter, p) which returns to the surface at separation x. For the self-compacting-powder model, the amplitude variation is estimated to be (see Appendix A)

$$A(x) = A_0(x/x_0)^{-(13-m)/12}, \quad m > 1, \tag{5}$$

where m is a measure of the source radiation pattern in the power-law-velocity medium. To insure integrability of

$$E = \int_0^\infty S(p)\,\mathrm{d}p,$$

where E is the energy radiated by the thumper source, we find $m > 1$ (see Appendix A). This indicates the amplitude decrease of the direct wave with separation is less in the powder-layer model than that in the constant-velocity model. This is consistent with the conclusion of Gold and Soter (1970) based on their analysis for a linearly increasing velocity with depth.

The determination of the amplitude variation with separation for the Apollo-14 and -16 ASE data is more difficult than determining the travel time data because of: (1) the coarseness of the amplitude sampling, (2) the variability of the thumper-shot strengths, (3) the variability of the geophone sensitivities (primarily due to siting and coupling of the geophones) and (4) the low S/N ratio for the larger separations. The coarseness of the amplitude data is significantly reduced by the interpolating effect of bandpass filtering. The variability due to the shot strengths, the geophone sensitivities and the low S/N ratio are reduced by the averaging inherent in stacking or summing traces (provided the signals are sufficiently coherent for a given source/receiver separation).

On the basis of the measured arrival times (at least for separations less than 22.86 m –

Table IV

Amplitude data (arbitrary units)

A. Bandpass: 3–66 Hz

x (m)	14–1†	14–2(1)§	14–3†	14–Σ¶	16–1†	16–2(3)§	16–3†	16–Σ¶	14,16–Σ¶
4.57	4.62	3.91	4.68	4.19		5.82	5.34	5.69	3.95
9.14	3.17	2.08	?	3.36	1.43	0.76	3.17	0.82	1.16
13.71	1.13	*	?	1.13	0.81	0.32	0.54	0.31	0.40
18.29	0.52	*	*	0.52	0.56	0.45	0.42	0.26	0.30
22.86	*	*	*	*	?	0.18?	0.23?	?	?
27.43	*	0.15	0.1?	0.17	0.13	?	0.18?	0.10	0.07
32.00	*	0.10?	*	0.10?	?	?	?	0.19?	?
Slope	1.55	1.83	2.15	1.78	1.77	− 2.01	− 2.01	1.97	− 2.04

B. Bandpass: 20–40 Hz

x (m)	14–1†	14–2(1)§	14–3†	14–Σ¶	16–1†	16–2(3)§	16–3†	16–Σ¶
4.57	2.38	2.17	2.65	2.26	–	2.94	2.48	2.34
9.14	1.75	0.93	1.49	1.75	0.66	0.39	1.70	0.44
13.71	0.56	*	0.22	0.56	0.38	0.20?	?	0.17
18.29	0.24	*	*	0.24	0.29	0.22	0.21	0.13
22.86	*	*	*	*	?	?	0.11	?
27.43	*	0.13	0.05	0.09	0.06	?	0.10	0.05
32.00	*	?	*	?	?	?	?	?
Slope	1.63	− 1.59	− 2.34	− 1.87	− 2.07	− 1.98	− 2.00	− 2.08

† 14–1 means Geophone 1, Apollo-14 ASE, etc.
¶ 14–Σ means stacked traces, Apollo-14 ASE.
§ 14–2(1) means traces on Geophone 2, Apollo-14 ASE, sources between Geophones 1 and 2, etc.
* Misfired shot.
– No shot available.
? Low S/N ratio.

see Table III, sufficient coherency of the signals exists so that averaging of the amplitudes should be possible by summing of traces. The measured amplitudes are given in Table IV. Both the amplitudes for individual traces and for stacked traces are given. Measurements were made on data that had been bandpass filtered by anti-aliased, fourth-order Butterworth filters with 3 dB frequencies of 3–66 Hz and 20–40 Hz. It can be seen that there is a great deal of scatter in the data. Some of this is due to the thumper-shot variability and some due to geophone siting, but the major part is due to low S/N ratio and the coarseness of the amplitude data. Straight lines were fitted, by least-squares, through the data points (on a log–log graph) and the slopes of these lines are included in Table IV. A representative plot of the amplitude data along with its least-squares-fitted line is shown in Figure 12. This represents one of the most complete sets of amplitude data available for a single geophone; namely, geophone 3 for the Apollo-16 ASE. The original traces were bandpass-filtered (3 dB frequencies at 3 and 66 Hz) prior to measuring the amplitudes.

Because of the low S/N ratio at the larger separations, it is not certain that a straight

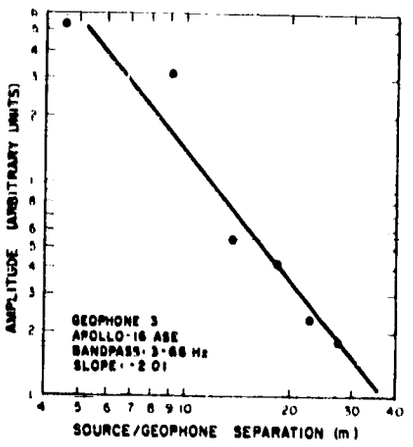

Fig. 12. Log–log plot of the amplitudes versus separations (Single geophone amplitudes; Geophone 3, Apollo-16 ASE; Bandpass: 3 to 66 Hz; measured slope: − 2.01).

line (on a log–log plot) is the appropriate fitting function. While all the data are fairly well fitted by the line in Figure 12 (with a slope equal to − 2.01), it is clear that the two largest amplitude values (at 4.57 and 9.14 m), which have the best S/N ratios, suggest a lower slope.

The slopes found for all the cases with fairly good data lie between − 1.5 and − 2.1. However, the possible errors on these slopes are of the order of ± 0.5. The fact that the slopes are more negative than − 1 and close to − 2, the slope predicted by a simple flat-layer model, does not mean the amplitude data verifies that model. From Equation (5), the slope predicted by the powder-layer model would be more positive than − 1. However, this equation and the theory used to predict a slope of − 2 for the flat-layer model are based on simplyfying assumptions; namely, that all the sources are of equal strength, the geophones are equally coupled to the regolith, there is no attenuation by absorption in either model, there is no energy loss by conversion of *p*-wave energy into *s*-wave energy (for the powder-layer model) and there are no scatters in the lunar regolith. The latter three effects would increase the amplitude loss with distance so that the predicted slopes (− 2 for the flat layer and $-(13-m)/12$ for the powder layer) should be considered upper bounds on the measured ones. The variability of the thumper-shot strengths and of the geophones would increase the scatter in the data.

While the amplitude data do not preclude either model conclusively (as they would have if the measured amplitudes decreased more slowly than inversely with separation), they do favor the powder-layer model. All the loss mechanisms lead to a greater decrease in amplitude than predicted by the simple analyses of the two models. However, the amplitude data do *not* show a more rapid decrease than that predicted for the homogeneous-layer models proposed by Kovach and Watkins (1973) while the data clearly do show a more rapid decrease with separation than that predicted by the simple

(first-order) theory for the powder-layer model. This discrepancy in the amplitude variation with distance can *not* be explained by interference of other waves with the direct wave. For the short separations where amplitude data is available (generally less than 27.43 m), interference from reflected or refracted waves would not affect the amplitudes by interference for the flat-layer models; nor would a velocity discontinuity at a depth greater than about 10 m effect the amplitude results (by the same types of interference) in the powder-layer model.

6. Geophone-Coupling and Shot-Strength Variability

To eliminate the effects of variability in the geophone coupling and the Thumper-shot strengths, an analysis of the amplitude data was made which determines both the geophone sensitivity (in place) and the shot strengths as well as the exponent of the amplitude variation when there is sufficient redundancy in the data.

If it is assumed that either the flat-layer model or the powder-layer model is valid, the measured amplitude at a particular geophone due to a particular source will be given by

$$A_{ij} = G_i S_j |x_i - x_j|^m, \tag{6}$$

where G_i is the sensitivity of the ith geophone (including coupling and siting effects) located at x_i, S_j is the strength of the jth shot located at x_j and m is the exponent of the amplitude variation.

Equation (6) can be normalized to the sensitivity of a particular geophone, say G_I ($I = 1$, 2 or 3), and to the strength of a particular shot, say S_J. This normalization is necessary because, quite clearly, each geophone sensitivity can be multiplied by some constant factor and each shot strength divided by the same factor without changing the resulting amplitude.

Letting $G_I S_J = A_0$, Equation (6) becomes

$$A_{ij} = A_0 (G_i/G_I)(S_j/S_J)|x_i - x_j|^m. \tag{7}$$

Equation (7) can be linearized in terms of the relative geophone sensitivities, the relative shot strengths, the exponent m and the arbitrary constant A_0 by taking its logarithm

$$\log A_{ij} = \log A_0 + \log (G_i/G_I) + \log (S_j/S_J) + m \log |x_i - x_j|;$$

or, for convenience in writing,

$$a_{ij} = a_0 + g_i + s_j + m X_{ij}, \tag{8}$$

where $a_{ij} = \log A_{ij}$, $X_{ij} = \log |x_i - x_j|$, $g_i = \log (G_i/G_I)$ and $s_j = \log (S_j/S_J)$.

The optimum values, in a least-squares sense, of a_0, g_i, s_j and m can be determined by minimizing the summed, weighted and squared error

$$E^2(a_0, m, \mathbf{g}, \mathbf{s}) = \sum_{i=1}^{I} \sum_{j=1}^{J} w_{ij}(a_0 + m X_{ij} + g_i + s_j - a_{ij})^2. \tag{9}$$

as a function of these parameters. The result (see Appendix B) is the matrix equation

$$\mathbf{a} = \mathbf{A} \cdot \mathbf{p}, \tag{10}$$

where $\mathbf{a}$ is a vector whose components depend only upon the measured amplitudes (a_{ij}), the weights (w_{ij}) and the measured separations (X_{ij}); A is a square matrix whose components depend only upon the weights and the measured separations while p is a vector whose components are the unknown parameters: $g_1, \ldots, s_1, \ldots, a_0$ and m. (The detailed form of this equation is given in Appendix B.) The solution to this matrix equation is

$$\mathbf{p} = \mathbf{A}^{-1} \cdot \mathbf{a}. \tag{11}$$

If there is sufficient redundancy in the data, the matrix will be well conditioned and nonsingular and will have a stable inverse.

The weights are established from the quality of the data. The weights for the Apollo-16 data are shown in Table V. From the table it is seen that only 14 of the 19 thumper shots gave useful amplitude data (shots 1, 11, 13, 14 and 19 were not useable) and, of these 14, only three (shots 6, 7 and 17) give measurable first-arrival amplitudes on more than one geophone. (Shots 12 and 17 gave amplitudes of 0.89 and 0.067, respectively, for the 3–66 Hz bandpassed traces on geophone 2; all other amplitudes are given in Table IV). Therefore, only six amplitude measurements (two for each shot) are available to determine the six parameters $a_0, m, g_1, g_3, s_6, s_{17}$ (when geophone 2 and shot 7 are used as the reference geophone and shot, respectively). With the relative geophone sensitivities, the constant a_0 and the exponent m set by these data, the remaining relative shot strengths will be determined by the assumed amplitude variation (Equation (6) or (7)) and the measured amplitude.

Having only six correlative amplitude measurements to determine six unknowns (by means of the linear equations (8) or (10)) means there is little redundancy in the amplitude data. Nevertheless, the solution of these six equations in the six unknowns do constitute a least-squares solution. This is because weighting factors are used in the equations; the weights can be interpreted to mean that more than six measurements of equal weight were made, some of which were identical measurements (i.e., same shot location), and the results combined together to give a single result of greater weight.

If we use six available correlative amplitude values, the matrix equation becomes

$$\begin{bmatrix} \langle w_{ij} a_{ij} \rangle \\ \langle w_{ij} a_{ij} X_{ij} \rangle \\ \langle w_{1j} a_{1j} \rangle \\ \langle w_{3j} a_{3j} \rangle \\ \langle w_{16} a_{16} \rangle \\ \langle w_{17} a_{17} \rangle \end{bmatrix} = \begin{bmatrix} \langle w_{ij} \rangle & \langle w_{ij} X_{ij} \rangle & \langle w_{1j} \rangle & \langle w_{3j} \rangle & \langle w_{16} \rangle & \langle w_{i,17} \rangle \\ & \langle w_{ij} X_{ij}^2 \rangle & \langle w_{1j} X_{1j} \rangle & \langle w_{3j} X_{3j} \rangle & \langle w_{16} X_{16} \rangle & \langle w_{17} X_{17} \rangle \\ & & \langle w_{1j} \rangle & 0 & \langle w_{16} \rangle & \langle w_{1,17} \rangle \\ & - & & \langle w_{3j} \rangle & \langle w_{26} \rangle & \langle w_{3,17} \rangle \\ & & & & \langle w_{16} \rangle & 0 \\ & - & - & - & & \langle w_{i,17} \rangle \end{bmatrix} \begin{bmatrix} a_0 \\ m \\ g_1 \\ g_3 \\ s_6 \\ s_{17} \end{bmatrix}.$$

Table V

Data weights and separations; Apollo-16 ASE

Shot No. (j)	Weights: w_{ij} Geophone No. (i)			Separations: $\lvert x_i - x_j \rvert$ Geophone No. (i)		
	1	2	3	1	2	3
1	0	0	0	91.44	45.72	0
2	0	0	1	86.87	41.14	4.57
3	0	0	1	82.30	36.58	9.14
4	0	0	1	77.72	32.00	13.71
5	0	0	1	73.15	27.43	18.29
6	0	½	½	68.58	22.86	22.86
7	0	1	¼	64.05	18.29	27.43
8	0	1	0	59.44	13.71	32.00
9	0	1	0	54.86	9.14	36.58
10	0	1	0	50.29	4.57	41.14
11	0	0	0	45.72	0	45.72
12	0	1	0	36.58	9.14	54.86
13	0	0	0	32.00	13.71	59.44
14	¼	0	0	27.43	18.29	64.05
15	0	0	0	22.86	22.86	68.58
16	1	0	0	18.29	27.43	73.15
17	1	¼	0	13.71	32.00	77.72
18	1	0	0	9.14	36.58	82.30
19	0	0	0	0	45.72	91.44

where $i = 1, 2$ and 3 and $j = 6, 7, 17$. In terms of assumed values of w_{ij} and the measured values of X_{ij} and a_{ij}, this equation becomes

$$\begin{bmatrix} 3.734 \\ -11.710 \\ -0.211 \\ -1.164 \\ -1.592 \\ -0.914 \end{bmatrix} = \begin{bmatrix} 3.50 & 10.35 & 1.00 & 0.75 & 1.00 & 1.25 \\ - & 30.84 & 2.62 & 2.39 & 3.13 & 3.48 \\ - & - & 1.00 & 0 & 0 & 1.00 \\ - & - & - & 0.75 & 0.50 & 0 \\ - & - & - & - & 1.00 & 0 \\ - & - & - & - & - & 1.25 \end{bmatrix} \begin{bmatrix} a_0 \\ m \\ g_1 \\ g_3 \\ s_6 \\ s_{17} \end{bmatrix}$$

If we solve this matrix equation, the relative geophone sensitivities and relative shot strengths are found to be

$$G_1/G_2 = 0.724; \quad G_3/G_2 = 1.40,$$

$$S_6/S_7 = 0.803; \quad S_{17}/S_7 = 0.848,$$

and the exponent is

$$m = -3.57.$$

Unfortunately, these values appear to be unreasonable; this is not surprising considering the lack of redundancy and quality in the amplitude data. The 30 to 40% differences in the relative geophone sensitivities are not too unreasonable, but are higher than expected. Also, the 15 to 20% variations in the shot strengths are possible, but again seem large. The value of the exponent ($m = -3.57$) is different by almost a factor of two compared to the values obtained using single-geophone profiles and stacked profiles (compare Table IV). The 30 to 40% differences in geophone sensitivity have no effect on the amplitude variation with distance as determined by a single-geophone profile. The 20% differences in shot strengths (of shots 6 and 17 relative to shot 7) would not cause appreciable differences in the slopes (or exponents) obtained from single-geophone profiles (provided, of course, that these differences are representative of the differences in the other shots). It is concluded that the least-squares analysis given above does not give reliable values for the parameters ($m, G_1/G_2, G_3/G_2, S_6/S_7, S_{17}/S_7$). However, the method is a valid one and the reason for the unreliability in the parameter values is the lack of redundancy and quality in the data.

While the method is not useful for this data set, it is presented in detail because there may be other instances where it would give valid results. It provides a rationale for the design of seismic experiments which test amplitude variation with separation when variability in source strengths and geophone sensitivities is anticipated (as is generally the case).

The same amplitude analysis could not be performed on the Apollo-14 ASE data because there were not correlative amplitude values for geophones 2 and 3 (due to misfires and poor signal-to-noise ratios).

7. Summary

The data from the thumper shots of the Apollo-14 and Apollo-16 ASE's have been reanalyzed to test whether the velocity variation in the shallow lunar crust (depths $\leqslant 10$ m) can be represented by a self-compacting-powder-layer as proposed by Gold and Soter (1972) and Gangi (1972) or by constant-velocity layers as proposed by Kovach *et al.* (1971, 1972, 1973).

Both the travel times and the amplitudes for the first arrivals were remeasured and compared with the values predicted by the self-compacting-powder-layer model proposed by Gangi ($v(z) = v_0(z/z_0)^{1/6}$) and the layered-velocity model proposed by Kovach *et al.* To improve the quality of the data, they were 'deglitched' to remove spurious values and bandpass filtered. Four-pole, anti-aliased Butterworth filters with bandpasses between 3 and 66 Hz and 20 and 50 Hz (3 dB frequencies) were used to improve the signal-to-noise ratio (S/N). In addition, traces from different thumper shots and with the same source-to-geophone spacing were summed together to improve the S/N. While these techniques improved the S/N, it still was not possible to measure travel times or amplitudes of the first arrivals for separations greater than 32 m.

While there is variability in the results obtained (see Table III), the travel times for the

direct arrival over a separation of 32 m can be fit by the 1/6-power velocity model. The measured values of the exponent for an assumed power-law velocity varied between approximately 1/3 to 1/7; that is, $0.67 < 1 - n < 0.86$ (see Table III) where n is the exponent for the depth variation of the velocity. The best (or average) model for both the Apollo-14 and Apollo-16 sites is $v(z) \simeq 350(z/z_0)^{1/6}\,\mathrm{m\,s^{-1}}$ for $z_0 = 1$ km or $v(z) \simeq 110z^{1/6}$, $0 \leqslant z \leqslant 10$ m. This is fairly close to the velocity variation, $v(z) \simeq 190z^{1/6}$, predicted by Gangi (1972) on the basis of Gassmann's analysis (1953) and the measured mechanical properties of the lunar soil.

The measured travel times of the first arrivals over the 32 m separation are in reasonable agreement with the values predicted by the layered model (see Table III). However, the biggest percentage deviations occur at the two shortest distances (4.57 and 9.14 m) where the S/N is high and the travel times can be measured most accurately. At these separations, the measured arrival times, which are accurate within at least one sample interval (or 1.89 ms), differs from those predicted by the layered model by 10 to 15 ms. The corresponding differences for the power-law model is generally less than 2 ms. While this indicates that the self-compacting-powder-layer model is probably the correct one, the quality of the data precludes a definitive distinction between the two models.

No comparison was made of the measured travel times with those predicted by the linear velocity variation used by Gold and Soter (1970), namely, $v(z) = v_0 + az$, because it was an assumed velocity variation which is not based on any physical mechanism. The travel time relationship for this velocity variation, $t = (2/a)\sinh^{-1}(ax/2v_0)$, should also fit the data to the same accuracy as that of the layered-velocity model. It, too, would have the largest percentage deviations at the shortest distances.

An analysis of the amplitudes of the first arrivals was performed to test the models. The predicted amplitude variation with separation, x – assuming no amplitude loss due to attenuation, scattering or conversion of p-wave energy into s-wave energy – for the layer model is x^{-2} while that for the 1/6-power velocity model is $x^{-(13-m)/12}$, $m > 1$. The measured exponent varied from −1.55 to −2.34 (see Table IV) with the average value near −2.0. While this result, at first glance, seems to favor the constant velocity model, the fact that there will be amplitude loss due to scattering, attentuation and wave-type conversion makes this result more consistent with the power-law model. However, the large errors in the amplitude data – which are more severe than the errors in the arrival times – preclude a *definitive* conclusion regarding which is the appropriate velocity model.

An attempt was made to eliminate the errors in amplitude, due to variations in the geophone sensitivities and shot strengths, by using a least-squares method. The method requires that the signals, from individual shots, be detected on two or more geophones. Unfortunately, only three thumper shots were detected on pairs of geophones, and no thumper shots gave detectable first arrivals on all three geophones. Consequently, there was too little redundancy in the data to give reliable values for the relative geophone sensitivities, relative shot strengths or the exponent for the amplitude variation with separation. Only for the Apollo-16 ASE was there sufficient data to perform this analysis at all, and it indicated that there could be 30 to 40% variability in the geophone

sensitivities and 15 to 20% variability in the thumper-shot strengths. An amplitude variation with separation equal to $x^{-3.6}$ was obtained from this analysis. It is not possible to give much credence to these values because the amplitudes used in this analysis were small and had large variability.

In conclusion, it has been demonstrated that the power-law-velocity model predicts: (1) the measured arrival times of the first arrivals as well as, if not better than, the layered-velocity model does and (2) the amplitude variation with separation as well as that model does. The quality of the data does not allow a definitive choice to be made between the two models. However, the power-law model predicts a very low velocity at the lunar surface which, in turn, implies that seismic rays will be nearly normally incident to the surface. This would explain why there is little correlation between the vertical and horizontal components of the motions detected by the Passive Seismic Experiment seismometers. It also implies that the long duration of the seismic signals detected on the Moon is due to scattering by even shallow undulations of the surface (Gold and Soter, 1970 and Gangi, 1972). The power-law velocity model also predicts that the lunar regolith is composed of fine particles (soil) down to a depth of 5 to 6 m. The power-law model indicates that the velocity below 6 meters is not 'sampled' by the first arrivals detected over separations less than or equal to 32 m.

Acknowledgements

This research was supported by the National Aeronautics and Space Administration (NASA) under NASA Grant NSG-7189. We thank Mrs. Mary Lynn McGuinness for her help in the preparation of the manuscript.

Appendix A. Variation in Amplitude with Distance in a Vertically Inhomogeneous Medium

An approximate analysis of the variation in amplitude of a compressional wave in a vertically inhomogeneous elastic medium can be made using ray theory. The analysis closely follows the developments givne in Bullen (1963) and Officer (1958).

The analysis is approximate in that it does not take into account either the variation in waveform of the propagating wave (i.e., dispersion) or the conversion of p-wave energy into s-wave energy (these assumptions are also made in the above references).

We assume that, for a source on the surface, the energy, dE, contained in a 'bundle of rays' with ray parameters between $p - dp/2$ and $p + dp/2$ is equal to the intensity (or energy per unit area), I, times the area subtended by the ray parameters (see Figure A1a)

$$dE(p) = I(x', p)\,dA = S(p)\,dp, \tag{A.1}$$

where $I(x', p)$ = the wave intensity for a ray with ray parameter, p, at a horizontal distance, x', away from the source point, dA = area contained between the circular 'cones' given by $p - dp/2$ = constant and $p + dp/2$ = constant ($dA = 2\pi x'\,dw$), $S(p)$ = energy

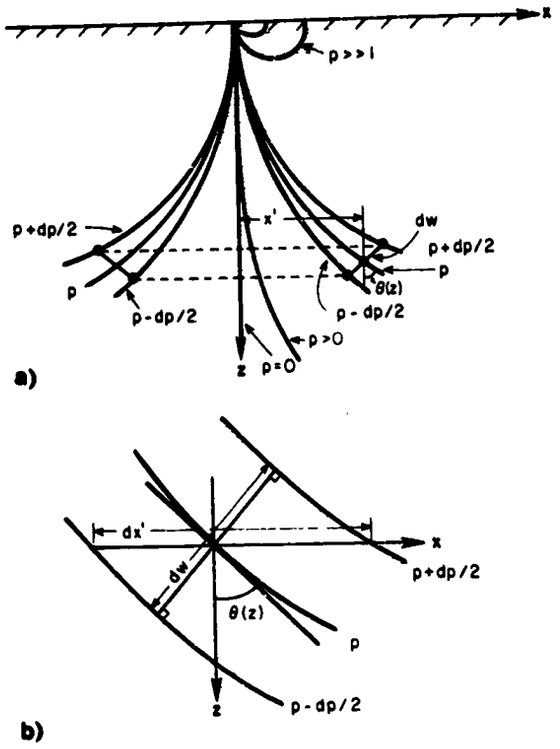

Fig. A-1. (a) Ray paths for a power-law velocity variation: $v(z) = v_0(z/z_0)^n$. (b) Detail of the wavefront, dw, in a ray bundle.

per unit change in the ray parameter, p = the ray parameter = $\sin\theta(z)/v(z)$, $\theta(z)$ = the angle between the ray and the vertical z axis and is measured counterclockwise from the z axis, and $v(z)$ = the velocity variation with depth.

The intensity for any point along the ray can be expressed as

$$I(x', p) = \frac{S(p)}{2\pi x'} \frac{dp}{dw}, \tag{A.2}$$

At a fixed depth, z, and for a particular ray bundle centered about ray parameter p, (see Figure A.1b)

$$dw(x', p) = \cos\theta dx'; \quad \text{or} \quad \frac{dw}{dp} = \cos\theta \frac{dx'}{dp}. \tag{A.3}$$

When the ray reaches the surface ($z = 0$), $\theta(0) = \pi$ ($\cos\theta(0) = -1$) and

$$x'(p, z = 0) \equiv x(p). \tag{A.4}$$

The intensity at the surface receiver then becomes

$$I(x,p) = \frac{S(p)\,dp}{2\pi x\,dx}. \tag{A.5}$$

Note that the intensity is positive since both $S(p)$ and x are positive but dp/dx is negative at the surface.

The general relationship for vertically inhomogeneous media

$$p = dt/dx \tag{A.6}$$

holds good, where $t(x)$ is the traveltime; therefore, we have

$$I(x,p) = -\frac{S(p)}{2\pi x}\frac{d^2t}{dx^2}. \tag{A.7}$$

It can be verified directly that $p = dt/dx$ for a velocity variation of the form

$$v(x) = v_0(z/z_0)^n \quad (0<n<1) \tag{A.8}$$

by using (1); the fact that

$$dt/dx = (dt/dp)/(dx/dp) \tag{A.9}$$

and (2) the parametric equations for the traveltime, $t(p)$, and the source/receiver separation, $x(p)$, (see, for example, Kaufman, 1953)

$$t(p) = C_n p^{-(1-n)/n}, \quad x(p) = (1-n)C_n p^{-1/n}, \tag{A.10}$$

where C_n is a constant and equal to

$$C_n = \frac{2\sqrt{\pi z_0}}{n v_0^{1/n}}\frac{\Gamma(1/2n+1/2)}{\Gamma(1/2n)}. \tag{A.11}$$

The problem that remains in determining the intensity is to express $S(p)$ in terms of x. The rays from a source at the surface propagate, initially, vertically; therefore, for a vertical-force source, most of the energy will be directed along the z-axis with little or no energy propagating along the surface. The rays received at the surface near the source correspond to large values of the ray parameter p, because

$$p = 1/v(z_T), \tag{A.12}$$

where z_T is the turning depth of the ray; i.e., its maximum depth of penetration. Therefore, if we assume an asymptotic expansion for $S(p)$ of the form (for $p \gg 1$)

$$S(p) \sim p^{-m}(1 + 1/p + 1/p^2 + \ldots); \quad m > 1, \tag{A.13}$$

and use the fact that (from Equation A.10)

$$p \sim x^{-n},$$

we have

$$S(p) \sim x^{mn}. \tag{A.14}$$

This indicates that the source radiation pattern contributes an increase to the intensity

as the separation increases. This is due to the fact that the rays detected at the larger separations come from that part of the radiation pattern where the intensity is higher; namely, closer to the z-axis. In order to insure integrability of $S(p)$ for the large values of p ($1 \ll p < \infty$), the exponent m must be greater than 1.

If we take advantage of the fact that

$$\frac{1}{x}\frac{d^2t}{dx^2} \sim x^{-(n+2)}, \tag{A.15}$$

the intensity variation with separation x becomes

$$I(x) \sim x^{-[1+n(1-m)]}; \tag{A.16}$$

and the amplitude variation is

$$A(x) \sim I^{1/2} \sim x^{-[2+n(1-m)]/2}. \tag{A.17}$$

For the self-compacting-powder model, $n = 1/6$ and we have

$$A(x) = A(x_0)(x/x_0)^{-(13-m)/12}; \quad m > 1. \tag{A.18}$$

Appendix B. The Relative Geophone Sensitivities, Shot Strengths and the Amplitude Variation; Least-Squares Analysis

The optimum values, in a least-squares sense, of (1) the relative geophone sensitivities, (2) the relative shot strengths and (3) the exponent of the amplitude variation with distance can be determined if there is sufficient redundancy in the amplitude data and the functional form of the amplitude function is known. The direct-wave-amplitude variation has the functional form given by Equation (6) both for a half space (i.e., constant velocity) and for a vertically inhomogeneous medium (i.e., $v(x, y, z) = v(z)$ only).

The summed, weighted and squared error, E^2, between the log of the measured amplitude values and the values predicted by the functional form (as expressed in Equation (8); see Equation (9)) is

$$E^2(a_0, m, \mathbf{g}, \mathbf{s}) = \sum_{i=1}^{I}\sum_{j=1}^{J} w_{ij}(a_0 + mX_{ij} + g_i + s_j - a_{ij})^2, \tag{B.1}$$

where $a_0 = \log(G_I S_J)$, G_I is the reference-geophone sensitivity, S_J is the reference-shot strength, $\mathbf{g}$ is the (vector of) relative geophone sensitivities, g_i is the relative sensitivity of the ith geophone, $\mathbf{s}$ is the (vector of) relative shot strengths, s_j is the relative strength of the jth shot, X_{ij} is the log of the separation between the ith geophone and the jth shot and a_{ij} is the log of the amplitude measured at the ith geophone for the jth shot.

We define a parameter vector $\mathbf{p}$ in the parameter space made up of the a_0, g_i, s_j and m as

$$\mathbf{p} = \sum_{i=1}^{I} \hat{\mathbf{g}}_i g_i + \sum_{j=1}^{J} \hat{\mathbf{s}}_j s_j + \hat{\mathbf{m}} m + \hat{\mathbf{a}}_0 a_0 = \sum_{n=1}^{I+J+2} \hat{\mathbf{p}}_n p_n = \mathbf{g} + \mathbf{s} + \mathbf{m} + \mathbf{a}_0, \tag{B.2}$$

where the symbols with carets above them (e.g., $\hat{\mathbf{g}}_i$) are unit vectors in the parameter space. They are assumed to be orthogonal (or independent), that is

$$\hat{\mathbf{p}}_n \cdot \hat{\mathbf{p}}_m = \delta_{mn} \quad \text{or} \quad \hat{\mathbf{g}}_i \cdot \hat{\mathbf{g}}_k = \delta_{ik}, \quad \hat{\mathbf{s}}_j \cdot \hat{\mathbf{s}}_r = \delta_{jr},$$
$$\hat{\mathbf{m}} \cdot \hat{\mathbf{a}}_0 = \hat{\mathbf{a}}_0 \cdot \hat{\mathbf{g}}_i = \hat{\mathbf{a}}_0 \cdot \hat{\mathbf{s}}_j = \hat{\mathbf{g}}_i \cdot \hat{\mathbf{s}}_j = 0; \tag{B.3}$$

where, for example, δ_{ik} is the Kronecker delta which is defined as $\delta_{ik} = 0$ if $i \neq k$, $\delta_{ik} = 1$ for $i = k$. Therefore,

$$a_0 + mX_{ij} + g_i + s_j = \mathbf{p} \cdot (\hat{\mathbf{a}}_0 + \hat{\mathbf{m}}X_{ij} + \hat{\mathbf{g}}_i + \hat{\mathbf{s}}_j). \tag{B.4}$$

The summed, weighted and squared error, $E^2(\mathbf{p})$, will have a minimum in the parameter space where its gradient is zero; i.e.,

$$\tfrac{1}{2}\partial_{\mathbf{p}} E^2 = \sum_i \sum_j w_{ij}(a_0 + mX_{ij} + g_i + s_j - a_{ij})(\hat{\mathbf{a}}_0 + \hat{\mathbf{m}}X_{ij} + \hat{\mathbf{g}}_i + \hat{\mathbf{s}}_j) = 0;$$

or

$$\sum_i \sum_j w_{ij}a_{ij}(\hat{\mathbf{a}}_0 + \hat{\mathbf{m}}X_{ij} + \hat{\mathbf{g}}_i + \hat{\mathbf{s}}_j) = \sum_i \sum_j w_{ij}[(\hat{\mathbf{a}}_0 + \hat{\mathbf{m}}X_{ij} + \hat{\mathbf{g}}_i + \hat{\mathbf{s}}_j) \times (\hat{\mathbf{a}}_0 + \hat{\mathbf{m}}X_{ij} + \hat{\mathbf{g}}_i + \hat{\mathbf{s}}_j)] \cdot \mathbf{p}, \tag{B.5}$$

where the term inside the brackets is a square, symmetric matrix obtained by the dyadic product of the two vectors.

$$\mathbf{A} = \begin{bmatrix}
\sum_i \sum_j w_{ij} & \sum_i \sum_j w_{ij}X_{ij} & \sum_j w_{1j} & \sum w_{2j} & \cdots & \sum w_{i_1} & \sum w_{i_2} & \cdots \\
\sum_i \sum_j w_{ij}X_{ij} & \sum\sum w_{ij}X_{ij}^2 & \sum w_{1j}X_{1j} & \sum w_{2j}X_{2j} & \cdots & \sum w_{i_1}X_{i_1} & \sum w_{i_2}X_{i_2} & \cdots \\
\sum_j w_{1j} & \sum w_{1j}X_{1j} & \sum w_{1j} & 0 & 0\,0\,0 & w_{11} & w_{12} & \cdots \\
\sum_j w_{2j} & \sum w_{2j}X_{2j} & 0 & \sum w_{2j} & 0\,0\,0 & w_{21} & w_{22} & \cdots \\
\cdot & \cdot & 0 & 0 & \cdot\,0\,0\,\cdot & \cdot & \cdot & \cdots \\
\cdot & \cdot & 0 & 0 & 0\,\cdot\,0\,\cdot & \cdot & \cdot & \cdots \\
\cdot & \cdot & 0 & 0 & 0\,0\,\cdot\,\cdot & \cdot & \cdot & \cdots \\
\sum_i \sum_j w_{i_1} & \sum w_{i_1}X_{i_1} & w_{11} & w_{21} & \cdots\ \sum w_{i_1} & 0 & 0\,0\,0 & \\
\sum\sum w_{i_2} & \sum w_{i_2}X_{i_2} & w_{12} & w_{22} & \cdots\ 0 & \sum w_{i_2} & 0\,0\,0 & \\
\cdot & \cdot & \cdot & \cdot & \cdots\ 0 & 0 & \cdot\,0\,0 & \\
\cdot & \cdot & \cdot & \cdot & \cdots\ 0 & 0 & 0\,\cdot\,0 & \\
\cdot & \cdot & \cdot & \cdot & \cdots\ 0 & 0 & 0\,0\,\cdot &
\end{bmatrix} \tag{B.6}$$

The resulting set of equations can be written in matrix form as

$$\mathbf{a} = \mathbf{A} \cdot \mathbf{p}, \tag{B.7}$$

(B.8)

where **a** is the vector

$$\mathbf{a} = \sum \hat{\mathbf{p}}_n a_n$$

$$= \sum \sum w_{ij} a_{ij} (\hat{\mathbf{a}}_0 + \hat{\mathbf{m}} X_{ij} + \hat{\mathbf{g}}_i + \hat{\mathbf{s}}_j), \tag{B.9}$$

the square-symmetric matrix **A** is defined in Equation (B.7) and the vector **p** is defined in Equation (B.2).

The parameter values (a_0, m, g_i and s_j) are just the components of the vector **p** and they are determined by inverting Equation (B.8) to give

$$\mathbf{p} = \mathbf{A}^{-1} \cdot \mathbf{a}. \tag{B.10}$$

This is the solution to the problem of determining the optimum (in a least-squares sense) parameters and it can be seen from Equation (B.10) that the accuracy of the solution depends upon the stability of the inverse of the matrix **A** and the errors in the vector **a**. These, in turn, depend upon the accuracy of the measurements of the separations, X_{ij}, and the amplitudes, a_{ij}, and the values of the weights, w_{ij}. The weights themselves are established by the accuracies of a_{ij} and X_{ij}. In the analysis of the amplitude data from the Apollo-16 ASE, it was assumed that the separations were measured with high accuracy; consequently, the weights were established only on the basis of the accuracy of the amplitude measurements.

From the form of matrix **A** (Equation (B.7)), it can be seen that it will have a stable inverse if there is high redundancy in the data; that is, the sums of the weights over the geophones (subscript i) and over the shot strengths (subscript j) as well as the double sums (over i and j) have large values. This will occur when the amplitude from each shot is measured accurately at each geophone; that is, all the $w_{ij} = 1$. Unfortunately, this is not the case in the Apollo-14 or Apollo-16 ASE's.

References

Bullen, K. E.: 1963, *An Introduction to the Theory of Seismology*, Third Edition, Cambridge University Press, New York, N.Y., Chapter 8.

Chang, G. K., Gunther, P., and James, D. B.: 1970, 'A Secondary Ejecta Explanation of a Lunar Seismogram', *Jour. Geophys. Res.* **75**, 7426.

Cooper, M. R., Kovach, R. L., and Watkins, J. S.: 1974, 'Lunar Near-Surface Structure', *Reviews of Geophysics and Space Physics* **12**, 291.

Dainty, A. M., Toksöz, M. N., Anderson, K. R., Pines, P. J., Nakamura, Y., and Latham, G.: 1974, 'Seismic Scattering and Shallow Structure of the Moon in Oceanus Procellarum', *The Moon* **9**, 11.

Gangi, A. F.: 1972, 'The Lunar Seismogram', *The Moon* **4**, 40.

Gassmann, F.: 1951, 'Elastic Waves Through a Packing of Spheres', *Geophysics* **16**, 673. See also *Geophysics* **18**, 269 (errata) (1953).

Gold, T. and Soter, S.: 1970, 'Apollo-12 Seismic Signal: Indication of a Deep Layer of Powder', *Science* **169**, 1071.

Kaufman, H.: 1953, 'Velocity Functions in Seismic Prospecting', *Geophysics* **18**, 289.

Kovach, R. L., Watkins, J. S., and Landers, T.: 1971, '7. Active Seismic Experiment', *Apollo 14 Preliminary Science Report*, NASA SP-272, pp. 163–174.
Kovach, R. L., Watkins, J. S., and Talwani, P.: 1972, '10. Active Seismic Experiment', *Apollo 16 Preliminary Science Report*, NASA SP-315, pp. 10.1–10.14.
Kovach, R. L. and Watkins, J. S.: 1973, 'The Velocity Structure of the Lunar Crust', *The Moon* 7, 63.
Latham, G., Ewing, M., Press, F., Sutton, G., Dorman, J., Nakamura, Y., Toksöz, N., Wiggins, R., Derr, J., and Duennebier, F.: 1970a, 'Apollo 11 Passive Seismic Experiment', *Proceedings of the Apollo 11 Lunar Science Conference, Geochim. Cosmochim. Acta, Suppl. 1*, 3, 2309.
Latham, G. V., Ewing, M., Press, F., Sutton, G., Dorman, J., Nakamura, Y., Toksöz, N., Wiggins, R., Derr, J., and Duennebier, F.: 1970b, 'Passive Seismic Experiment', *Science* 167, 455.
Latham, G., Ewing, M., Press, F., Sutton, G., Dorman, J., Nakamura, Y., Toksöz, N., Wiggins, R., and Kovach, R.: 1970c, '3. Passive Seismic Experiment', *Apollo 12 Preliminary Science Report*, NASA SP-235, pp. 39–53.
Latham, G. V., Ewing, M., Dorman, J., Press, F., Sutton, G., Meissner, R., Duennebier, F., Nakamura, Y., Kovach, R., and Yates, M.: 1970d, 'Seismic Data from Man-made Impacts on the Moon', *Science* 170, 620.
Lauderdale, W. and Eichelman, W.: 1974, Tech. Eds., 'Active Seismic Experiment (NASA Experiment S-033)', Section 5, *Apollo Scientific Experiments Data Handbook*, NASA TMX-58131.
Mukhamedzhanov, A. K.: 1970, 'The Nature of the Lunar Seismic Echo', translated from *Priroda*, 3, pp. 74–75 (1970) by E. R. Hope, Can. Tech. Sc., Moscow, Defence Scientific Information Service, DRB Canada, Translation *T-542R*, June.
Officer, C. B.: 1958, *Introduction to the Theory of Sound Transmission*, McGraw-Hill Book Co., Inc., New York, N.Y., pp. 49f.
Sutton, G. H. and Duennebier, F. K.: 1970, 'Elastic Properties of the Lunar Surface from Surveyor Spacecraft Data', *J. Geophys. Res.* 75, 7439.
White, J. E.: 1965, *Seismic Waves*, McGraw-Hill Book Co., Inc., New York, N.Y., p. 215.

APPENDIX II

VELOCITY DETERMINATION OF THE VERY SHALLOW LUNAR CRUST

A Thesis

by

TZUHUA EDWARD YEN

Submitted to the Graduate College of
Texas A&M University in
partial fulfillment of the requirement for the degree of

MASTER OF SCIENCE

August 1979

Major Subject: Geophysics

ABSTRACT

Velocity Determination of the Very Shallow Lunar Crust

(August 1979)

Tzuhua Edward Yen, B.S.

National Central University; Rep. of China

Chairman of Advisory Committee: Dr. A.F. Gangi

The very shallow lunar crust (for depths less than 15 m) at the Apollo 14 and 16 landing sites has been determined to be a self-compacting powder layer overlying a homogeneous layer. The velocity function of the powder layer is given by $V(z)=V_o(z/z_o)^{1/6}$, where $V_o=340\pm20$ m/sec is a reference velocity at a depth of $z_o=1$ km. The thickness of the powder layer is approximately 10 ± 1 m. The constant velocity in the homogeneous layer is approximately 250 ± 20 m/sec with an unknown thickness.

The data of the Active Seismic Experiments of Apollo 14 and 16 missions are improved by deglitching, filtering, and stacking. However, the measurements of the traveltimes and the amplitudes of the first arrivals from the stacked profiles are difficult for separations beyond 32.0 m, while the traveltime determinations of the first arrivals from the single geophone profiles are difficult for separations beyond 45.72 m.

The traveltime determinations of Apollo 16 ASE grenade launchings at Geophone 3 are also difficult because of the

low amplitudes. Also, there is a maximum of 57 msec time offset among the instants of grenade launchings. The amplitude measurements for the grenade launchings are impossible at Geophones 2 and 3. Because of the high noise levels existing in the grenade data of the Apollo 16 ASE, the measurements of both the traveltimes and amplitudes have low accuracy.

The slope, m, on the log/log traveltime graph is related to the exponent, n, of the velocity function, $V(z)=V_o(z/z_o)^n$. That is, the slope, m, is 5/6 for the one-sixth power variation (n=1/6) while m equals 1 for the constant velocity function (n=0). The measured slope lies between 0.65 and 0.82. The best-fitted reference velocity, V_o, at the Apollo 14 and 16 landing sites are 345 and 357 m/sec, respectively, by forcing the slope to be 5/6. A homogeneous layer with a constant velocity of 254 and 302 m/sec at Apollo 14 and 16 landing sites, respectively, is found underlying the surface powder layer. However, the constant velocity, 302 m/sec, at Apollo 16 landing site is questionable because of little and poor data.

An amplitude analysis (Gangi and Yen, 1979) indicates that the amplitude/separation variation is $x^{-(13-s)/12}$, where $s > 1$, for the powder layer model and x^{-2} for the homogeneous and layered model. These variations are based on the assumptions that: 1) there is no energy loss either by conversion or by attenuation, 2) there are no scatterers in the lunar regolith, 3) all the thumper shots are of equal

strength, and 4) all the geophones are equally oriented and coupled. The exponent of the amplitude variation from the measured data, for separations up to 32.0 m, lies between -1.5 and -2.5. These values seem to favor the homogeneous and layered model; however, the predicted values of the exponents for these two models should be treated as upper bounds for the measured data. We also find that there are 30 to 40% differences in the relative geophone sensitivities and 15 to 20% differences in the thumper-shot strengths. These variations seem high but are not too unreasonable. The coefficient of attenuation which dominates the amplitude variation at larger separations is 0.047 /m.

A velocity-spectrum analysis indicates that the signal-to-noise ratio for the Apollo 14 and 16 ASEs varies from 0.5 to 1.5. Velocity spectra of the direct and reflected waves for the Apollo ASE data suggest that the reference velocity of the powder layer, V_o, is approximately 320 m/sec. From the velocity spectra of the reflected and refracted waves, the thickness of the surface powder layer is evaluated to be approximately 9 m and the constant velocity in the homogeneous medium is 230 m/sec. These values of the parameters are consistent with those vlaues found from the traveltime investigations. All of them are within 10%.

To my parents, in appreciation for
their love and encouragement.

ACKNOWLEDGEMENTS

I would like to thank Dr. Anthony F. Gangi for suggesting the problem, for providing me with the opportunity to perform this research, and for reading and commenting on the first draft of this thesis. I am also indebted to Dr. D.A. Fahlquist and Dr. S.K. Jones.

My appreciation goes to Dr. R.L. Kovach and Dr. J. Minear for their help and suggestions concerning this thesis.

I wish also to thank the National Space Science Data Center of Goddard Space Flight Center for providing the data.

This research was supported, in part, by NASA Grant NSG-7417, "Velocity Model of the Shallow Lunar Crust.

TABLE OF CONTENTS

LIST OF FIGURES

FIGURE PAGE

FIGURE

LIST OF TABLES

TABLE

CHAPTER I. INTRODUCTION

Before the first astronauts landed on the surface of the moon, NASA had tried sending seismometers to it, but without success. The first seismometer for the Passive Seismic Experiment (PSE) was installed on the moon by astronauts Aldrin and Armstrong of the Apollo 11 mission on July 20th, 1969. The seismic data sent back showed some unusual characteristics which are not found on Earth's seismic records (Figure 1; from Toksoz et al, 1974). These unusual characteristics (summarized by Gangi, 1972) are:

1) the long duration of the signal.
2) the variable character of the signals (variable durations, variable onset and shape of the envelope).
3) the lack of correlation between the vertical and horizontal displacement components.
4) the variation of the spectrum of a signal over its duration.
5) the variation of the near-surface, P-wave velocity (measurements from 45 m/sec to 104 m/sec).

Motivated by those characteristics, various authors

The citations on the following pages follow the style of Geophysics.

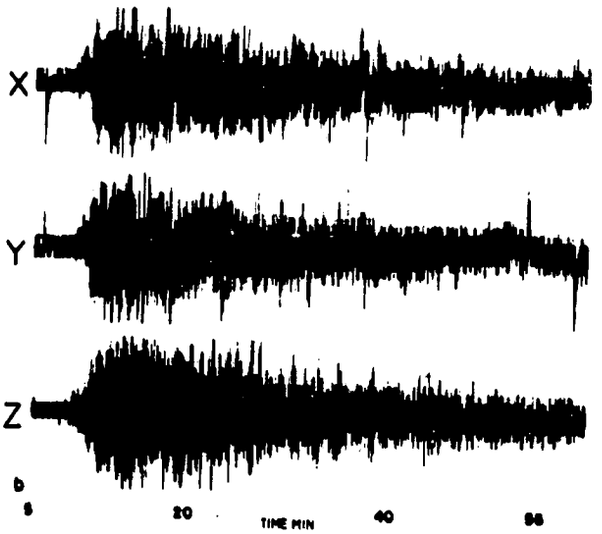

Figure 1. The A1 moonquake. May 23, 1970, as received by the ALSEP 12 station. Here X is the N-S component (S positive), Y is E-W (W positive), and Z is vertical (up positive). Seismogram starts at 1305 UT. Distance between traces is 22 digital units. (From Toksoz et al, 1974)

(Gold and Soter, 1970; Gangi, 1972) suggested that the topmost layer of the lunar crust consists of compacted powder.

Gold and Soter (1970) investigated seismic-wave propagation for an assumed linear velocity increase with depth for a self-compacting powder layer; i.e., $V=V_o(1+az)$ with V_o=395 m/sec, a=1.97 /km, and z in km. At full compaction, at whatever depth this may occur, they assumed the P-wave velocity may be as high as 6 km/sec. In such a situation, there would be a propagation channel in which the velocity gradient is steep between the top and the depth of full compaction.

Gangi (1972) proposed a sixth-power velocity model for the lunar surface layer based on Hertz's theory of the deformation of spheres in contact and Gassmann's (1951) determination of the P-wave velocity for dry, hexagonal-closed-packed, self-compacting, uniform spheres. This velocity variation has a rapid increase of velocity with depth near the surface. Rays in such a velocity variation come back to the surface at (or near to) 0^o from the vertical because the velocity at the surface is zero. This would explain the lack of correlation between the vertical and horizontal components.

Kovach et al (1971, 1972, 1974) took a more conventional approach in interpreting the data from the Apollo 14 and 16 Active Seismic Experiment (ASE) shown in

Figure 2 (from Kovach et al, 1971). They assumed the lunar crust was horizontally layered with each layer having a constant velocity. The velocity of each layer is determined by assuming there are refraction arrivals which travel, for most of their paths, along the interfaces between the layers.

Latham et al (1970) explained the long duration, the variable character of the signals and the lack of correlation between vertical and horizontal components of motion by postulating a high quality factor ($Q \approx 3000$) for a highly-fractured or brecciated crustal layer. They proposed that the long duration was due to multiple scattering of the waves from the fractures and showed that this would give rise to signals similar to those shown in Figure 1 if the intrinsic Q of the medium was as high as 3000.

A comparison of the traveltime curves of the first arrival using the models of Gold and Soter (linear velocity variation), Gangi (power-law velocity variation) and Kovach et al (horizontally-layered crust) is shown in Figure 3 (from Cooper et al, 1974). All three models can be made to fit the traveltime reasonably well. Also included in Figure 3 is the $z^{\frac{1}{4}}$ velocity variation suggested by Carrier (1971) to Gangi and which is described in detail in Gangi (1972).

If the wave velocity increases in a stepwise fashion with depth, the traveltime curve for the first arrival will be composed of linear segments. If the velocity function is continuous, the traveltime curve will be a smooth continuous

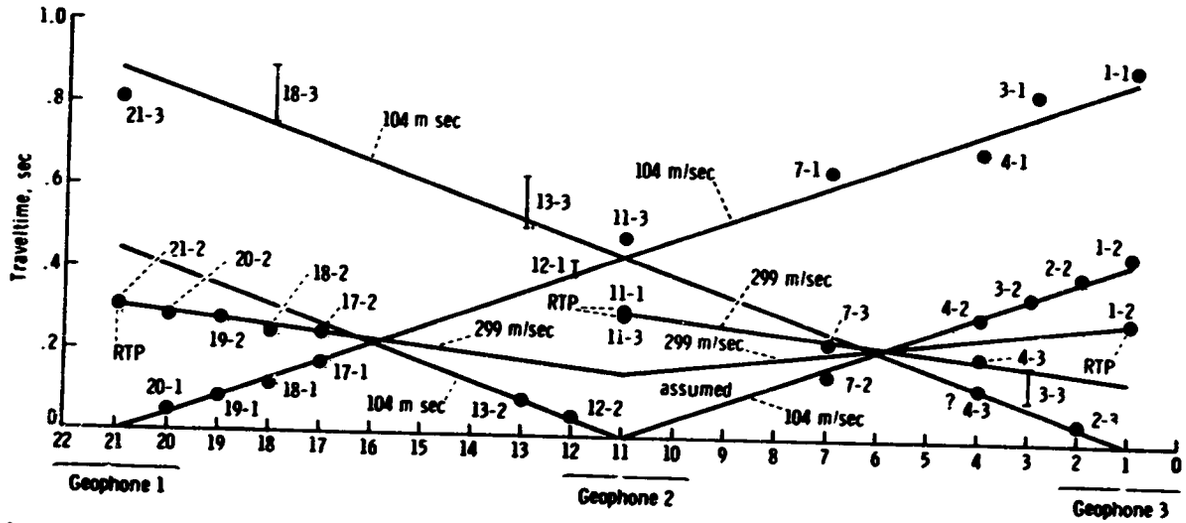

Figure 2. Seismic arrivals from the thumper firings plotted on a traveltime/distance graph for Apollo 14 ASE. The data points are shown as black circles; the first number refers to the thumper firing, the second number to the geophone on which the data were recorded. Reverse tie points are indicated as RTP; distance between thumper shot location is 4.6 m. (From Kovach et al, 1971)

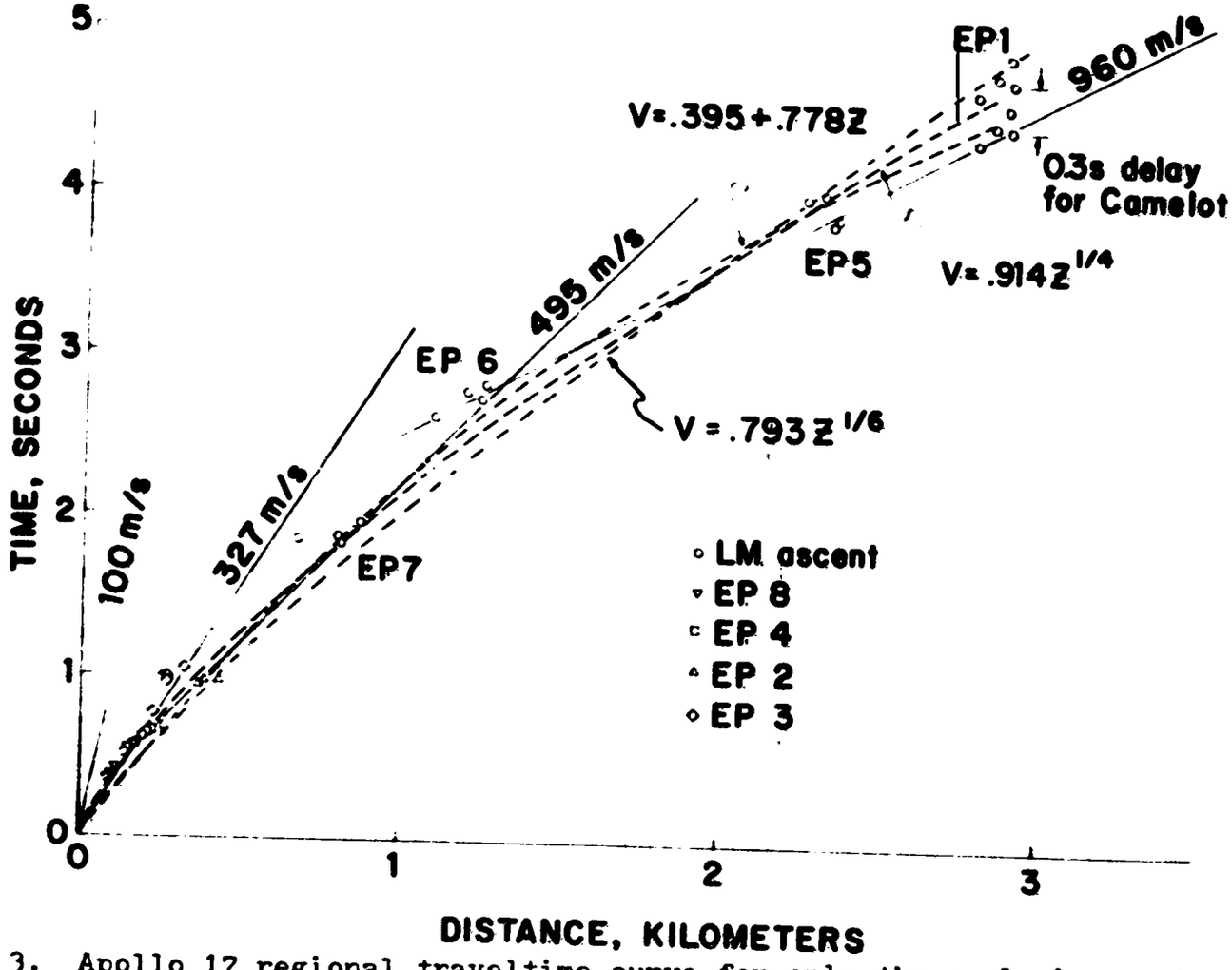

Figure 3. Apollo 17 regional traveltime curve for only the explosive packages. Dot-dash and dashed curves are best-fitting traveltime curves derived for linear and power-law velocity/depth relationships, respectively. The double dot-dash curve refers to a one-sixth power velocity/depth relationship. (From Cooper et al, 1974)

curve. The accuracy and sparseness of the data shown in Figure 3 do not preclude any of the models. The question of which is the correct or best-fitting velocity function will have to be answered by more accurate determination of the traveltime data and by determining which of the models explain most of the unusual characteristics of the lunar seismogram.

Kovach et al (1971, 1972, 1974) do not address the question of the long duration of the lunar seismogram which lasts for over 50 minutes. Both Gold and Soter (1970) and Gangi (1972) suggest that "random walking" of the seismic waves, caused by undulations of the lunar surface, would explain this phenomenon. Latham et al (1970) suggest the long duration is due to the multiple scattering of the waves from the fractures in the shallow lunar crust.

CHAPTER II. PREVIOUS GEOPHYSICAL INVESTIGATIONS

For Apollo 12 Passive Seismic Experiment (PSE), Latham et al (1970) constructed three lunar seismic-velocity models (Figure 4; from Latham et al, 1970) based on the measurements of the physical properties of lunar samples to estimate the velocity-depth variation.

Model I assumed the same variation in elastic parameters with pressure (or depth) as measured in the laboratory on a breccia sample. Model III was based on the laboratory measured properties of a homogeneous, igneous, lunar rock. Model II was an attempt to combine the properties of the igneous-rock and breccia samples to produce a model that would have the elastic parameters of a highly fractured igneous material. The traveltimes for the first and second arrivals, which were assumed to be the direct P and S waves, respectively, fall in between those predicted for the homogeneous, igneous model III and the fractured igneous model II. Thus, the correct model for the upper 20 km of lunar material in the vicinity of the Apollo 12 landing site must have a velocity-depth function that falls between models II and III but is closer to the model of homogeneous igneous rock (model III).

From the thumper firings of Apollo 14 ASE, Kovach et al (1971) obtained the traveltime curves shown in Figure 2. They found velocities of 104 m/sec and 299 m/sec for the

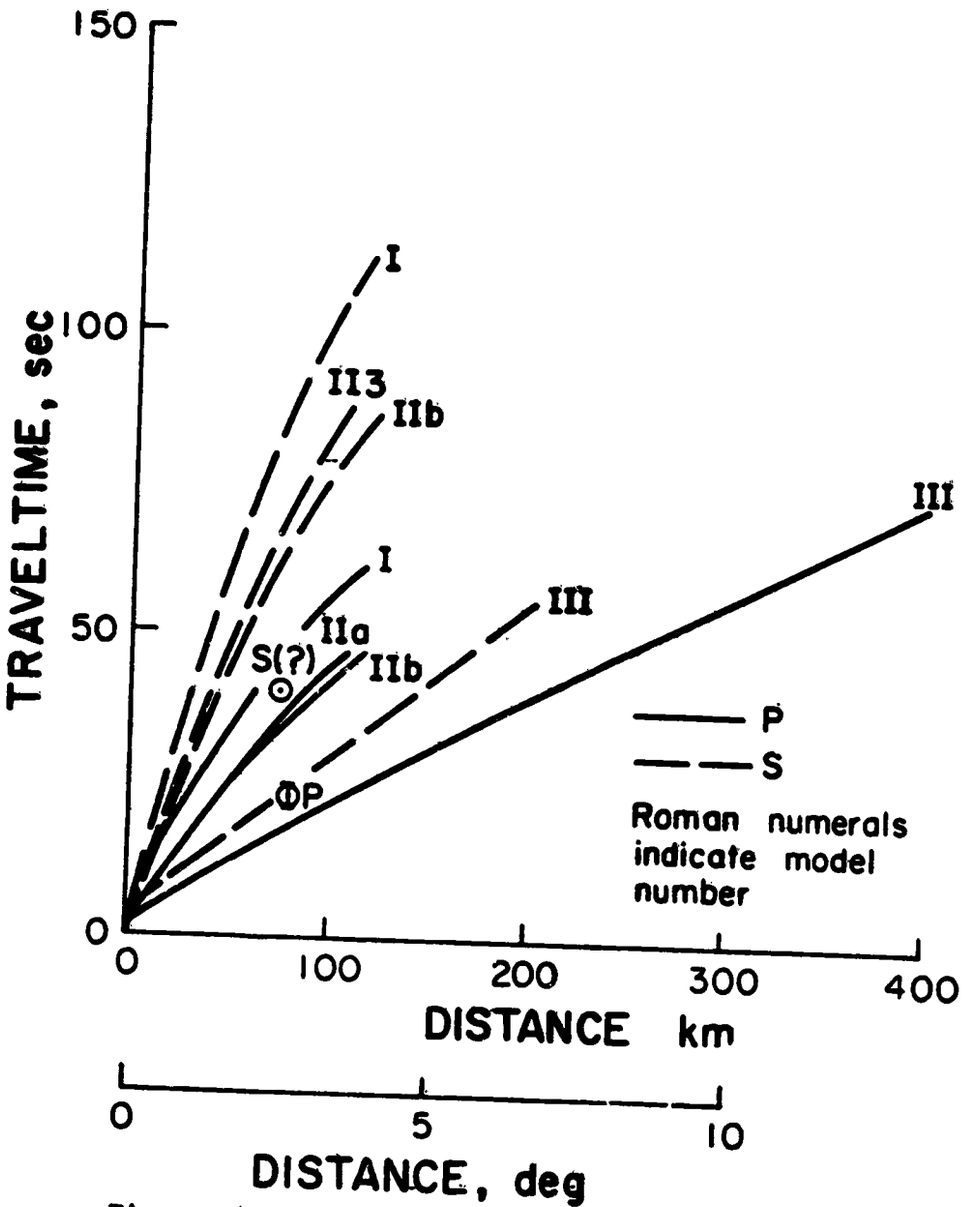

Figure 4. First and second arrivals from the LM impact plotted on the traveltime distance curves based on the Apollo 11 lunar sample data.
(From Latham et al, 1970)

direct and refracted waves, respectively (See Figure 2).

Kovach et al (1972, 1974) assumed that the lunar crust is homogeneous and horizontally layered with constant velocity and thickness in each layer. Within each layer, the velocity may increase slightly with depth without violating the assumptions of the interpretation, but the first arrivals observed on the surface must have travelled either as direct waves or as head waves; that is, waves critically refracted along the top of each layer. Thus, each layer generates a straight-line segment in the traveltime curve. They obtained the velocity structures shown in Figures 5 and 6 (from Kovach et al, 1972 and 1974) for the Apollo 16 and 17 landing sites, respectively.

A deep layer of dust on the moon may provide a very good seismic-wave transmission channel. In order to investigate the seismic properties of such a medium, Gold and Soter (1970) performed a computer simulation using ray theory for a linear velocity/depth variation, $V(z)=V_o(1+az)$. If the surface of the moon were perfectly flat, a ray, leaving the origin initially at an angle θ_o, would be reflected back at the angle θ_o at each subsequent step and, after n cycles, would have moved a distance nx_o in a time nt_o. However, the lunar surface in the vicinity of the seismic experiment is not flat but is gently undulating as is characteristic of mare regions. If the undulations are random, the ray, at the i-th reflection, will be reflected from the surface at an angle

$$\theta_i = \theta_{i-1}+2\alpha_i$$

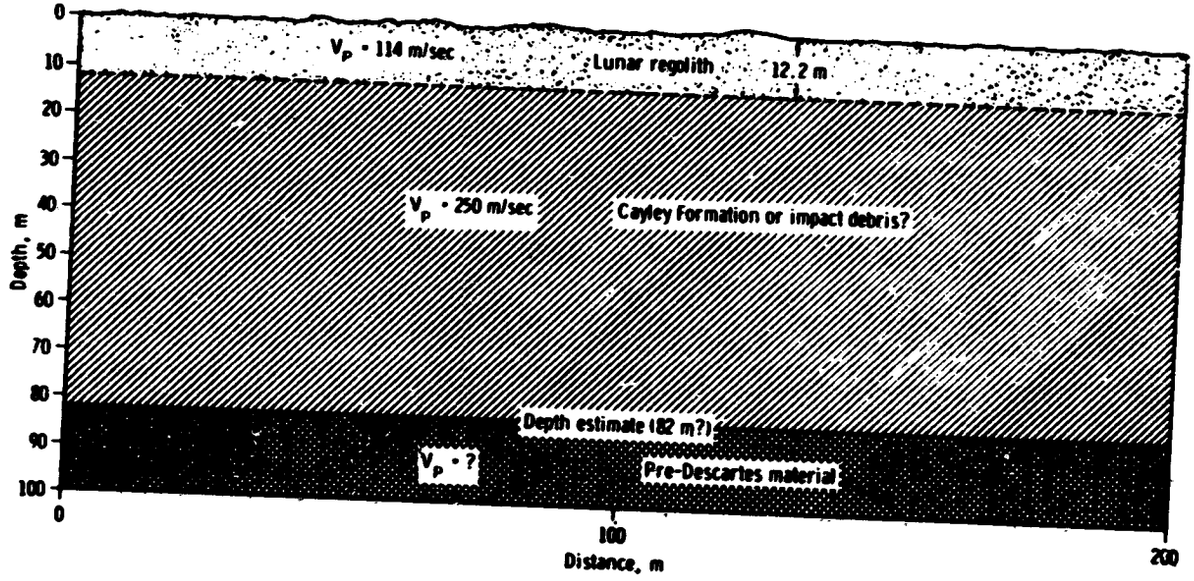

Figure 5. Seismic cross section at the Apollo 16 landing site. (From Kovach et al, 1972)

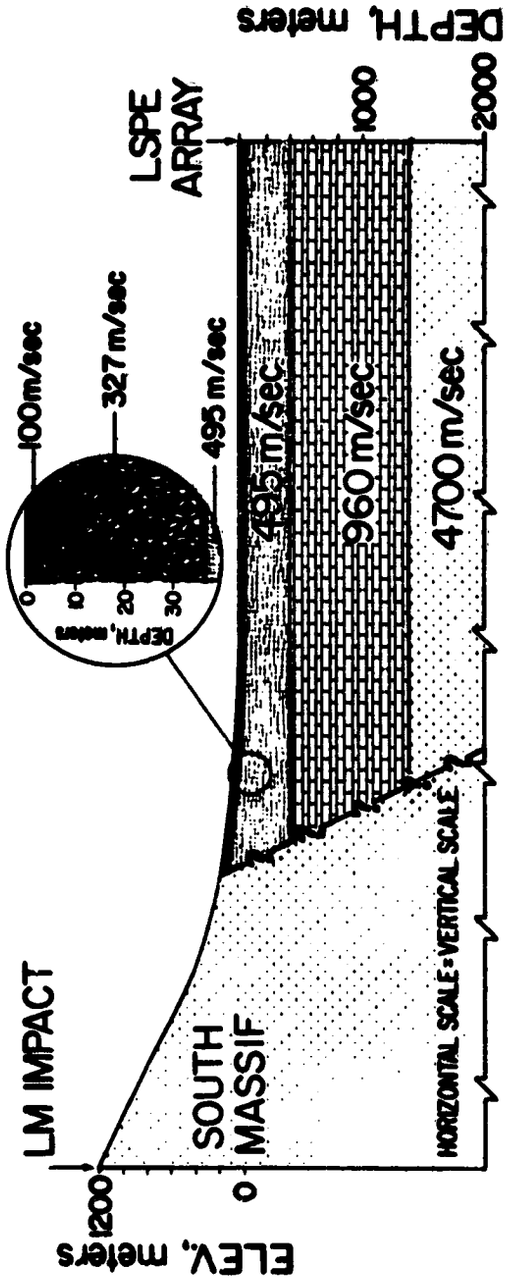

Figure 6. Seismic cross section at Apollo 17 landing site. (From Kovach et al, 1974)

where α_i is the angle of the random slope encountered (positive if tilted up away from the origin). After n+1 reflections, the ray would have travelled from the origin a net distance

$$R_n = \frac{2}{a} \left| \sum_{i=0}^{n} \tan \theta_i \right|$$

Since the α_i have random signs and magnitudes (up to some cutoff α_{max}), tan θ_i would occasionally change sign; that is, the ray would be reversed in direction. Thus, a ray encountering random slopes would have travelled a considerably smaller net distance from the origin in a given time than would be the case for a perfectly flat surface. The introduction of random walking would explain the long-duration characteristic of the lunar seismograms.

Dainty et al (1974) interpreted the long duration of the seismic record as a result of scattering in a surface layer overlying a non-scattering elastic medium. Seismic-model experiments (Dainty et al, 1974) were used to demonstrate this interpretation. Figure 7 (from Dainty et al, 1974) diagrammatically illustrates the seismic-modelling apparatus used to produce the seismograms shown in Figure 8 (from Dainty et al, 1974). Two experiments (Dainty et al, 1974) are illustrated: 1) propagation across a plate with grooves cut half-way through, and 2) propagation along the edge of a plate with holes drilled within a skin depth (for Rayleigh waves) of the edge. The first experiment produces a seismogram of the nature of that shown in Figure 1. They

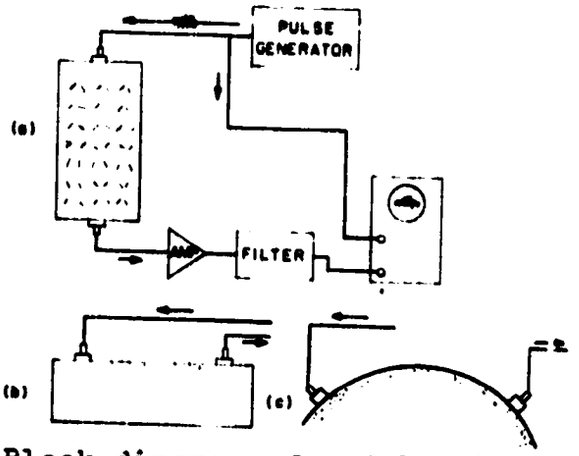

Figure 7. Block diagram of model seismic experiments on scattering. (a) Retangular plate (body wave) experiment. (b) Surface wave scattering experiment. (c) Lunar seismogram simulation experiment. (From Dainty et al, 1974)

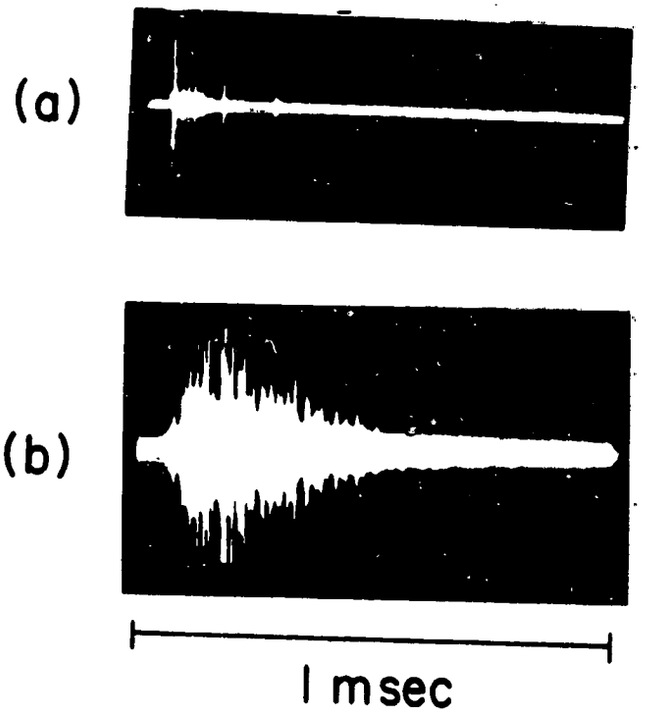

Figure 8. Production of the scattered envelope. (a) Retangular plate 36 cm wide, 24 cm across as in Figure 7(a) without scatters. (b) Same plate with 0.6-cm-diameter holes, 0.56 holes/cm^2. The P-wave velocity is 5.6 mm/μs; a Poisson's ratio of 0.25 is assumed. (From Dainty et al, 1974)

found that most surface-wave energy scattered into body waves and the surface wave disappeared.

Gangi (1972) proposed a 1/6-power velocity-depth variation (i.e., $V=az^{1/6}$) for the lunar surface layer. This variation is based on Hertz's theory of the deformation of spheres in contact and Gassmann's (1951) determination of the P-wave velocity for dry, hexagonal-closed-packed, self-compacting, uniform spheres. Gassmann found

$$V_{hp} = B_o(gz)^{1/6}$$

where B_o is a constant.

By using the values obtained from lunar samples by Kanamori et al (1970, 1971), Gangi (1972) found

$$V_{hp} \approx 600(z/z_o)^{1/6} \text{ m/sec}$$

where z_o=1 km. This depth dependence of the vertical P-wave velocity (Figure 9; from Gangi, 1972) gives rise to a very rapidly varying velocity with depth. This velocity dependence is consistent with the measured velocity dependence on pressure for lunar samples (Figure 10; from Gangi, 1972).

The ray parameter, p, which is given by Snell's law, $p=\sin\theta(z)/V(z)$, is a constant along any ray in a horizontally homogeneous but vertically inhomogeneous elastic medium. Since, for the power-law velocity model, the velocity at the surface (z=0) is zero, a finite ray-parameter value requires all rays to be normally incident to the surface. This would explain the lack of correlation of the vertical and horizontal displacement components.

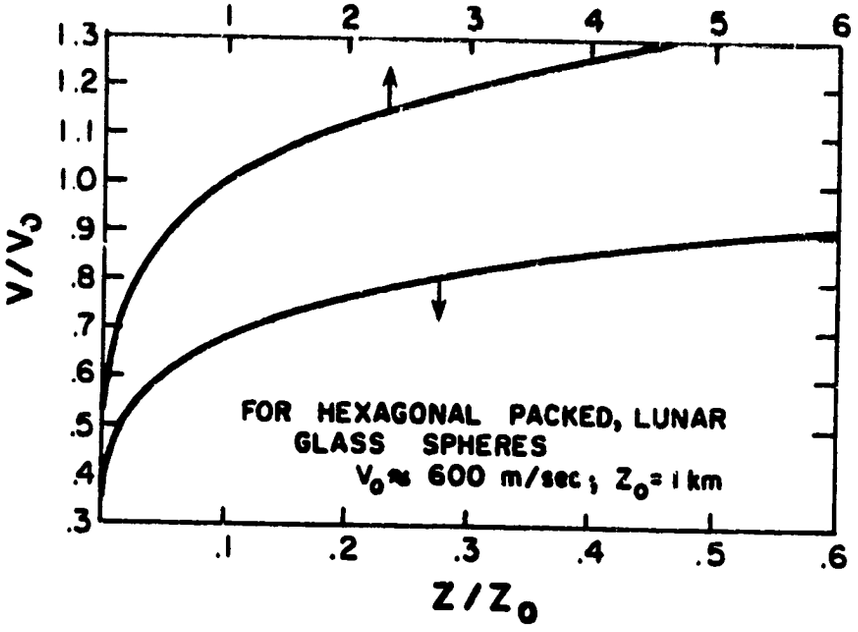

Figure 9. Velocity-depth variation for self-compacting dry sphere (From Gangi, 1972)

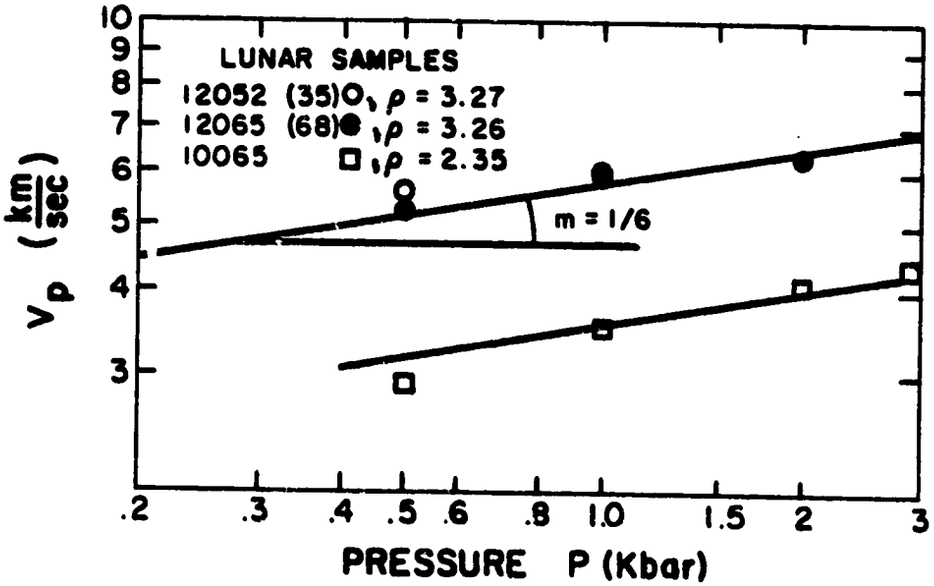

Figure 10. P-wave velocity vs. pressure (Lunar samples 12052(35), 12065(68) and 10065). Refs: Kanamori et al (1971) and Kanamori et al (1970). (From Gangi, 1972)

In addition, rays emanating from a surface source would all be directed vertically into the lunar interior at the surface.

Carrier (1971) suggested to Gangi that the velocity may increase as the fourth-root of depth near the surface; i.e., $V=V_o(z/z_o)^{\frac{1}{4}}$. Gangi (1972) and Cooper (1974) found that the traveltime curves with V_o equals 0.748 km/sec and 0.914 km/sec, respectively, and z_o=1 km will fit the results from Kovach's model very well. But the values of V_o were so chosen to make a good fit. Because the velocity at the surface is zero, this model would also require all rays to be normally incident to the surface.

CHAPTER III. FIELD PROCEDURES

The Active Seismic Experiments (ASE) are part of the Apollo Lunar Surface Experiment Package (ALSEP) of the Apollo 14 and 16 missions. The purpose of the experiments (Lauderdale et al, 1976a) is to study the internal structure and characteristics of the moon to a depth of less than one hundred meters. The purpose of the Apollo 17 Lunar Seismic Profiling Experiment (LSPE) (Lauderdale et al, 1976b) is to determine these characteristics to a depth of about one kilometer.

Locations and Site Descriptions:

On Feburary 5th, 1971, the Apollo 14 Lunar Module (LM) landed at 3.65° S latitude and 17.48° W longitude (Figure 11 and Table 1) (Lauderdale et al, 1976c). At about 1100 m east of the landing site is the Cone Crater which is located on a ridge of Fra Mauro Formation (Lauderdale et al, 1976c). Cone Crater is a sharp-rimmed crater. The Fra Mauro Formation is an extensive blanketlike deposit lying on a broad band around the basin and is interpreted as ejected from the impact. Detailed studies (Lauderdale et al, 1976c) by the geologists indicate that the Fra Mauro Formation is mainly composed of moderately coherent breccias. The main characteristic features of the Fra Mauro

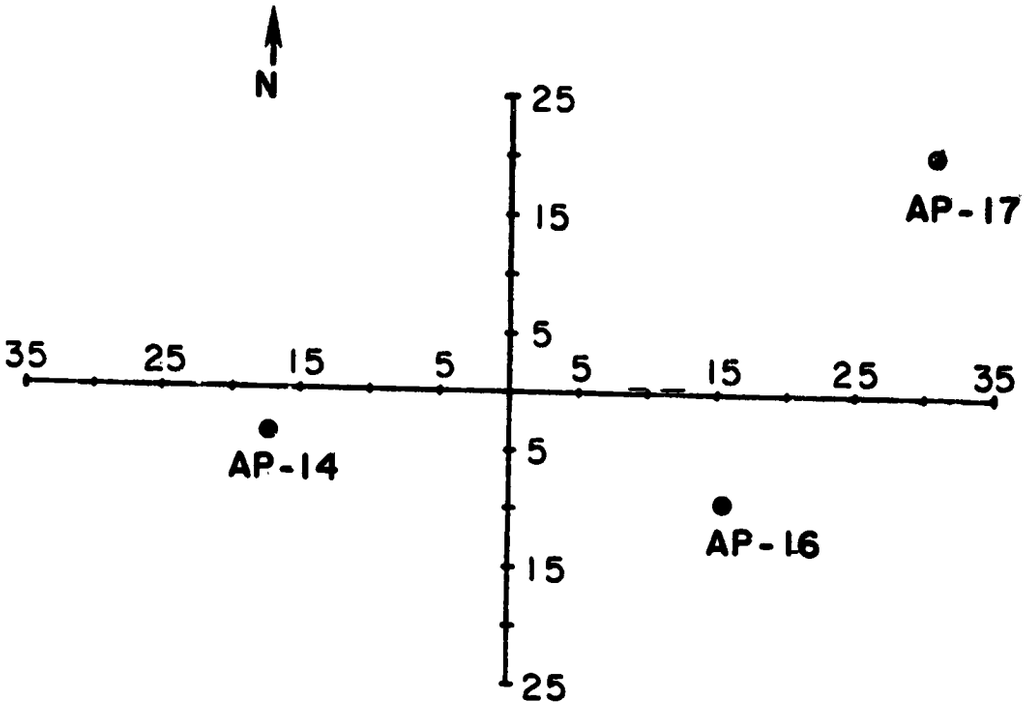

Figure 11. Map of the locations of Apollo 14, 16, and 17 landing sites.

Table 1. Locations of the landing sites and the relative distances to each other.

Apollo	Location	Distance, km, to Apollo-		
		14	16	17
14	3.65 S; 17.48 W	-	1007	1607
16	8.97 S; 15.51 E	-	-	994
17	20.17 N; 30.77 E	-	-	-

Formation are ridges which are mostly 1 to 4 km wide and a few to several tens of meters high in the vicinity of the landing site. They also suggested that the ridges were formed by flowage of material along the ground during the excavation of the basin by meteorites.

On April 21st, 1972, the Apollo 16 LM landed at 8.97° S latitude and 15.51° E longitude (Figure 11 and Table 1) (Lauderdale et al, 1976c) which is at about 1007 km southeast of Apollo 14 landing site. The LM landing site is at the western edge of the Descartes Highlands which is the lunar central highlands encompassed by highland plains and adjacent mountainous areas of hilly and furrowed terrain (Lauderdale et al, 1976c). This area, which is underlain by impact-generated breccias, may represent a remnant of an ancient lunar surface sculptured by impact of material. It may also be attributed to igneous and volcanic activity from within the moon.

On December 12th, 1972, the Apollo 17 LM landed at 20.17° N latitude and 30.77° E longitude which is at about 1607 km and 994 km to the northeast of Apollo 14 and 16 landing sites, respectively (Figure 11 and Table 1) (Lauderdale et al, 1976c). The LM landing site is on the floor of a deep valley, the Taurus-Littrow Valley, which is at the eastern rim of and is radial to the Serenitatis basin (Lauderdale et al, 1976c). The Taurus-Littrow Valley is interpreted as a deep graben formed by the Serenitatis

impact. Ejecta around many craters on the valley floor consists of basalt. It shows that the graben is partly filled by lava flow underlying a relatively thick layer of unconsolidated material.

Apparatus:

The Lunar-Surface-Experiment Package (ALSEP) of both Apollo 14 and 16 consisted of three geophones deployed in a linear array, a thumper, a mortar package assembly (MPA) which contained four grenades, and the ALSEP central station (Lauderdale et al, 1976a). The Apollo 14 and 16 Active Seismic Experiment (ASE) data were obtained from an astronaut-activated thumper, four mortar-launched grenades, and four grenade launchings. The Apollo 17 ALSEP consisted of four geophones deployed in a T-array, eight explosive packages (EP), and the ALSEP central station (Lauderdale et al, 1976b). The Apollo 17 Lunar Seismic Profiling Experiment (LSPE) data were generated by eight EP's weighing from 57 grams to 2722 grams (Cooper and Kovach, 1975).

Thumper shots. The astronaut-activated thumper was a short staff (Figure 12; from Kovach et al, 1972) which was used to detonate small explosive charges. The thumper was so mounted that it was perpendicular to the base plate at the lower end of the staff. An arm-switch and an initiator-selector switch were located at the upper end of

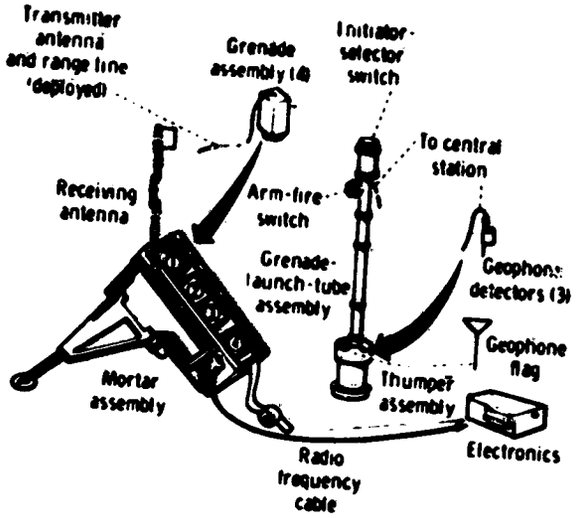

Figure 12. Drawing of the ASE. (From Kovach et al, 1972)

the staff. A pressure switch in the base plate detected the the instant of shot initiation. A cable connected the thumper to the central station to transmit the firing time of the shot.

There were twenty-one thumper shots planned for the Apollo 14 ASE and nineteen thumper shots planned for the Apollo 16 ASE (Lauderdale et al, 1976a). But thumper shots 5, 6, 8, 9, 10, 14, 15, and 16 of Apollo 14 ASE misfired. The amount of explosive used for the thumper shots are not known. The first thumper shots for both Apollo 14 and 16 ASE's were fired at Geophone 3. The Thumper/Geophone-3 distance was then increased in increments of 4.57 m toward Geophone 1 for the rest of the thumper shots (Table 2; from Lauderdale et al, 1976a); that is, thumper shots 11 for both the Apollo 14 and 16 ASE's were fired at Geophone 2, and

Table 2. The ASE geophone/thumper distances. (After Lauderdale et al, 1976a)

Distance, m, to --			Shot No.	
Geophone 1	Geophone 2	Geophone 3	AP-14	AP-16
91.44	45.72	0.00	1	1
86.72	41.14	4.57	2	2
82.30	36.58	9.14	3	3
77.72	32.00	13.71	4	4
73.15	27.43	18.29	5	5
68.58	22.86	22.86	6	6
64.00	18.29	27.43	7	7
59.44	13.71	32.00	8	8
54.86	9.14	36.58	9	9
50.29	4.57	41.14	10	10
45.72	0.00	45.72	11	11
41.14	4.57	50.29	12	-
36.58	9.14	54.86	13	12
32.00	13.71	59.44	14	13
27.43	18.29	64.05	15	14
22.86	22.86	68.58	16	15
18.29	27.43	73.15	17	16
13.71	32.00	77.72	18	17
9.14	36.58	82.30	19	18
4.57	41.14	86.87	20	-
0.00	45.72	91.44	21	19

Note: Shots 5, 6, 8, 9, 10, 14, 15, and 16 of Apollo 14 ASE misfired.

thumper shots 21 and 19 for Apollo 14 and 16 ASE's, respectively, were fired at Geophone 1. However, two thumper shots were omitted between Geophones 1 and 2 for the Apollo 16 ASE; namely, those at a distance of 4.57 m from these two geophones.

The mortar-package assembly (MPA). The MPA consisted of a mortar box, a grenade-launch-tube assembly, and connecting cable (Figure 12; from Kovach et al, 1972). The launch-tube assembly, which contained four grenades, was mounted in the mortar box. The mortar box was deployed at approximately 45^{o} to the surface so that the grenades would be sent to their maximum distances, ranging from 150 m for Grenade 4 to 1500 m for Grenade 1. The four grenades were identical except for the amount of launching explosive, which weighed from 10 grams to 42 grams, and the high-explosive charges, which weighed from 45 grams to 454 grams (Table 3; from Lauderdale et al, 1976a). The MPA was located about 14 m north-north-east of Geophone 1 (Figure 13; from Kovach and Watkins, 1973). The grenade firing direction was parallel to the geophone array and toward Geophone 3. The geophone/source distances (Table 3; from Lauderdale et al, 1976a) ranged from 61.87 m to 1017.42 m.

The Apollo 14 ASE grenades were not fired because a study of the photographs and the astronaut's descriptions of the position of the MPA suggested that the back-blast might effect other experiments (Lauderdale et al, 1976a). The decision was that the grenades would not be fired until

Table 3. Grenade parameters of the Apollo 16 ASE.
(After Lauderdale et al, 1976a)

	Distance, m, to			Firing Range, m	Launching Charge, g	Explosive Charge, g
	GP 1	GP 2	GP 3			
Grenade 1	-	-	-	1500	42	454
Grenade 2	1017.42	971.70	925.98	900	27	272
Grenade 3	444.70	398.98	353.26	300	15	136
Grenade 4	154.23	107.29	61.87	150	10	45
Launch*	14.00	50.00	95.00	-	-	-

* Obtained from Kovach and Watkins, 1972

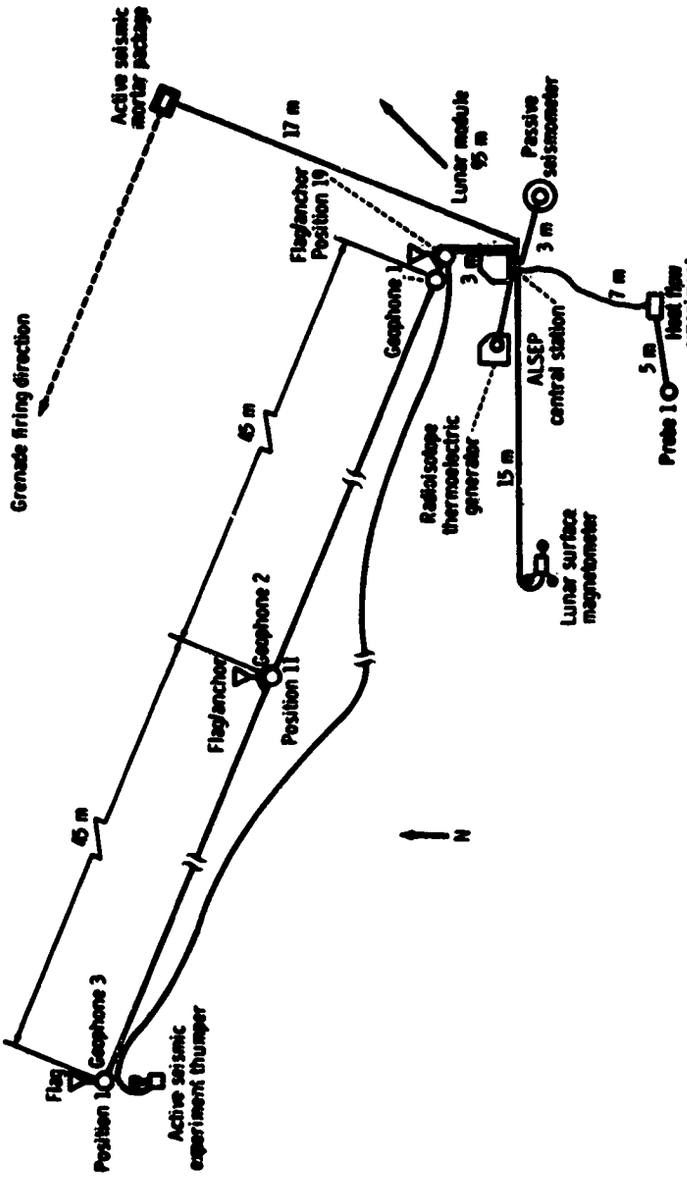

Figure 13. Deployment configuration for Apollo 16 ALSEP. (From Kovach and Watkins, 1973)

all other experiments fail. Three of four grenades of Apollo 16 ASE were launched in a sequence of 2-4-3. Grenade 1 was not launched because the angle sensor went off scale.

Geophones. The geophones of both ASE's and the LSPE were miniature seismometers of the moving-coil, magnet type. The coil was the inertial mass suspended by springs in the magnetic field. Above the natural resonant frequency of the geophone (at 7.5 Hz), the output was proportional to the ground motion. The three geophones of Apollo 14 and 16 ASE's were deployed in a linear array at approximately 3 m, 49 m, and 94 m from the ALSEP central stations and were connected to it by cables (Figure 13; from Kovach and Watkins, 1973). The four geophones of the Apollo 17 LSPE were deployed in a T-array at approximately 150 m west of the LM and were also connected to the ALSEP central station by cables (Figure 14; from Cooper et al, 1974).

The ASE's and LSPE characteristics are given in Tables 4 and 5 (from Lauderdale et al, 1976a,b), respectively. The output voltages from the amplifiers for a 5 nm zero-to-peak signal at 10 Hz are given in Table 6. Note that there is a 0.02 V (or 12%) difference between Geophone 2 (GP 2) of Apollo 14 ASE and Geophone 3 of Apollo 16 ASE. These differences in amplitude sensitivities will cause moderate errors when we measure the amplitudes. It is necessary to correct the output voltages from the

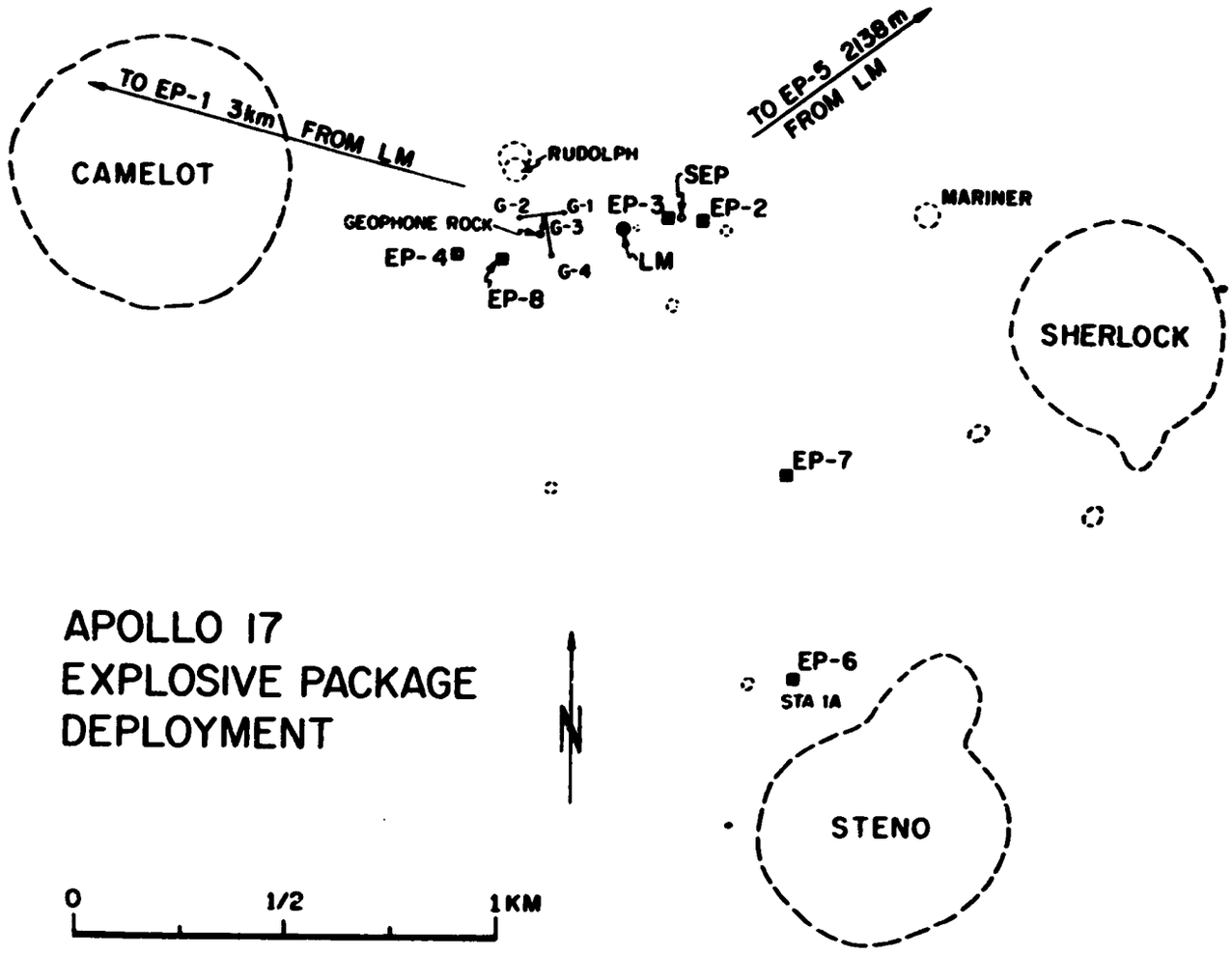

Figure 14. Map of Apollo 17 landing site showing position of geophone array (G-1 to G-4) and locations of explosive charges (EP 4 etc.) deployed during traverses. Location of lunar module is shown as LM. (From Cooper et al, 1974)

Table 4. The Apollo 14 and 16 ASE characteristics.
(from Lauderdale et al, 1976a)

Component Characteristics	Geophone Number					
	AP-14			AP-16		
	1	2	3	1	2	3
Geophones:						
Generator constant, V/m/sec	250.4	243.3	241.9	255	255	257
Frequency, Hz	7.32	7.22	7.58	7.42	7.44	7.39
Resistance, ohm	6065	6157	6182	6090	6212	6204
Amplifiers:						
Noise level, mV rms at input	0.300	0.325	0.272	-	-	-
mV rms at input	-	-	-	.266	.100	.133
Dynamic range, rms signal to rms noise in dB	86.8	86.5	87.5	84.4	92.4	90.0
Gain (at 10 Hz) and V_{in} = 5.0 mV rms	666.7	666.7	675.7	-	-	-
V_{in} = 2.75 mV peak to peak	-	-	-	698	684	709
Log compressor (compression accuracy for temperature range 288 to 323°k):						
Positive signal error, percent	3.79	4.71	2.00	4.04	3.63	4.83
Negative signal error, percent	2.07	1.32	3.33	2.46	1.87	1.88
System:						
Signal-to-noise ratio (rms signal to rms noise in dB for a 10-nm peak-to-peak signal at 10 Hz)	33.6	33.1	32.9	38.9	37.9	45.0

Table 5. Apollo 17 LSPE characteristics.
(After Lauderdale et al, 1976b)

Component Characteristics	Geophone Number			
	1	2	3	4
Geophones:				
Generator constant, V/m/sec at 40 Hz	235.6	239.2	237.1	235.3
Frequency, Hz	7.38	7.31	7.40	7.35
Resistance, ohm	5970	5953	6080	6153
Amplifiers:				
Noise level, mV rms at input	0.75	0.75	0.83	0.83
Dynamic range, rms signal to rms noise in dB at 10 Hz	73.4	76.2	75.6	75.8
System:				
Signal-to-noise ratio (rms signal to rms noise in dB for a 6-nm rms signal at 10 Hz)	24.4	26.9	26.8	26.8
Amplitude sensitivity (measured at input to log compressor), V/μm of peak-to-peak ground displacement at 10 Hz	7.33	7.02	7.12	7.13

Table 6. Output voltages from the ASE amplifiers for a 5 nm zero-to-peak signal at 10 Hz.

	Apollo 14			Apollo 16		
	GP 1	GP 2	GP 3	GP 1	GP 2	GP 3
Voltage, V Normalized, %	.167 100.	.162 97.	.163 97.6	.178 106.6	.174 104.2	.182 109.

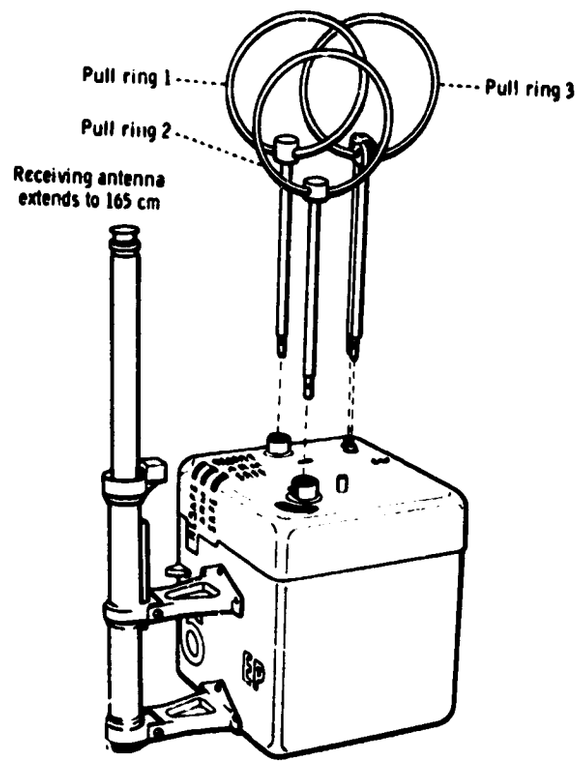

Notes: (1) Pull ring 1 - pulls one pin to start SAFE/ARM slide timer

(2) Pull ring 2 - swing up ring; rotate 90° counterclockwise; pull pin to release SAFE/ARM plate

(3) Pull ring 3 - pulls two pins to free firing pin and start thermal battery timer

Figure 15. Arming sequence for an LSPE explosive package. (From Lauderdale et al, 1976b)

the amplifiers for the differences in the gains and generator constants.

The Explosive Packages (EP). An EP (Figure 15; from Lauderdale et al, 1976b) was activated by removing three pull pins. Removal of the first pull pin activated the SAFE/ARM slide timer. Removal of the second pull pin released the SAFE/ARM slide from its constrained SAFE position. Removal of the third pull pin removed a constraint on the firing pin and activated the thermal battery timer.

The eight EP's were placed on the lunar surface by the Apollo-17 astronauts at various locations (Figure 14; from Cooper et al, 1974), and were identical except for the amount of charges (weighing from 57 grams to 2722 grams, Table 7; from Cooper and Kovach, 1975) and the preset runout time of the timers. The farther the distance, the larger the amount of explosive used. The geophone/source distances (Table 7; from Cooper and Kovach, 1975) ranged from 101 m (GP 2-EP 8) to 2870 m (GP 4-EP 1).

Log Compression:

The seismic data from the geophones were sampled every 1.9 msec and 8.5 msec (which correspond to Nyquist frequencies of approximately 265 Hz and 59 Hz) for the ASE's and the LSPE systems, respectively (Lauderdale et al, 1976a,b). To cover a large dynamic range with only a few

Table 7. The LSPE geophone/EP distances. (Modified from Cooper and Kovach, 1975)

EP No.	Explosive Weight, g	Distance, m, to --			
		GP-1	GP-2	GP-3	GP-4
1	2722	2855	2758	2818	2870
2	113	327	425	371	366
3	57	242	341	288	287
4	57	269	172	215	220
5	1361	2230	2330	2290	2320
6	454	1195	1240	1195	1095
7	227	800	865	810	672
8	113	179	101	122	112

bits per sample, the seismic data were log compressed. The analog output of the logarithmic compressor was converted into five-bit binary data for the ASE's, and into seven-bit binary data for the LSPE by an analog-to-digital convertor and transmitted to the earth through the ALSEP communication networks.

The binary data stored on the tapes had to be expanded from the output, V_{out}, of the log compressor to obtain the actual seismic data. The relationships between the binary levels and the outputs, V_{out}, of the log compressor are given in Table 8 (from Lauderdale et al, 1976a). For the Apollo 14 and 16 ASE systems, Equations 1a and 1b give the relationships between the output, V_{out}, and input, V_{in}, voltages of the "log compressor" (Lauderdale et al, 1976a).

$$V_{in} = \pm \exp ((V_{out}-V_1)/V_2). \qquad (1a)$$

For binary levels 0 to 13, the "-" sign was used, and 17 to

Table 8. Apollo ASE log compression
(From Lauderdale et al, 1976a)

The ASE has 32 binary levels for representing the log-compressed data. Compression is linear if V_{out} is between 2.170 and 2.670 V.

Binary level	Log compressor output, V_{out}	
0	0.059060	
1	.216540	
2	.374020	
3	.531500	
4	.688980	
5	.846460	
6	1.003940	
7	1.161420	
8	1.318900	
9	1.476380	Negative input signals
10	1.633860	
11	1.791340	
12	1.948820	
13	2.106300	
14	2.263780	
15	2.421260	Linear portion of compressor
16	2.578740	
17	2.736220	
18	2.893700	
19	3.051180	
20	3.208660	
21	3.366140	Positive input signals
22	3.523620	
23	3.681100	
24	3.838580	
25	3.996060	
26	4.153540	
27	4.311020	
28	4.468500	
29	4.625980	
30	4.783460	
31	4.940940	

Linear portion of compressor

31, the "+" sign was used; and

$$V_{in} = (V_{out} - 2.420)/V_3 \qquad (1b)$$

for binary levels 14, 15, and 16.

The values of V_1, V_2, and V_3 for the Apollo ASE systems are given in Table 9 (from Lauderdale et al, 1976a). For example, if the binary level is 27 for Geophone 1 of the Apollo 16 ASE, then the true input voltage is

$$V_{in} = \exp((4.311020 - 4.55779)/0.267730)$$
$$= 0.3978 \text{ volts}$$

For the Apollo LSPE system, the logarithmic compressor has the function (from Lauderdale et al, 1976b)

$$V_{out} = \pm M \ln \left| V_{in} \right| + b$$

where V: voltage

M: constant which determines the slope of the transfer function

b: is specified by the DC offset of the compressor output and the system noise level

The values of M and b are determined by calibration of the system to provide at least 6% accuracy of the data referenced to the level of the input signal.

Table 9. The values of V_1, V_2, and V_3 for the ASE systems. (Modified from Lauderdale et al, 1976a)

Geophone	V_1		V_2		Apollo Mission Number
	Negative, levels 0 to 13	Positive, levels 17 to 31	Negative, levels 0 to 13	Positive, levels 17 to 31	
1	0.29296	4.551350	-0.26996	0.27046	14
2	.28192	4.543420	-.26996	.26984	
3	.27628	4.556939	-.27128	.27088	
1	.28260	4.557799	-.26858	.26773	16
2	.30123	4.557980	-.26983	.27065	
3	.26124	4.553029	-.27054	.26813	

For both Apollo 14 and 16 systems, V_3 equals 332.0 V for all geophones.

CHAPTER IV. DATA ANALYSES AND INTERPRETATIONS OF APOLLO 14 AND 16 ASE'S

The ASE data are obtained from: 1) an astronaut-activated thumper (thirteen thumper shots for the Apollo 14 ASE and nineteen thumper shots for Apollo 16's), 2) three mortar-launched grenades for the Apollo 16's, and 3) three grenade launchings for the Apollo 16's. The geophone/thumper-source distances are increased, in increments of 4.57 m, from 0 m up to 91.44 m (Table 2; page 23). The amount of charge used for the thumper shots is not known. The three grenades of the Apollo 16 ASE are launched, in a sequence of 2-4-3, to distances of 900 m, 150 m, and 300 m, respectively. Grenade 1, planned for a launch distance of 1500 m, was not launched because the angle sensor went off scale. The geophone/source distances ranged from 61.87 m to 1017.42 m, and the explosive charges weighed from 45 grams to 454 grams for the grenades and from 10 grams to 42 grams for the thrusts of the grenade launchings (Table 3; page 25). The three grenade launchings had the same distances to Geophones 1 (14 m), 2 (50 m), and 3 (95 m).

Deglitching:

The lunar seismograms from the Apollo ASE thumper shots and grenades show severe "glitches". Most are almost

uniformly spaced and of uniform amplitude at binary level 27 but others are of varying amplitudes and locations in Geophone 1, while extraneous random glitches exist in the data for Geophones 2 and 3 for both Apollo 14 and 16 ASE's.

Figure 16 shows three representative traces of the raw data from the Apollo 14 and 16 ASE thumper shots and grenades. These data are from the tenth thumper shot and the geophone/source distances are 50.29 m, 4.57 m, and 41.14 m to Geophones 1 (GP 1), 2, and 3, respectively. The thumper firing time is 1.21 seconds after the beginnings of the traces. The data show that there are glitches throughout the records; they are recognized by the fact that they are of short duration -- generally, only one sample value -- and have values which are inconsistent with the preceding and/or following sample values. Figure 17 shows another three traces of raw data. These data are from the second grenade launching of the Apollo 16 ASE. The geophone/source distances are 14 m, 50 m, and 95 m to Geophones 1, 2, and 3, respectively. The grenade launching time is approximately 0.60 seconds after the beginnings of the traces. Figure 17 shows there are relatively fewer glitches for these data than there are for the ASE thumper shots (see Figure 16) and grenades. Furthermore, no glitches are found in the grenade launching data for the second and third geophones.

The first data-improving operation performed is to go through the data by hand and remove the extraneous values

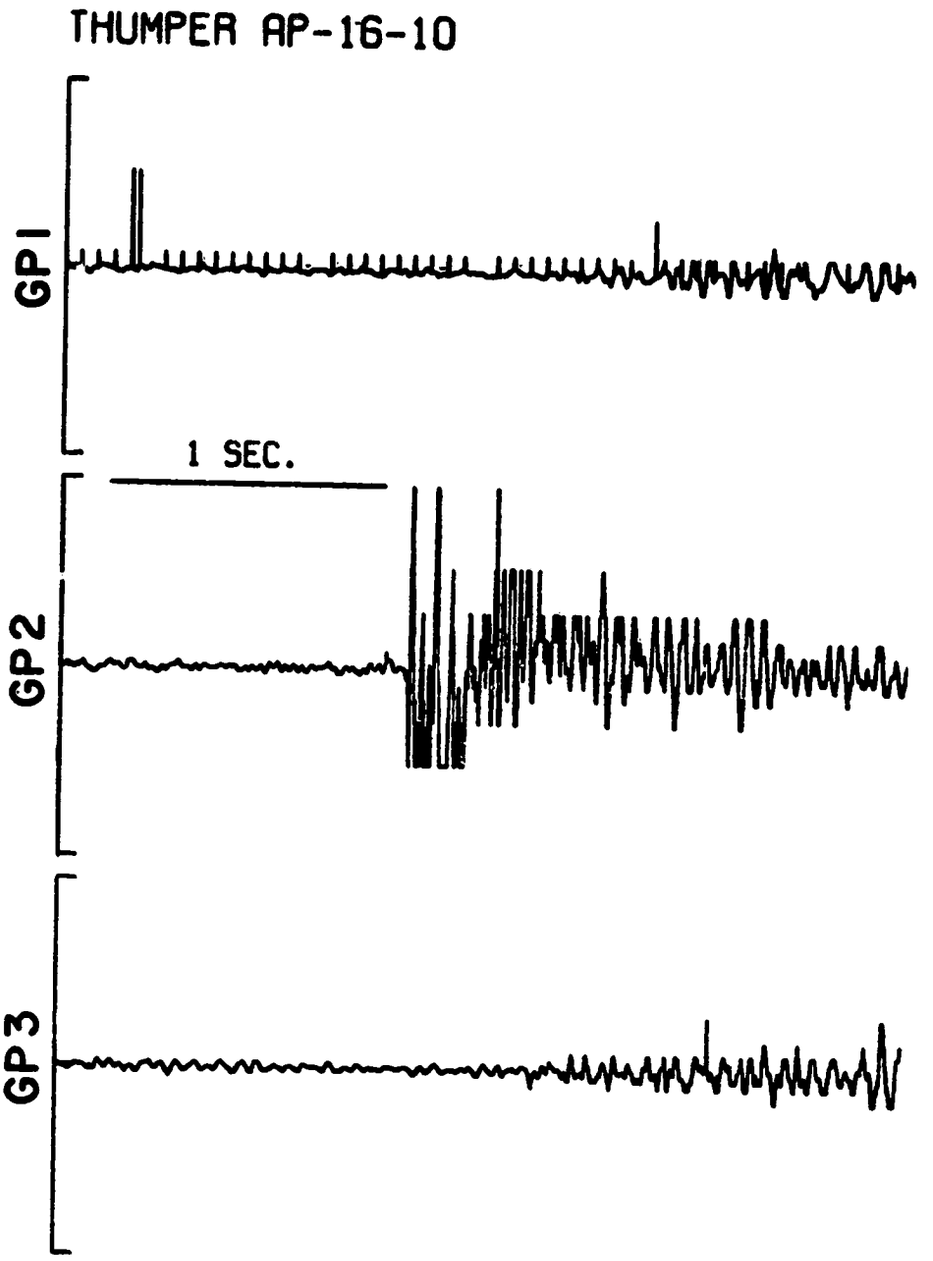

Figure 16. Representative raw data which is from the tenth thumper shot of Apollo 16 ASE. The geophone/source distances are 50.29 m, 4.57 m, and 41.14 m to Geophones 1 (GP 1), 2, and 3, respectively. The firing time is 1.21 seconds after the beginnings of the traces.

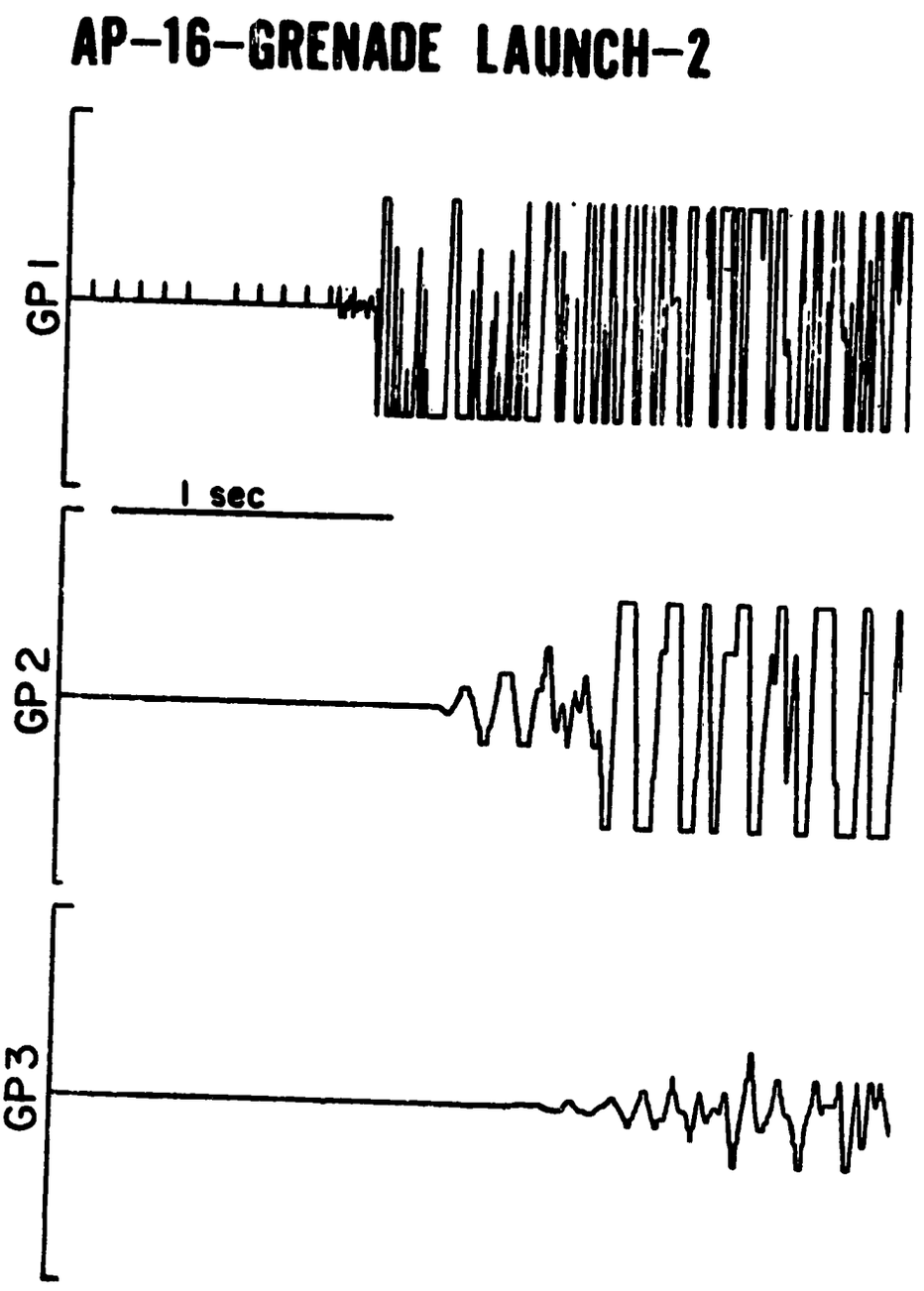

Figure 17. Representative raw data which is from the second grenade launching of Apollo 16 ASE. The geophone/source distances are 14 m, 50 m, and 95 m to Geophones 1 (GP 1), 2, and 3, respectively. The firing time is 0.64 seconds after the beginnings of the traces.

and replace them by values interpolated from neighboring values. A deglitching program is not used in this process because: 1) there are relatively few glitches (excluding the regular, periodic ones in GP 1, there are fewer than 1%), 2) the coarseness of the amplitude values precludes automatic, computer interpolation, and 3) a criteria is used to identify and correct the bad sample values; that is, we change the value of the binary level of the bad sample by one bit and this makes its amplitude consistent with the preceding and/or following sample values. The results of the "deglitching" process is shown in Figure 18 for the same traces shown in Figure 16. The seismic traces are smoother and much clearer than before.

Amplitude Spectrum Analyses and Filtering:

For the ASE thumper shots, the inconsistency of the amplitude spectra is observed. The spectra shown in this section are taken from approximately the first one second, 512 sample points, of the data after the firing time. Figure 19 shows the amplitude spectrum from the second geophone of the tenth thumper shot of the Apollo 16 ASE. The geophone/source distance is 4.57 m. Most of the energy of the signal is concentrated between approximately 10 Hz and 40 Hz. There are two peaks in the amplitude spectrum (with amplitudes of approximately 0.6 and 0.5) at

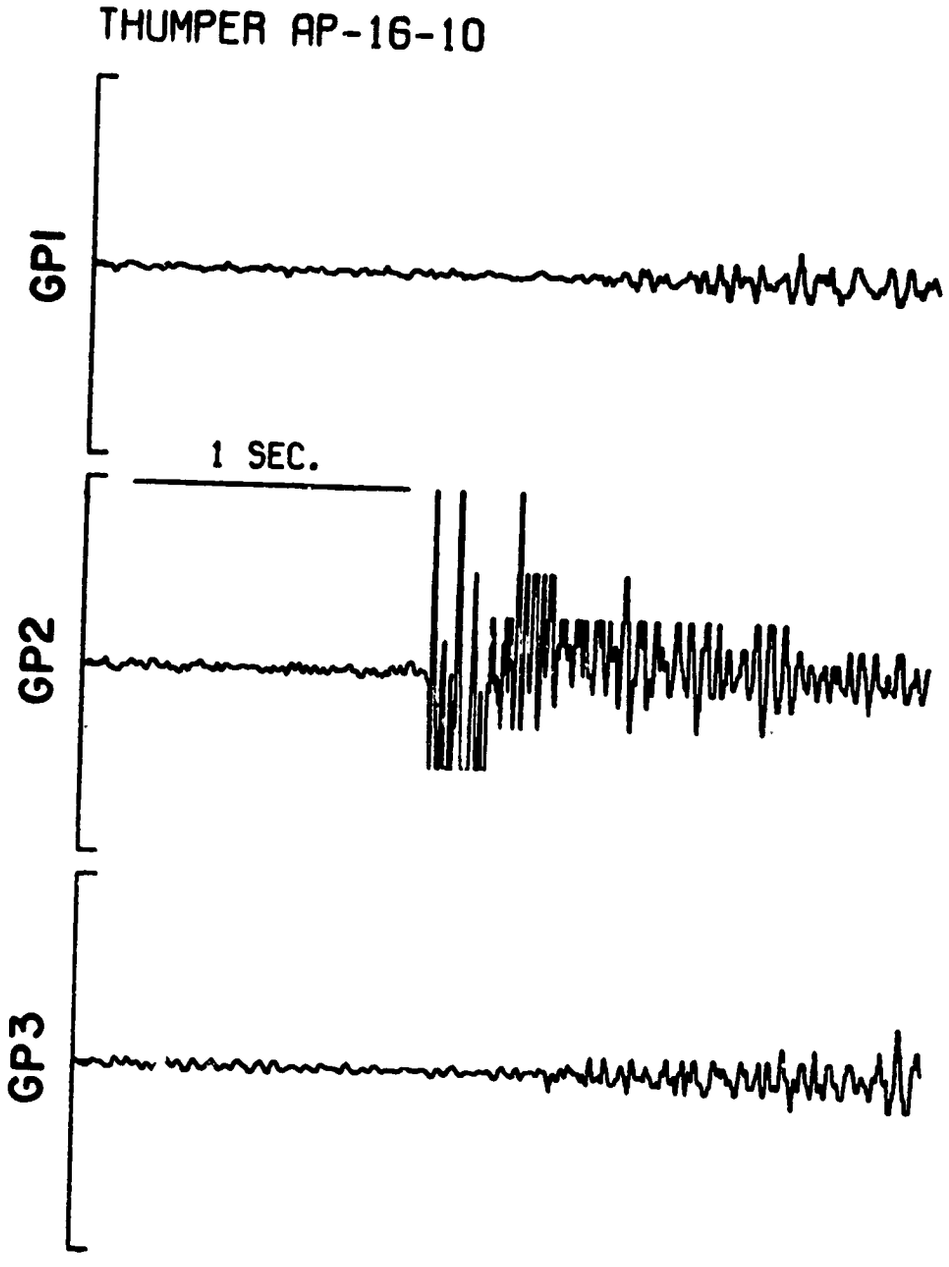

Figure 18. Representative of deglitched data of the ASE. It is from the tenth thumper shot of Apollo 16 ASE.

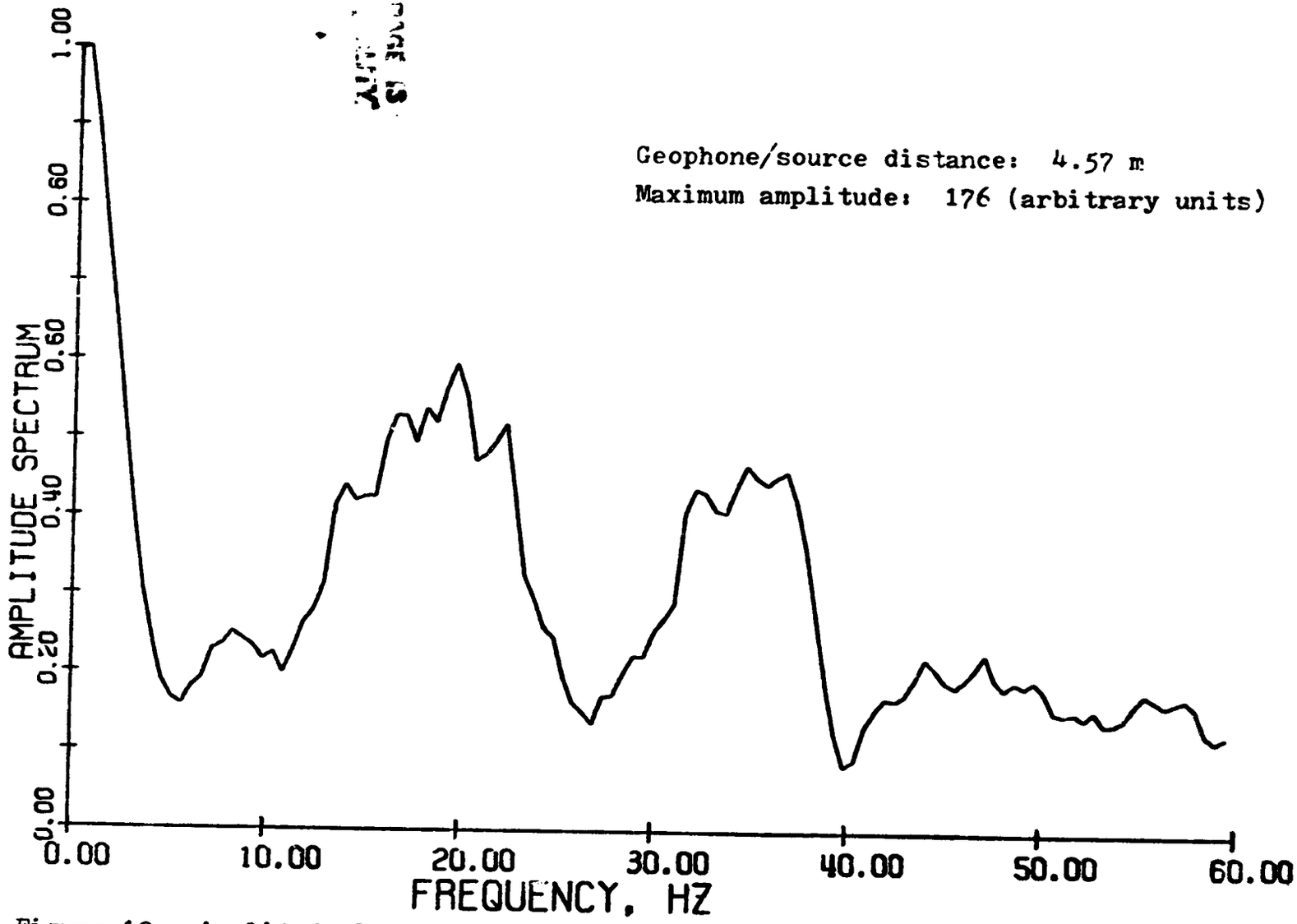

Figure 19. Amplitude Spectrum of Geophone 2 of Thumper-shot 10 of Apollo 16 ASE.

about 18 Hz and 33 Hz, respectively. The noise level (with amplitude of approximately 0.1) is reached at frequencies greater than 90 Hz. Figure 20 shows the amplitude spectrum from the first geophone of the seventeenth thumper shot of the Apollo 14 ASE. The geophone/source distance is 18.29 m. The energy of the signal is still concentrated but harmonically distributed between approximately 10 and 40 Hz. The maximum amplitude (at 18 Hz) is approximately 87% that of the maximum amplitude in Figure 19.

The amplitude spectra of the ASE grenades and grenade launchings show more consistency than those of the ASE thumper shots. The amplitude spectrum has the broadest frequency band (approximately from 4 to 30 Hz) for the shortest geophone/source distance, 61.87 m; namely, the signal at Geophone 3 of Grenade 4. In general, the frequency band of the signal narrows when the geophone/source distance increases, both the maximum amplitude and the frequency band shift toward lower frequencies. The longer the distance the seismic waves travel, the more high frequency components the moon filters out. For example, the amplitude spectrum of the signal from Geophone 3 for Grenade 3, whose geophone/source distance is 353.26 m, has a frequency band from about 7 Hz to 25 Hz and a maximum amplitude at about 17 Hz. The frequency band of the signal from Geophone 1 for Grenade 2, which has the largest geophone/source distance (1017.42 m), is from about 5 Hz to

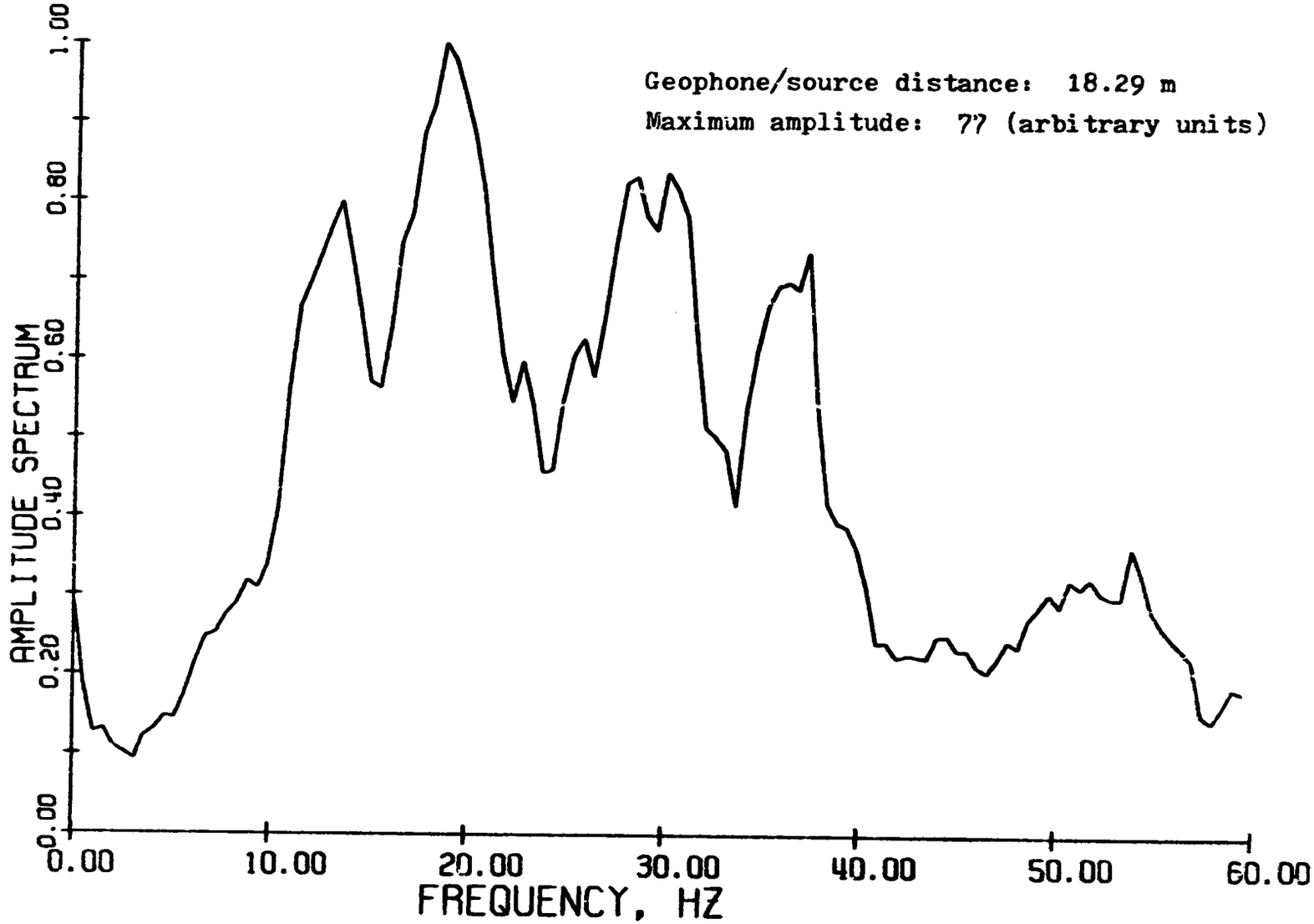

Figure 20. Amplitude spectrum of Geophone 1 of Thumper-shot 17 of Apollo 14 ASE.

20 Hz, and its maximum amplitude is at about 11 Hz.

To improve the S/N ratio, the ASE thumper data are bandpass filtered by a four-pole, anti-aliased, Butterworth filter with -3 dB frequencies at about 3 Hz and 66 Hz (0.01 f_n and 0.25 f_n, respectively, where $f_n \approx 265$ Hz is the Nyquist frequency). The ASE grenade and grenade launching data are bandpass filtered by a similar Butterworth filter with -3 dB frequencies at 3 Hz and 40 Hz (0.01 f_n and 0.15 f_n, respectively). The Butterworth filter (Oppenheim and Schafer, 1975) has the properties: 1) the amplitude response is maximally flat in the passband and 2) the approximation is monotonic in the passband and stopband. The amplitude, A(n), and the phase, $\theta(n)$, functions of a 2^N-point version of a Butterworth bandpass filter are:

$$A(n) = ((1+B^4)(1+C^4))^{-\frac{1}{2}}$$

$$\theta(n) = \tan^{-1}\left(\sqrt{2}C/(1-C^2)\right) - \tan^{-1}\left(\sqrt{2}B/(1-B^2)\right)$$

where $B = \tan(n\pi/2^{N+1})/\tan(\pi f_n/2f_H)$

$C = \tan(\pi f_n/2f_L)/\tan(n\pi/2^{N+1})$

f_H and f_L: are the high and low cutoff frequencies, respectively.

$n = 0, 1, 2, \ldots, 2^N-1$

These improve the S/N ratio significantly. Representative results are shown in Figure 21 (compare with Figure 18). The traces are smoother, and the high frequency noise and the low frequency characteristic have been eliminated.

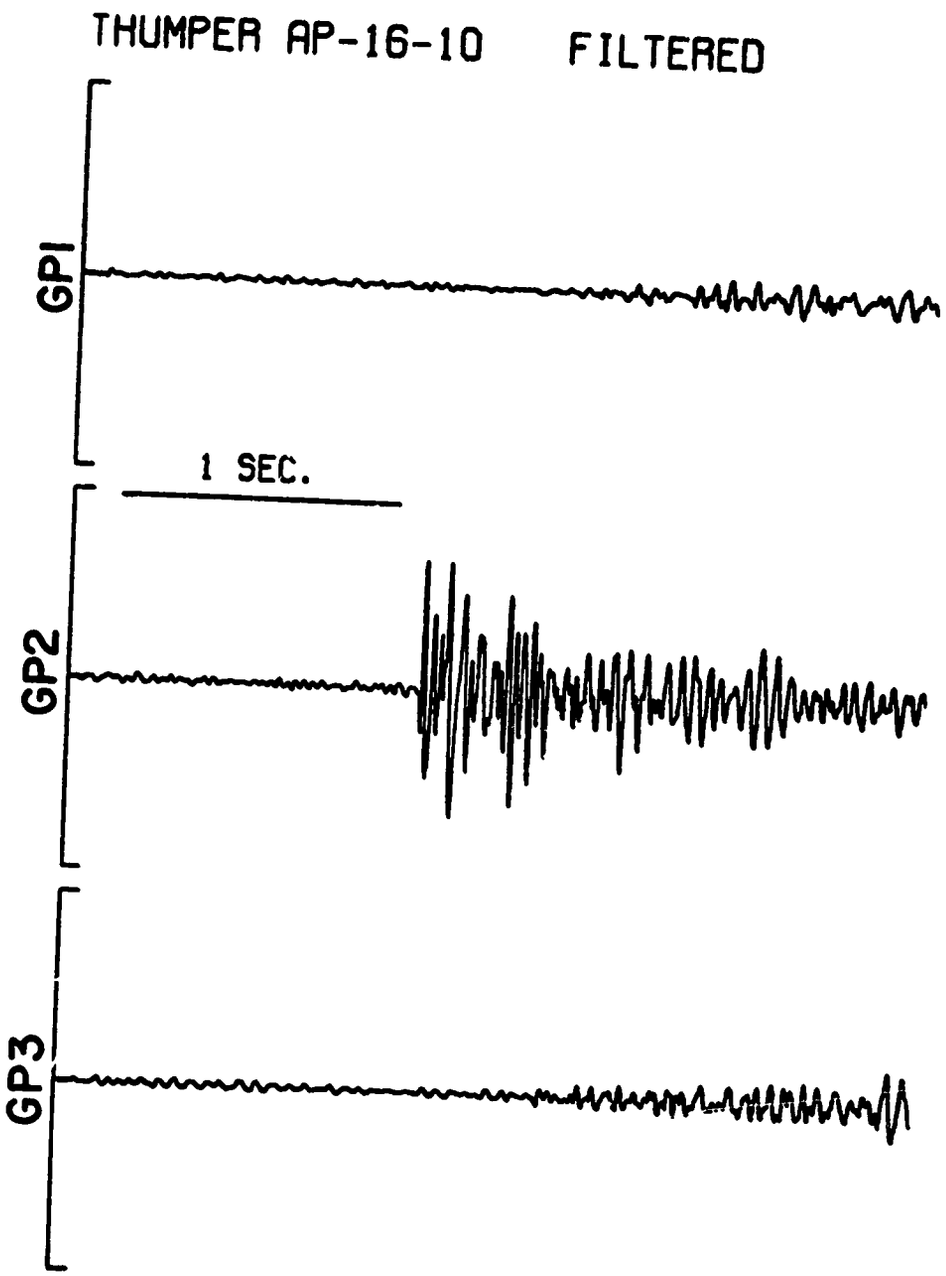

Figure 21. Representative of the bandpass filtered ASE data. It is from the tenth thumper shot of Apollo 16 ASE.

While a high S/N ratio exists for the shortest ASE thumper distance (4.57 m, GP 2; Figure 21), the S/N ratios for the other two traces in Figure 21 are so low that it is difficult, if not impossible, to pick the first arrivals or to measure their amplitudes. The low S/N ratio at larger distances is caused by the decrease of the first-arrival amplitudes. Kovach et al (1972) also indicate that the onsets become emergent when the separations are larger than 15 m and the determination of the signal onsets from the background noise is difficult for the Apollo 14 and 16 ASE thumper shots for separations greater than 45 m. Consequently, large uncertainties arise when picking traveltimes for greater separations. Furthermore, there is strong noise throughout the data for the third geophone of Apollo 14 ASE thumper shots. Strong reveberations exist in the data of thumper shots 1 through 7 for the second geophone of Apollo 14 ASE. The first breaks of the signal onsets can not be determined with any accuracy for these data. Also, the amplitudes of the first arrivals of Apollo 16 ASE thumper shots are smaller than those of Apollo 14's at the same geophone/source distances.

There is little noise in the grenade launching data. However, the onsets on the third geophone (95 m) of all the grenade launchings are still too low to determine first-arrival times. The traveltimes of the first arrivals are expected to be the same at each geophone for these three

grenade launchings because they have the same geophone/source distance to each geophone. But we find a maximum of 57 msec difference in the traveltimes between Grenade Launchings 2 and 4. The traveltime differences might be caused by the difficulties in recording the initiations of the launchings. For the ASE grenade data, the first arrivals at all three geophones merge into the background noise so that the traveltimes of the first arrivals can not be determined.

Stacking and Amplifying:

To further improve the data, those traces which have the same geophone/source distances were stacked together. The stacking would be destructive to the noise and constructive to the signal because of the randomness of the noise from trace to trace and the coherence of the signal. Consequently, stacking the traces for equal separations will increase the amplitude of the signal by the number of traces stacked while the noise will increase by the square root of the same number. This gives a S/N ratio improvement equal to the square root of the number of traces stacked.

For the ASE thumper-shot data, those traces which have the same geophone/source distances are listed in Table 10. The numbers listed on the right-hand side of the table are the thumper-shot numbers which have the given separations at

Table 10. Stacking parameters of Apollo ASE's.

Geophone-source distance, m	No. of traces stacked	Amplification	Thumper Shot No. to --					
			AP-14			AP-16		
			GP 1	GP 2	GP 3	GP 1	GP 2	GP 3
0.00	3	2	21*	11	1*	19	11	1*
4.57	4	2	20	12	2*	-	10	2
9.14	6	2	19	13*	3	18	9,12	3
13.71	6	4	18	-	4	17	8,13	4
18.29	5	4	17	7*	-	16	7,14	5
22.86	4	4	-	-	-	15	6,15	6
27.43	6	4	-	17	7	14	5,16	7
32.00	5	4	-	4*18	-	13	4,17	8
36.58	5	8	13*	3*19	-	12	3,18	9
41.14	4	8	12	2*20	-	-	2	10
45.72	7	8	11	1*21	11	11	1,19	11
50.29	2	8	-	-	12	10	-	-
54.86	3	8	-	-	13	9	-	12
59.44	2	8	-	-	-	8	-	13
64.00	3	8	7	-	-	7	-	14
68.58	2	8	-	-	-	6	-	15
73.15	3	8	-	-	17	5	-	16
77.72	4	16	4	-	18	4	-	17
82.30	4	16	3	-	19	3	-	18
86.87	3	16	2	-	20	2	-	-
91.44	4	16	1	-	21	1	-	19

* Noisy trace which was not stacked.

their left. However, those thumper shots with an asterick above their numbers (ten are from the Apollo 14 ASE and one is from the Apollo 16's) have such high noise levels that they were not used in stacking. The number of traces stacked are given in the second column of Table 10. There are between 2 and 7 traces with the same separations for the ASE thumper shots. The stacking would give S/N improvements between $\sqrt{2}$ and $\sqrt{7}$. The stacked data are then amplified so that they are plotted at almost full scale for each stacked trace. This helps us pick the first arrivals. The amplifications used are given in the third column of Table 10.

Figure 22 shows the results of the stacked, filtered, and amplified profile of Apollo 14 and 16 ASE thumper shots. Remember that the thumper firing time is 1.21 seconds after the beginnings of the traces, and the increment of the geophone/source separation between traces is about 4.57 m. The first arrivals could be determined easily and accurately for separations up to 32.0 m.

Figure 22 also shows a smooth curve for the first arrivals on the profile which suggests that the continuous velocity variation model might be the better one. If the velocities increase in a stepwise fashion, the traveltime curve of the first arrivals on the profile will then be straight lines. However, it was still not possible to pick first-arrival times for distances greater than 32.0 m.

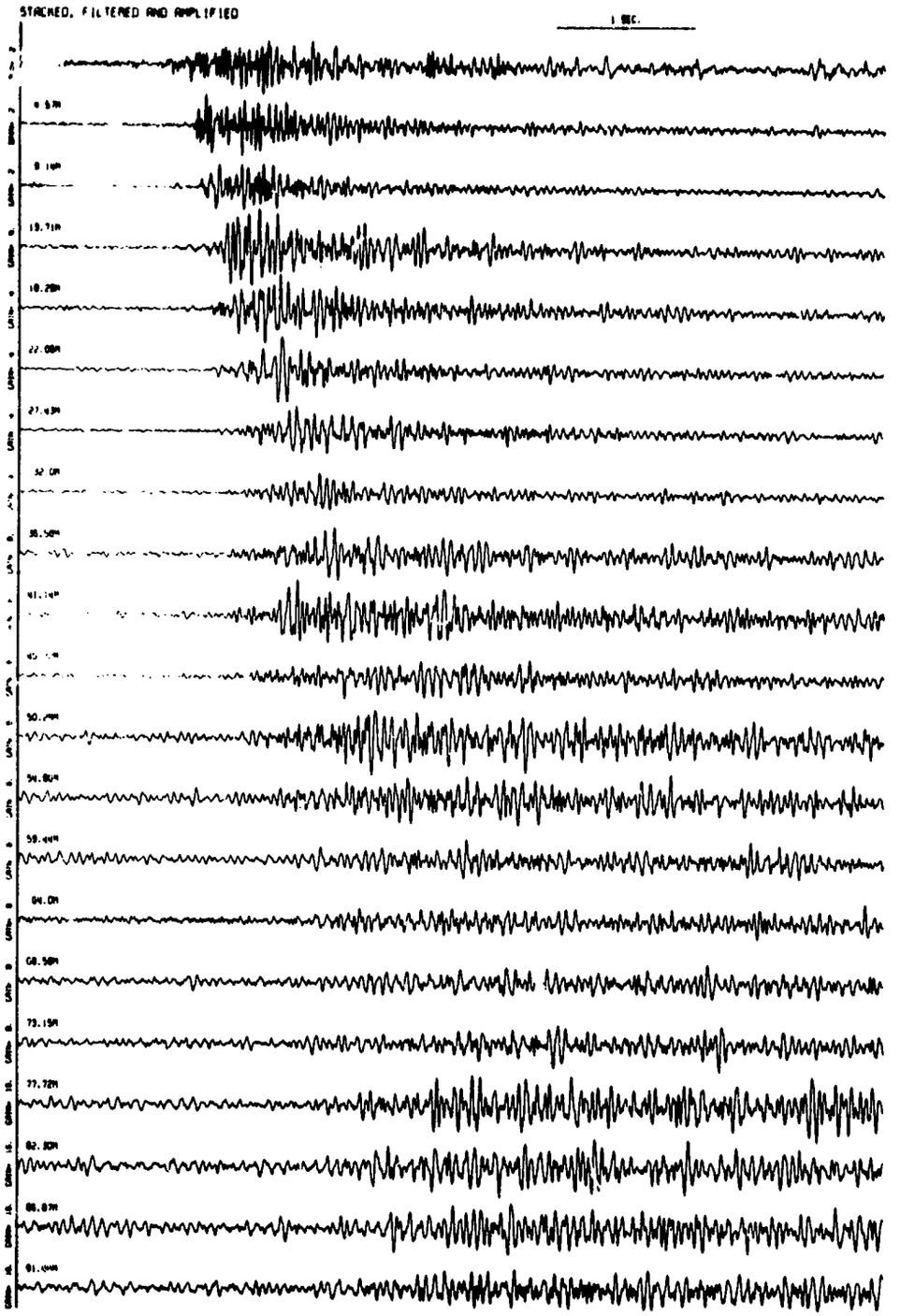

Figure 22. Stacked, filtered, and amplified profile of Apollo ASE's.

The stacked profiles and the single geophone profiles of Apollo 14 and 16 ASE thumper shots are compared with the results of the stacked profile of the Apollo 14 and 16 ASE thumper shots. If there are any significant differences in the velocity structures at these two sites, the results of these profiles will show the differences. Little difference is found.

Traveltime Variations:

Using Kaufman's (1953) result, a velocity function with depth, z, given by $V(z)=V_o(z/z_o)^n$ has a traveltime function, t(x), with separation, x, given by

$$t(x) = cx^m/V_o$$

where c is a constant, m equals 1-n, and V_o is the velocity at a depth of z_o. The above equation also represents the traveltime/separation function of the direct waves for the homogeneous and layered model (m=1); where $c/V_o=1/V'$ and V' is the constant velocity of the surface layer. The slope of the traveltime data plotted on a log t (traveltime) versus log x (geophone/source separation) graph would determine the exponent, m.

The traveltime data of the first arrivals measured from the Apollo 14 and 16 ASE stacked profiles for separations up to 32.0 m are listed in Table 11 (from Gangi and Yen, 1979). The questionable data are given a weight

Table 11. Traveltimes of the first arrivals both measured from the ASE stacked profiles and calculated from the Kovach and Watkins models. (Modified from Gangi and Yen, 1979)

Separation, m	Measured traveltimes@, msec			Calculated traveltimes, msec	
	1	2	3	A	B
4.57	55	53	56	44	40
9.14	91	91	-	88	80
13.71	123	123	124	132	120
18.29	151	149	152	176	160
22.86	-	-	-	220	201
27.43	206?	230	196?	*245	241
32.00	255?	274?	264?	*260	281
Slope	.76	.80	.74	-	1
V_o, m/sec	590	430	630	104	114

@ Traveltimes with question marks indicated uncertainties existed.
* Traveltimes of the first refracted waves
1 Measured from Apollo 14 and 16 stacked and amplified data (3-66 Hz)
2 Measured from Apollo 14 stacked (only) and amplified data (3-66 Hz)
3 Measured from Apollo 16 stacked (only) and amplified data (3-66 Hz)
A From Apollo 14 homogeneous and layered model (Kovach and Watkins, 1973)
B From Apollo 16 homogeneous and layered model (Kovach and Watkins, 1973)

of one quarter that of the high-S/N data; the V_o's are calculated from the slopes of the least-square-fitted straight lines and extrapolated to z_o=1 km. However, the V_o at a depth of z_o= 1 km does not imply that the powdered layer would extend to 1 km. The V_o at 1 km is, for convenience, a constant of reference used to characterize the velocity model. The depth, z_o, can be chosen at any other depth, say z_1, then the V_o's in Table 11 will be multiplied by $z_1^{-1/6}$. Table 11 (from Gangi and Yen, 1979) shows a greater variation of the reference velocities, V_o's, than of the slopes. The reference velocities vary between 430 m/sec and 630 m/sec while the slopes vary between 0.74 and 0.80. While the measured slopes are variable, they are all consistently lower than m=1-n=1, the value that would be obtained for the homogeneous and layered model. They tend to the value predicted by the self-compacting-powder model; namely, m=1-1/6=0.833.

The traveltimes of the first arrivals calculated for the Kovach and Watkins models (1973) at the Apollo 14 and 16 landing sites are tabulated in Columns A and B of Table 11 (from Gangi and Yen, 1979). There are not large differences between the measured traveltimes and the calculated traveltimes. However, the biggest differences between the Kovach and Watkins models and the measured values occur at the smallest separations. They assumed that the traveltimes at zero separations are zeros, and

they fitted most of the data points simply by forcing the least-squared traveltime curves to pass through the zero separations (Figure 2, page 5).

In stacking, we assume that the separations are exactly the same for each trace. Stacking should improve the S/N ratio by the square root of the number of traces stacked. However, the S/N improvement obtained from the stacked data is not that expected theoretically. This might be due to the time offsets introduced into the individual traces by differences in separations and small differences in elevations at the source and receiver locations. Figure 23 shows the second geophone profile of the Apollo 14 ASE thumper data (the firing time is approximately 1.21 seconds after the beginnings of the traces). Thumper shots 14, 15, and 16 of Apollo 14 ASE (corresponding to separations of 13.71 m, 18.29 m, and 22.86 m, respectively) misfired. Notice that some good first arrivals can be found at separations greater than 32.0 m (Figure 23). However, strong reveberations exist in the data of thumper shots 1 through 7; the first arrivals could be detected but the accuracy of the onset determinations is very questionable.

In Table 12, the traveltime data from the first and second geophone profiles of Apollo 14 ASE thumper shots up to 45.72 m are tabulated; that is, traveltimes from thumper shots 11 through 21 are listed except for those

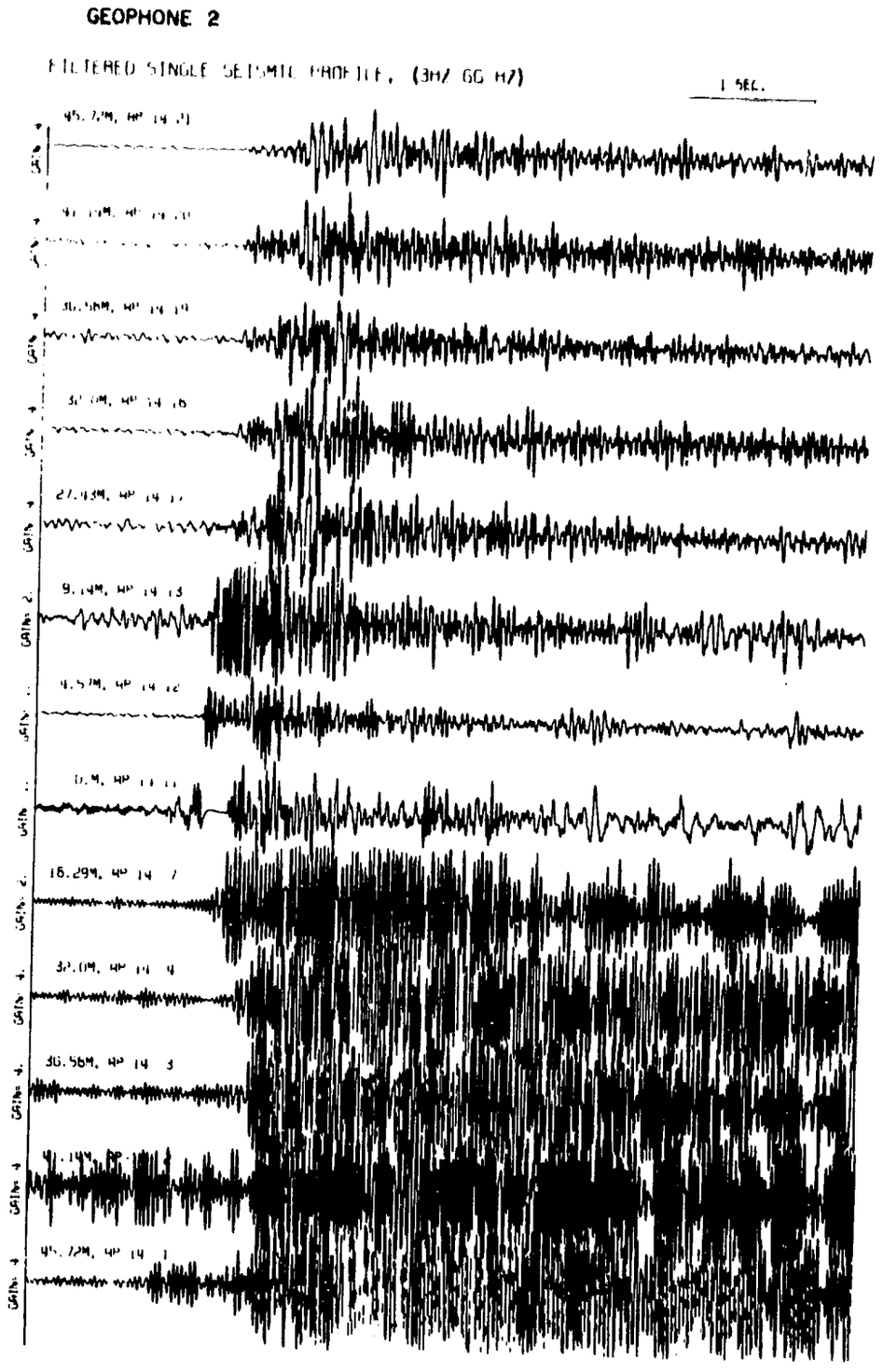

Figure 23. Filtered and amplified profile of the second geophone of Apollo 14 ASE.

Table 12. Measured and calculated traveltimes of the first arrivals.

Separation, m	Traveltime, msec			
	Measured[§]		Calculated	
	GP 1	GP 2	A	B
4.57	53	53	53	52
9.14	94	94	95	93
13.71	132	-	132	131
18.29	164	-	168	166
22.86	-	-	201	200
27.43	-	230	234	233
32.00	-	260	*259	*259
36.58	?	276	*277	*277
41.14	?	293	*295	*295
45.72	312	315	*313	*313
Slope	0.82[†]		0.82	0.833
V_1, m/sec	254[††]		254	254

§ Measured from the first and second geophone profiles of Apollo 14 ASE. Data are filtered between 20 and 40 Hz.

A For $V=373(z/z_o)^{0.18}$ in the surface powder layer overlying a homogeneous medium with V_1=254 m/sec.

B For $V=345(z/z_o)^{1/6}$ in the surface powder layer overlying a homogeneous medium with V_1=254 m/sec.

* Refracted first arrivals

\- Misfire

? Noisy data

† Least-square fitted, for separations less than 30 m.

†† Least-square fitted, for separations between 32.0 m and 45.72 m, inclusive.

** The thickness of the powder layer is 11 m.

misfired. Beyond those separations, the first arrivals are ambiguous. The third-geophone profile of Apollo-14 ASE thumper shots is not used because of the low S/N ratio. On a linear traveltime/separation plot (Figure 24), the first arrivals show a smooth curve up to approximately 30 m; no straight line could be fitted to those data points which would pass through the origin in the same time. It strongly suggests that the power-law velocity model might be a more suitable representative for the velocity structure on the very shallow lunar crust. Beyond 30 m, a straight line is observed. Those data points are assumed to be associated with refracted waves from the second layer which is assumed to be homogeneous with a constant velocity of 254 m/sec. However, the velocity in the second layer is still questionable because there only are five data points and uncertainties increase in the data at larger separations.

The log/log traveltime plot for the single geophone profiles of Apollo 14 ASE thumper shots is shown in Figure 25 along with the least-square-fitted line with a slope of 0.82. It can be seen from the figure that the straight line is an excellent fit to the data. The reference velocity, V_o=373 m/sec, is evaluated from the slope of the least-square-fitted line and the time intercept at x=1 m. If the exponent of the traveltime function, $t(x)=cx^m/V_o$ (where x is in meters), is 0.82,

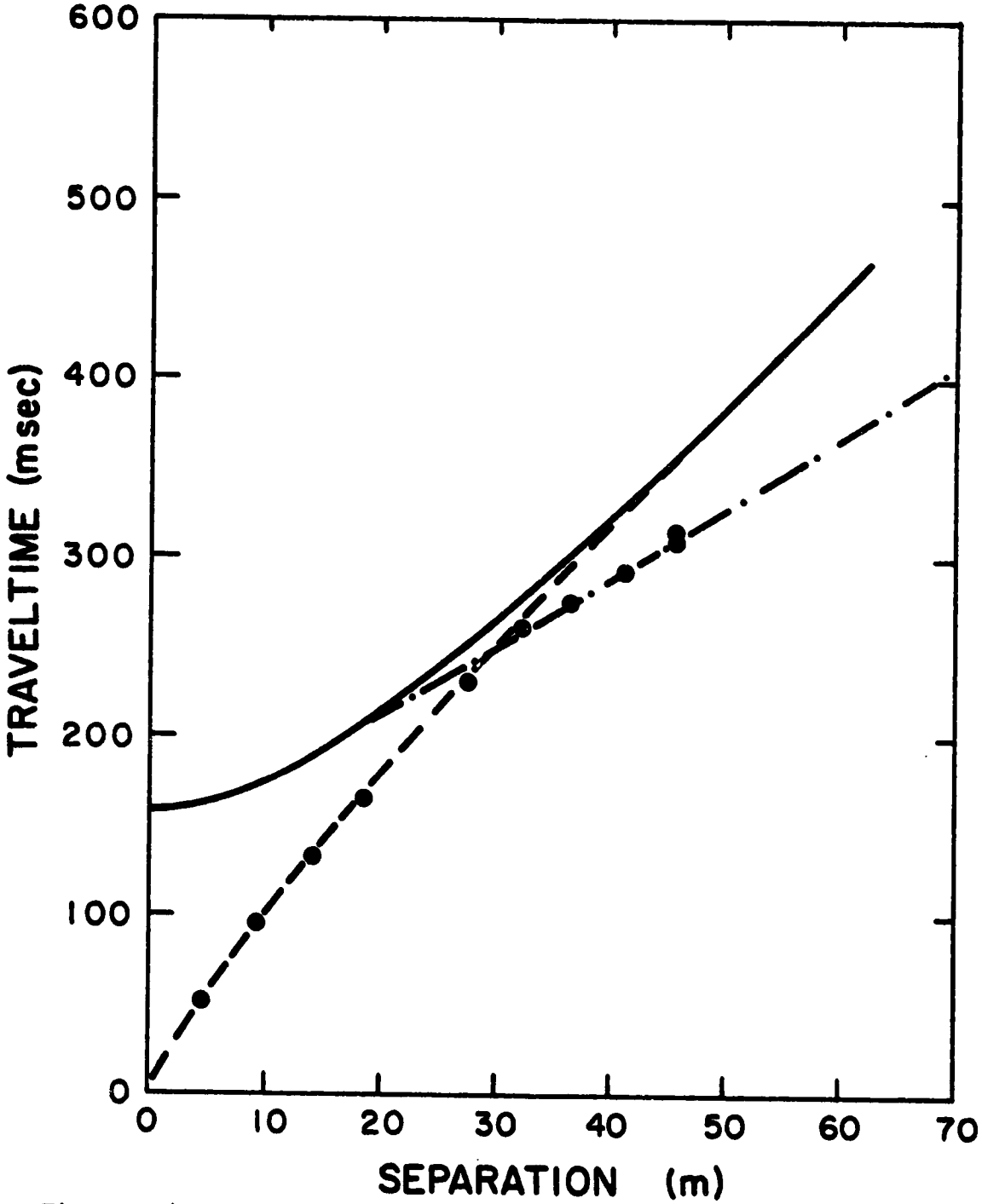

Figure 24. Theoretical and measured traveltime curves. Measured data are obtained from the first and second geophone profiles of Apollo 14 ASE thumper shots 11 through 21. Direct waves are in dashed line. Refracted waves are in dot-dashed line. Reflected waves are in solid line.

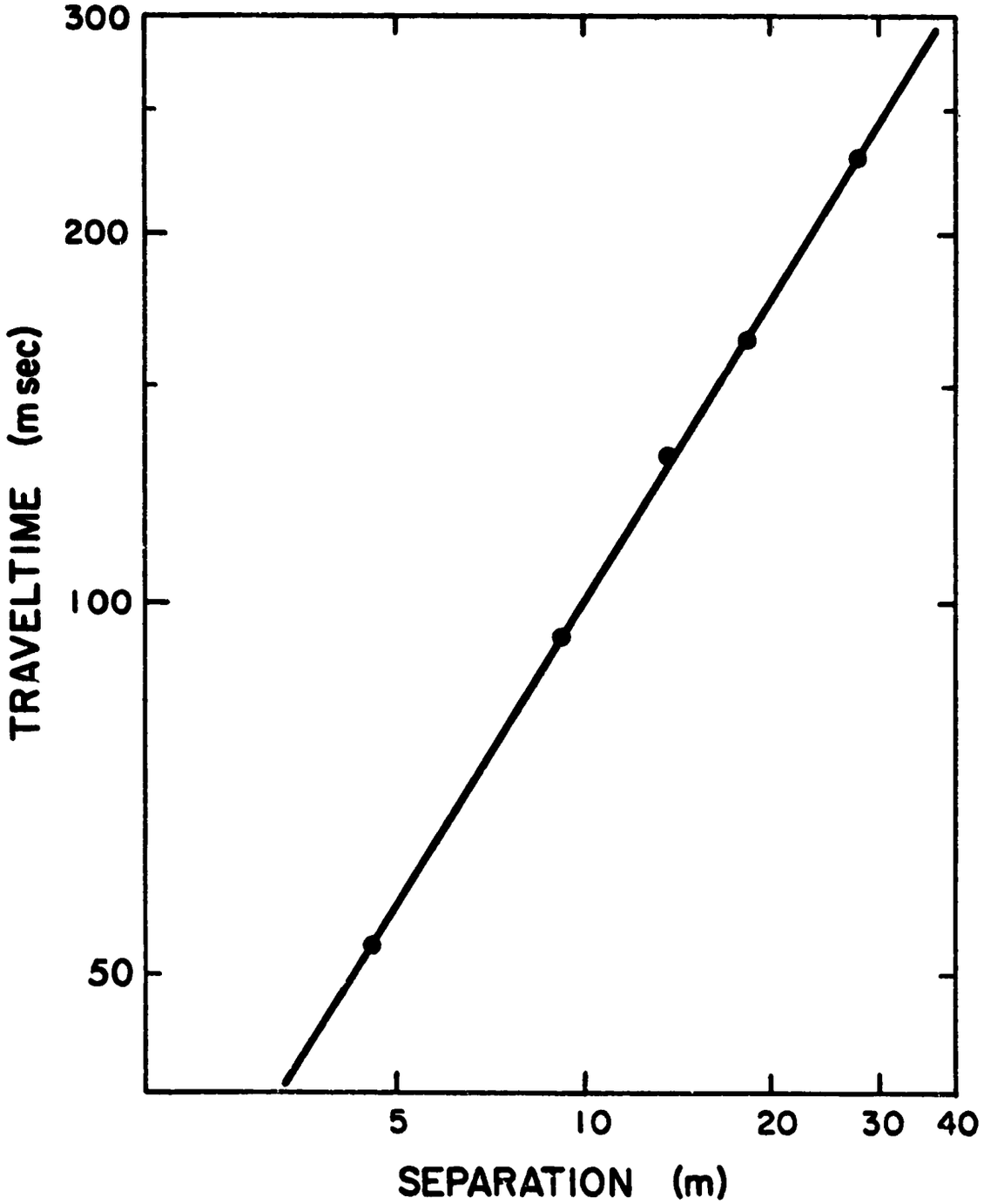

Figure 25. Least-square-fitted traveltimes in log/log plot from the first and second geophone profiles of Apollo 14 ASE thumper shots for separations up to 27.43 m.

c equals 5.77. However, the slope of the least-square-fitted line is almost identical to the value, m=1-1/6=0.833, predicted by the self-compacting-powder model that the one-sixth power velocity variation is very possible. Using Kaufman's (1953) result, a velocity function with depth, z, given by

$$V(z) = V_o(z/z_o)^{1/6}$$

has a traveltime function, t(x), with separation, x, given by

$$t(x) = 1.2(15\pi z_o/8)^{1/6}x^{5/6}/V_o. \qquad (2)$$

A least-squares fit of this function to the measured traveltimes gives V_o=345 m/sec. The theoretical traveltime curve of the direct waves with V_o=345 m/sec fits the data points very well (Dashed line; Figure 24, page 60).

If this is the velocity model for the very shallow lunar crust, we can derive the traveltime equations for the refracted and reflected waves. That is, we assume there is a one-sixth power velocity variation of a self-compacting-powder layer on the lunar surface with a reference velocity of 345 m/sec at 1 km and a thickness of H overlying a homogeneous layer with a constant velocity of 254 m/sec. For the traveltime equation, t_R, of the refracted waves, we have

$$t_R = x/V_1+(z_oV_1^5/4V_o^6)F(\theta_c) \qquad (3)$$
$$= x/V_1+t_o$$

where x: separation

V_o: reference velocity of the powder layer at z_o=1 km

V_1: constant velocity of the homogeneous layer

$F(\theta_c) = 3\theta_c - \sin\theta_c \cos\theta_c (3+2\sin^2\theta_c - 8\sin^4\theta_c)$

θ_c: critical angle; where $\sin\theta_c = (V_o/V_1)(H/z_o)^{1/6}$

H: thickness of the powder layer

t_o: intercept time

The thickness, H=11 m, of the powder layer is calculated from the V_o, V_1, and t_o using the fixed-point iterative method (see, for example, Conte and de Boor, 1972, page 44). The maximum separation for the direct waves is x=5.89H=64.8 m (Gangi, 1972).

The traveltime equation of the reflected waves must be expressed in a parametric form. That is, the traveltime and separation relationships, $t_r(p)$ and $x_r(p)$, for the reflected waves are (in terms of the ray parameter, p, which is given by the Snell's law, $p=\sin\theta(z)/V(z)$)

$$t_r(p) = (3z_o/2pV_o^2)(3a^4\sin^{-1}(b/a) - (3a^2+2b^2)bc)$$
$$x_r(p) = (z_o/4)(15a^6\sin^{-1}(b/a) - (15a^4+10a^2b^2+8b^4)bc) \qquad (4)$$

where $a = 1/pV_o$

$b = (H/z_o)^{1/6}$

$c = (a^2-b^2)^{\frac{1}{2}}$

$= ((1/pV_o)^2 - (H/z_o)^{1/3})^{\frac{1}{2}}$

The theoretical traveltimes for the refracted and reflected waves, dot-dashed and solid lines, respectively, are also

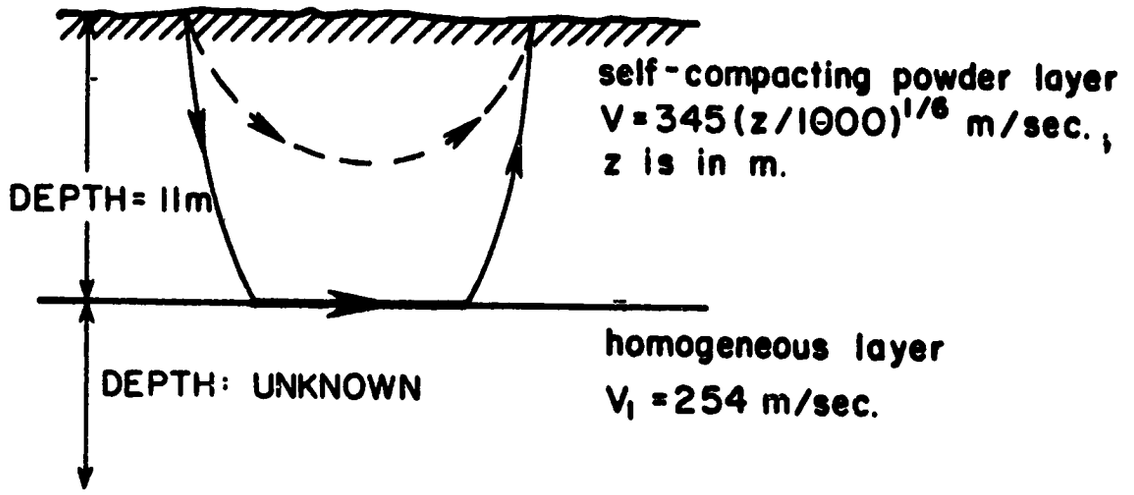

Figure 26. Velocity structure at the Apollo 14 landing site.

shown in Figure 24 (page 60) based on the values found. Figure 26 shows the velocity model at the Apollo 14 landing site. Notice that the velocity at the lunar surface, z=0 m, is zero based on the velocity function, and the thickness of the second layer, the homogeneous layer, is unknown. However, whether the second layer is homogeneous is still unknown.

For the first geophone profile of Apollo 16 ASE, the first arrivals can be picked for separations up to 18.29 m and, with difficulty, for 27.43 m (see Table 13). After 27.43 m, the first arrivals are buried in the noise. The slopes (see Table 13) of the least-square-fitted lines are, again, lower than that predicted by the Kovach and Watkins model (1973). For the three single-geophone profiles, the variation of the reference velocities is

Table 13. Traveltimes measured from single geophone profiles of Apollo 16 ASE thumper shots. Data are filtered between 20 and 40 Hz.

Separation, m	Traveltime, msec		
	GP 1*	GP 2†	GP 3†
4.57	-	57	58
9.14	98	94	89
13.71	128	121	-
18.29	155	145	151
22.86	-	185?	189
27.43	201	-	196?
Slope	0.65	0.71	0.71
V_o, m/sec	1059	773	789

* Thumper shots 12 through 19

† Thumper shots 1 through 11

greater than that of the slopes; the values of the reference velocities vary from 1059 m/sec to 773 m/sec. The values of the reference velocities are almost doubled or tripled that of Apollo 14 ASE. The slopes of the least-square-fitted line vary from 0.65 to 0.71. Empirically speaking, the velocity variation on the lunar surface at the Apollo 16 landing site tends to the fourth-root velocity variation rather than the sixth-root velocity variation. However, if we also assume that the velocity variation on the lunar surface at the Apollo 16 landing site is one-sixth power, a least-squares fit of the traveltime function (Equation (2), page 62) for the direct waves to the measured traveltimes gives V_o=357 m/sec.

The traveltimes for the Apollo 16 ASE grenade launchings are tabulated in Table 14. Notice that there is a maximum time offset of 57 msec between Grenade Launchings 2 and 4. The time offsets between the other two pairs of grenade launchings are approximately 30 msec. The same traveltimes are expected at each geophone because the geophone/source separations are the same. Furthermore, the first arrivals for Grenade Launchings 3 and 4 at Geophone 3 are undetectable, and the first arrival at Geophone 3 of Grenade Launching 2 is also questionable because of the extremely low amplitudes. Based on the previous knowledge obtained, we assume that the direct waves are the first arrivals at Geophone 1 (14 m)

Table 14. Traveltimes measured from grenade launchings of Apollo 16 ASE. Data are filtered between 3 and 40 Hz.

Grenade Launching Number	Traveltime, msec		
	GP 1(14 m)	GP 2(50 m)	GP 3(95 m)
2	177	359	508?
3	151	338	-
4	121	302	-

while the refracted waves are the first arrivals at Geophones 2 (50 m) and 3 (95 m). We find the velocity, 302 m/sec, of the refracted waves from the traveltime data of the second and third geophones of the second grenade launching.

An attempt was made to correlate the grenade launching data with the results of the thumper-shot data of Apollo 16 ASE. Using the reference velocity, 357 m/sec, of the powder layer and holding the traveltime differences among those at the geophones of the grenade launching to be the same, we correct the traveltime at Geophone 1 for Grenade Launching 2 to 129 msec, determine the intercept time of the refracted waves to be 145 msec and find the thickness, H=12 m, of the (surface) powder layer.
It is of some interest to notice that the deviations of the velocity structures between the Apollo 14 and 16 landing sites are within 16%; namely, 4% for the reference

velocity, 8% for the thickness of the powder layer, and 16% for the constant velocity of the homogeneous layer. However, it is not surprising that a larger deviation occur for the constant velocity of the homogeneous layer because we essentially have only two data points to be interpreted for the constant velocity of the refracted waves, and the one at Geophone 3 of Apollo 16 ASE grenade launching is very questionable because of the extremely low amplitude of the first arrivals. If we let the constant velocity, V_1, of the homogeneous layer be either 302 m/sec or 254 m/sec and vary the reference velocity, V_o, of the powder layer from 300 to 420 m/sec, we find the depth varies from 11 to 13 m and 9 to 10 m, respectively (Table 15).

Amplitude Variations:

The amplitudes of the first arrivals for separations up to 32.0 m are measured from the profiles. The measurements of the amplitudes for the ASE data are more difficult than that of the traveltimes. These difficulties (summarized by Gangi and Yen, 1979) are caused by: 1) the coarseness of the amplitude sampling, 2) the variabilities of the thumper-shot strengths, 3) the variabilities of the geophone siting and coupling, and 4) the low S/N ratio for larger separations. However, the interpolating effect of the Butterworth bandpass filter reduces the coarseness of the amplitude data, the stacking reduces the

Table 15. Calculated values of the intercept time, T_o, and their related depth, H.

T_1 msec	V_o, m/sec	V_1=302 m/sec		V_1=254 m/sec	
		T_o, msec	H, m	T_o, msec	H, m
150	300	169	11	137	9
139	330	155	11	123	9
128	360	144	12	112	9
118	390	134	12	102	10
110	420	126	13	94	10

T_1: traveltime at Geophone 1 based on the V_o on its right

T_o: intercept time, if we assume a V_1 given on above it

ΔT_{12}=182 msec; traveltime difference between the first arrivals at Geophones 1 and 2

ΔT_{23}=149 msec; traveltime difference between the first arrivals at Geophones 2 and 3

variabilities of the shot strengths and the geophone sensitivities. The amplitude data, again, are plotted on a log/log graph and compared with the amplitude/separation variation predicted by the two models.

Since the thumper shots give primarily vertical forces and the geophones are vertically oriented, the amplitude function of the direct arrivals for the homogeneous and layered model is given by

$$A(x) = A_o(x/x_o)^{-2}$$

for small separation (see, for example, White, 1965, page 215), while the amplitude/separation variation for the power-law-velocity model is estimated to be (Gangi and Yen, 1979)

$$A(x) = A_o(x/x_o)^{-(13-s)/12} \quad ; \; s > 1 \qquad (5)$$

where s is a measure of the source radiation pattern in the vertically inhomogeneous medium. The decrease of the amplitude with separation of the direct waves in the powder-layer model is less than that in the homogeneous and layered model.

The measured amplitudes along with the slopes of the least-square-fitted lines are given in Table 16 (from Gangi and Yen, 1979). Both the amplitudes for the single geophone profiles and the stacked profiles are given in the table. Measurements are made on the data that have been bandpass filtered with -3 dB frequencies of 3 to 66 Hz and 20 to 40 Hz. Notice that there is a great deal of scatter in the

Table 16. Amplitude data (arbitrary units) (From Gangi and Yen, 1979)

A. Bandpassed: 3-66Hz

x (m.)	14-1*	14-2(1)§	14-3*	14-Σ¶	16-1*	16-2(3)§	16-3*	16-Σ¶	14,16-Σ¶
4.57	4.62	3.91	4.68	4.19	-	5.82	5.34	4.69	3.95
9.14	3.17	2.08	?	3.36	1.43	.76	3.17	.82	1.16
13.71	1.13	*	?	1.13	.81	.32	.54	.31	.40
18.29	.52	*	*	.52	.56	.45	.42	.26	.30
22.86	*	*	*	*	?	.18?	.23?	?	?
27.43	*	.15	.1?	.17	.13	?	.18?	.10	.07
32.00	*	.10?	*	.10?	?	?	?	.19?	?
Slope	-1.55	-1.83	-2.15	-1.78	-1.77	-2.01	-2.01	-1.97	-2.04

B. Bandpassed: 20-40Hz

x (m.)	14-1*	14-2(1)§	14-3*	14-Σ¶	16-1*	16-2(3)§	16-3*	16-Σ¶
4.57	2.38	2.17	2.65	2.26	-	2.94	2.48	2.34
9.14	1.75	.93	1.49	1.75	.66	.39	1.70	.44
13.71	.56	*	.22	.56	.38	.20?	?	.17
18.29	.24	*	*	.24	.29	.22	.21	.13
22.86	*	*	*	*	?	?	.11	?
27.43	*	.13	.05	.09	.06	?	.10	.05
32.00	*	?	*	?	?	?	?	?
Slope	-1.63	-1.59	-2.34	-1.87	-2.07	-1.98	-2.00	-2.08

*14-1 means Geophone 1, Apollo-14 ASE, etc.; ¶14-Σ means stacked traces, Apollo-14 ASE
§14-2(1) means traces on Geophone 2, Apollo-14 ASE, sources between Geophones 1 and 2, etc.
*misfired shot; -, no shot available; ?, low S/N ratio.

data. Some of it is because of the variabilities of the shot strengths and geophone sitings, while some is due to the low S/N ratio and the coarseness of the amplitude sampling. Figure 27 (from Gangi and Yen, 1979) shows a representative amplitude plot (for Geophone 3, Apollo 16 ASE). While all the data are well fitted by the straight line with a slope of -2.01 in the figure, the two largest amplitude data, which have the highest S/N ratio, suggest a lower slope.

Table 16 (from Gangi and Yen, 1979) shows the slopes for the fairly good data lie between -1.5 and -2.5. The slopes are closer to the slope predicted by the homogeneous and layered model than that predicted by the powder-layer model. However, the slopes predicted by these two models are made on the following assumptions: 1) all the thumper sources are of equal strength, 2) all the geophones are equally coupled and oriented to the lunar surface, 3) there is no attenuation, 4) there is no energy loss by conversion of P-wave energy into S-wave energy, and 5) there are no scatterers in the lunar regolith. The first two effects would increase the scatter in the data, while the latter three effects would decrease the amplitudes. Therefcre, the two predicted slopes should be considered as upper bounds on the measured data. However, energy loss does exist when seismic waves propagate through a medium. The energy loss is called the attenuation or absorption. In general, the attenuation

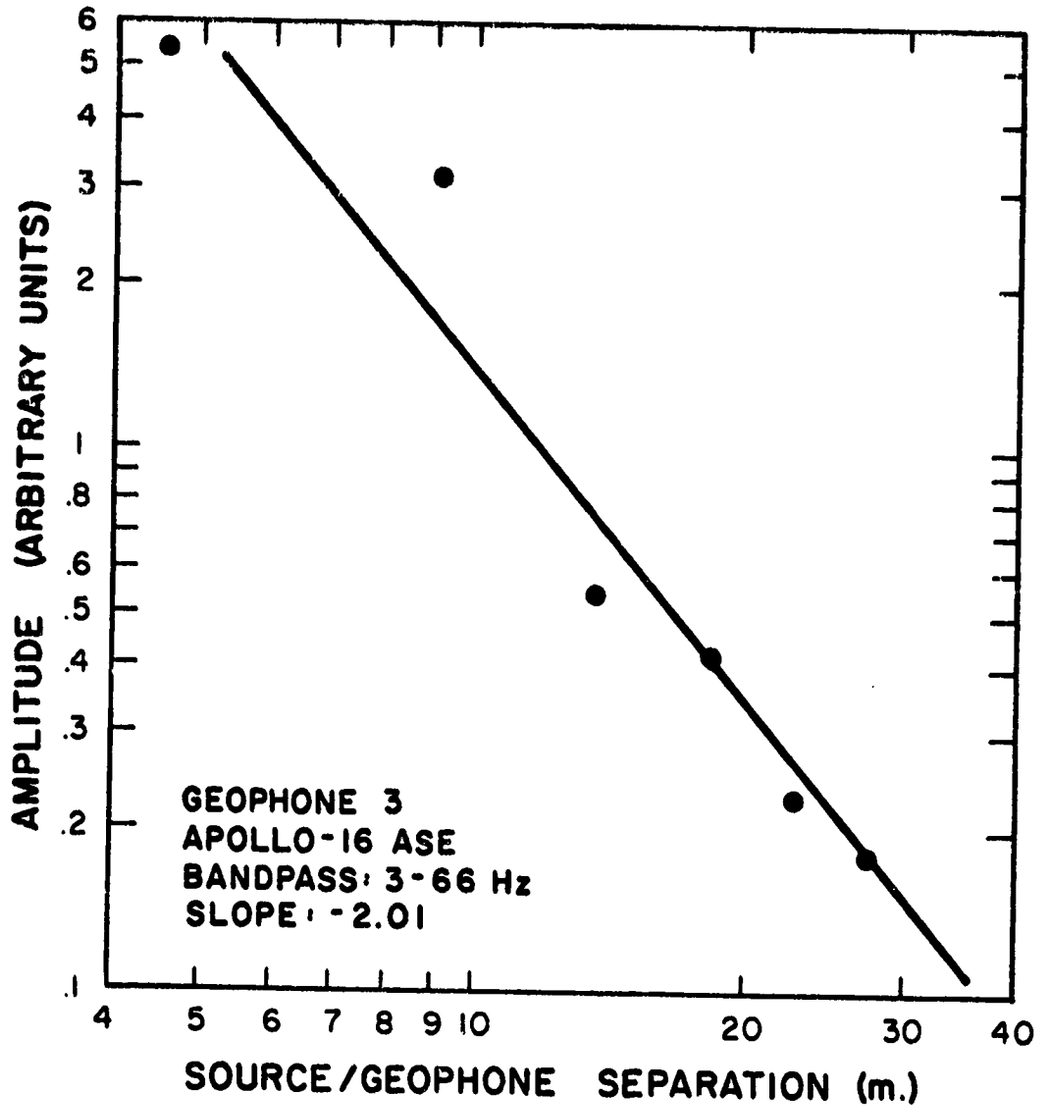

Figure 27. Log/log plot of the amplitudes versus separations. (From Gangi and Yen, 1979)

in a medium is an exponential function with distance (see, for example, Dobrin, 1976, page 39) as follows

$$A(x) = A_o x^{-n} e^{-\alpha x}$$

where α is the coefficient of attenuation. Using the amplitude data of the third geophone profile of Apollo 16 ASE thumper shots, we find (also see Figure 28)

$$A_o = 71.66$$

$$n = 1.463$$

$$\alpha = 0.047 \ m^{-1}$$

For the powder-layer model, the exponential factor, -n, results in a negative value for s which contradicts the condition $s > 1$ (also see Equation (5), page 70). However, the exponential factor, -n, is close to but less negative than the slopes shown in Table 16, and the predicted values for the powder-layer model and the homogeneous and layered model are treated as upper bounds on the measured data. This value, -n=-1.463, seems to favor the powder-layer model. Figure 28 shows that the amplitude decreases exponentially at larger separations, while the factor x^{-n} dominates the amplitude variation at small separations.

Velocity-Spectrum Analyses:

The velocity-spectrum technique used in this research was pioneered by Taner and Koehler (1969). The semblance of the velocity spectrum shows the power of the signals arriving at different vertical two-way traveltime, t_o, over

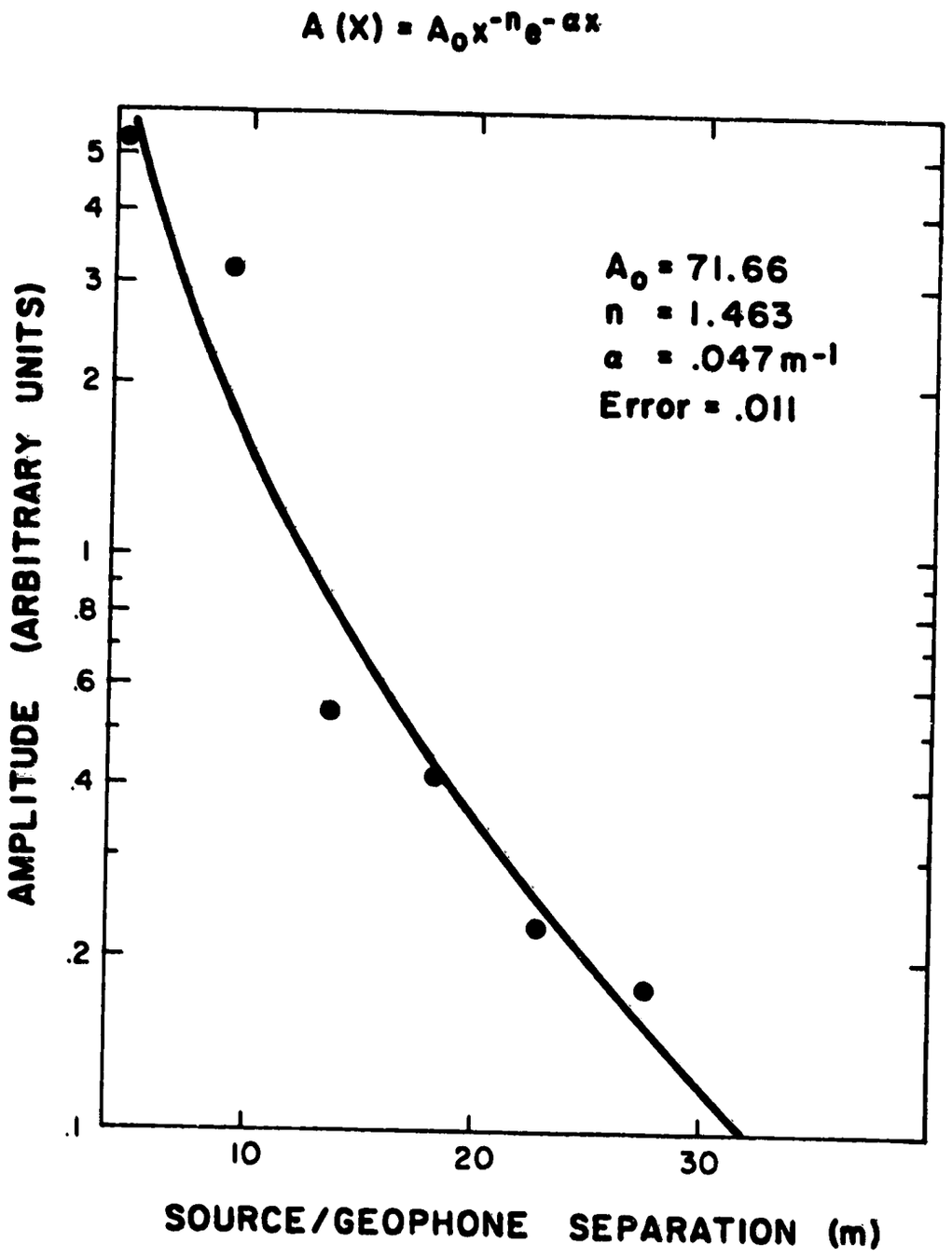

Figure 28. Amplitude attenuation with separation.

a spectrum of (assumed) root-mean-squared (RMS) velocities, $\bar{V}$. This technique is used to search for the parameters of the (assumed) velocity model for the direct, reflected, and refracted waves by delaying and summing the traces along a profile. The delay is computed on the basis of the (assumed) velocity model and the maximum amplitude for the sum over a time window is obtained when a proper velocity model is used. That is, the semblance is calculated for the digitized data by

$$S(t_o,\bar{V}) = \frac{\sum_{j=J_o}^{J_o+N} \left(\sum_{i=1}^{M} A_{ij}\right)^2}{M \sum_{j=J_o}^{J_o+N} \sum_{i=1}^{M} A_{ij}^2} \qquad (6)$$

where A_{ij} is the amplitude of the j-th sample point of the i-th trace on the profile, M is the number of the traces, and N is the width of the time window. The sampling point, J_o, in the i-th trace is obtained by

$$J_o = \mathrm{INT}\left(T(t_o,\bar{V},X_i)/\Delta t \right) \qquad (7)$$

where t_o is the vertical two-way traveltime or the intercept time, $\bar{V}$ is the RMS velocity, X_i is the geophone/source separation for the i-th trace, Δt=1.89 msec/sample is the sampling interval, INT represents INTEGER in computer language, and T is the traveltime function based on the (assumed) velocity model and the event of interest.

The velocity spectrum is generated by measuring the semblance, using Equation (6), for various t_o and $\bar{V}$.

An intercept time, t_o, is chosen and the semblance is calculated for $\bar{V}$, which varies (in increments of $\Delta\bar{V}$) from $\bar{V}_{min}$ to $\bar{V}_{max}$. The intercept time is then increased in increments of Δt_o and the same procedure is repeated. The maximum semblance value will occur at the values of t_o and $\bar{V}$ associated with the traveltime curve of the event (Figure 29; from Taner and Koehler, 1969). The semblance value of the velocity spectrum is also related to the S/N ratio in the data. The amplitude, A_{ij}, in Equation (6) consists of both the signal, s_{ij}, and the noise, n_{ij}, so that Equation (6) can be rewritten as

$$S(t_o,\bar{V}) = \frac{\sum_{j=J_o}^{J_o+N} \left(\sum_{i=1}^{M} (s_{ij}+n_{ij}) \right)^2}{M \sum_{j=J_o}^{J_o+N} \sum_{i=1}^{M} (s_{ij}+n_{ij})^2}$$

$$= \frac{M^2 \sum_{j=J_o}^{J_o+N} s_{Ij}^2}{\sum_{j=J_o}^{J_o+N} s_{Ij}^2 + M \sum_{j=J_o}^{J_o+N} \sum_{i=1}^{M} n_{ij}^2}$$

where we assume that the summation of noise is zero and the signal and noise do not correlate. Let P_s and P_n be the average signal and noise powers, respectively, of the data in the time window, the above equation then can be rewritten as

$$S(t_o,\bar{V}) = P_s/(P_s+P_n)$$

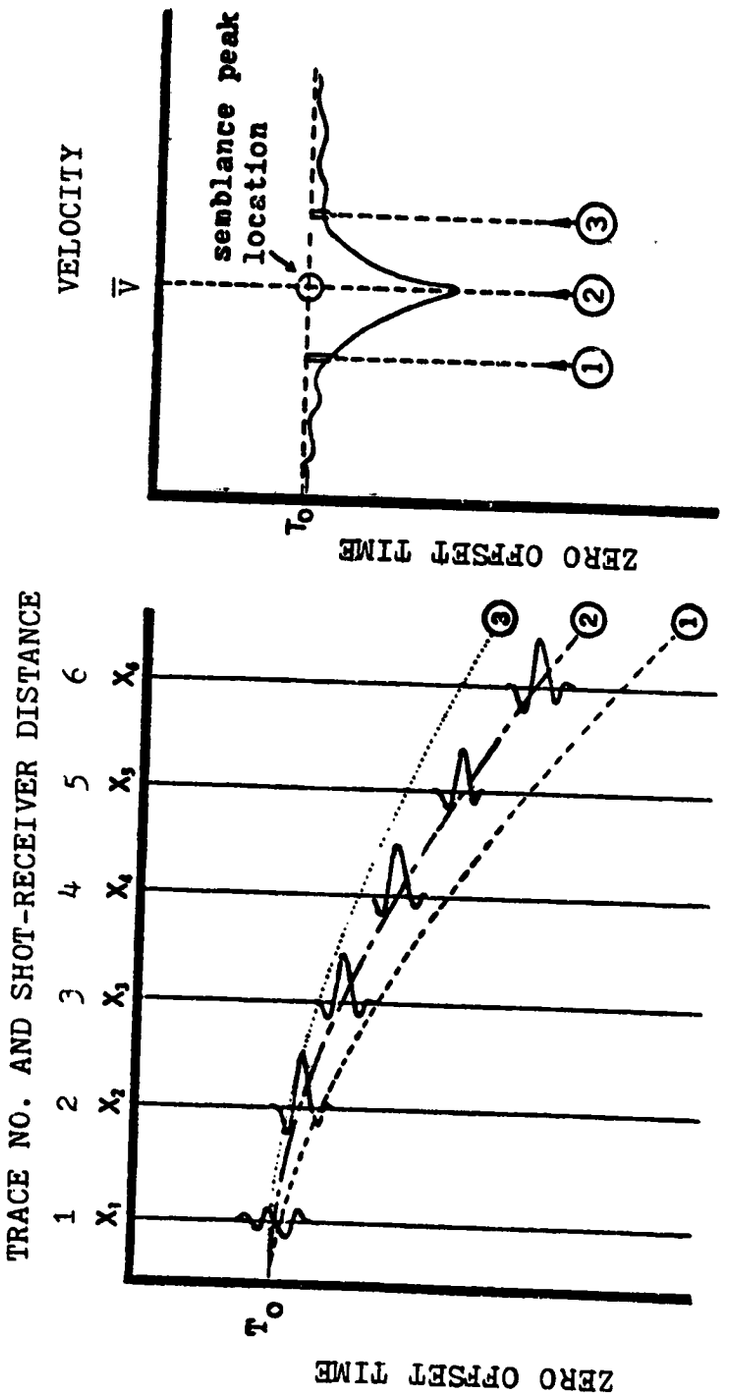

Figure 29. Principle of velocity spectra.
(Modified from Taner and Koehler, 1969)

or

$$P_s/P_n = S/(1-S)$$

Notice that the maximum value of the semblance is 1 when there is only signal in the time window and its minimum value is 0 when there is no signal but noise. The S/N ratio can then be estimated by taking the square root of P_s/P_n. The semblance read on the peaks of the velocity spectra varies from approximately 0.2 to 0.7 which correspond to S/N ratio of 0.5 to 1.5, respectively.

The assumed velocity model based on the previous investigation is that there is a self-compacting, powder layer overlying a homogeneous medium. For the direct waves, the traveltime function $T(t_o,\bar{V},X_i)$ of Equation (7) (page 76) has the form

$$T(t_o,\bar{V},X_i) = AX_i^{5/6}/\bar{V}$$

where t_o equals zero, A is a constant (also see Equation (2), page 62), and $\bar{V}$, in this case, is the reference velocity at 1 km for the powder layer. Also, Gangi (1972) demonstrated that the traveltime, T_n, for a ray reflected n times (the n^{th}-surface-reflected waves) from the surface is

$$T_n = (1+n)^{1/6}T_o$$

where T_o is the traveltime of the primary direct waves. The above equation shows that the apparent velocity of the n-th-surface-reflected waves is equal to the product of $(1+n)^{-1/6}$ and $\bar{V}$ for the direct waves.

For the reflected waves, Taner and Koehler (1969)

find that the traveltime equation (also see Equation (4), page 63) can be approximated by

$$t(x) = (c_1 + c_2 x^2 + c_3 x^4 + \ldots)^{\frac{1}{2}}$$

where $c_1 = a_1^2$

$c_2 = a_1/a_2 = \bar{V}^{-2}$

$c_3 = (a_2^2 - a_1 a_3)/4a_2^4$

.

.

.

$$a_m = 2\int_0^H V^{2m-3}(z)dz$$

$V(z)$: the sixth-power velocity function with depth

H: the depth of the powder layer

Furthermore, they conclude that the first-two-term approximation of the above equation will converge quite rapidly and accurately to the exact traveltime/separation curve for most cases of pratical interest. The first-two-term approximation has the same form as Dix's (1955) formula. That is,

$$T(t_o, \bar{V}, X_i) = (t_o^2 + X_i^2/\bar{V}^2)^{\frac{1}{2}}$$

For (n-1)-th multiply reflected waves, the above equation is also valid. Its intercept time, $t_{o,n}$, is n times that of the primary reflected waves, while the apparent RMS velocity remains the same. The relationships among the c_i's, $t_{o,n}$, and $\bar{V}$ can be obtained immediately as follows

$$c_1^{\frac{1}{2}} = t_{o,n} = 2n\int_0^H dz/V(z)$$

$$= n(288/5)^{\frac{1}{2}} H^{5/6}/V_o$$

$$c_2^{-1} = \bar{V}^2 = 2n\int_0^H V(z)dz \Big/ 2n\int_0^H dz/V(z)$$

$$= \frac{2n}{t_{o,1}}\int_0^H V(z)dz$$

$$= n(72/245)^{\frac{1}{2}}V_o H^{7/6}/t_{o,1}$$

or

$$H \approx 0.493\bar{V}t_{o,1}/n$$

$$V_o \approx 4.210\bar{V}^{5/6}(t_{o,1}/n)^{-1/6}$$

where $t_{o,n}=nt_{o,1}$. Obviously, we would expect to have the semblance peaks at every grid point of $(nt_{o,1},\bar{V}')$ for the (n-1)-th multiply reflected waves; where $t_{o,1}$ and $\bar{V}'$ are the intercept time and the (assumed) RMS velocity, respectively, of the primary reflected waves and n is equal to or greater than 2.

For the refracted waves, the traveltime function $T(t_o,\bar{V},X_i)$ (also see Equation (3), page 62) is

$$T(t_o,\bar{V},X_i) = t_o + X_i/\bar{V}$$

where $\bar{V}$ is the constant velocity, V_1, of the homogeneous medium. This velocity remains unchanged for the n-th multiply refracted waves, while its intercept time is n+1 times that of the primary refracted waves. However, the intercept time is a transcendental function in terms of V_o, H, and V_1. Either V_o or H has to be assumed to determine the other one.

A synthetic seismogram and computer program have been used to test this velocity-spectrum technique.

The synthetic seismogram consists of the primary direct, surface reflected, reflected, and refracted waves; the assumed velocity model is a powder layer, with a thickness of 10 m and a reference velocity of 330 m/sec at a depth of 1 km, overlying a homogeneous layer with a constant velocity of 250 m/sec. The geophone/source distances of the synthetic profile are from 4.57 m, in increments of 4.57 m, to 45.7 m. The arrival signals are one and half cycles of a sinc function with a duration of approximately 57 msec (Figure 30 (a)). Random noise is introduced in the synthetic profile. Figure 30(b) shows a synthetic velocity spectrum of the direct waves. The first-surface-reflected waves are contained in the profile and its reflection coefficient is 0.35. The S/N ratio is approximately 2.6. The solid, dot, and dash curves represent the semblances for time windows with durations of approximately 19, 38, and 57 msec, respectively. The spectrum indicates that the longer the duration of the time window, the lower the semblance value at the peak and the wider the spread of the semblance peak. Notice that the semblance curves shift to the right at the neighborhood of the velocity, 330 m/sec, of the primary direct waves and shift to the left at the velocity, 294 m/sec, of the surface-reflected waves as the duration of the time window increases. These tests also show that interfering signals on one or more seismic traces or high noise may cause spurious peaks and lower the

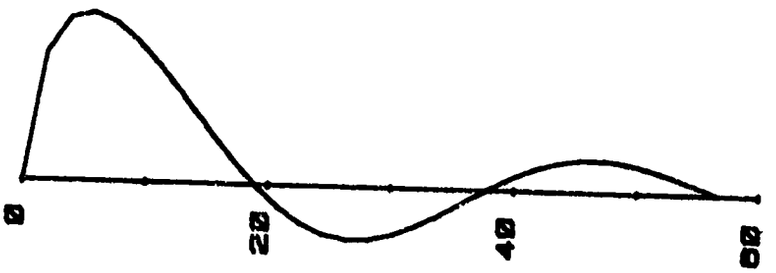

TIME, msec

(a)

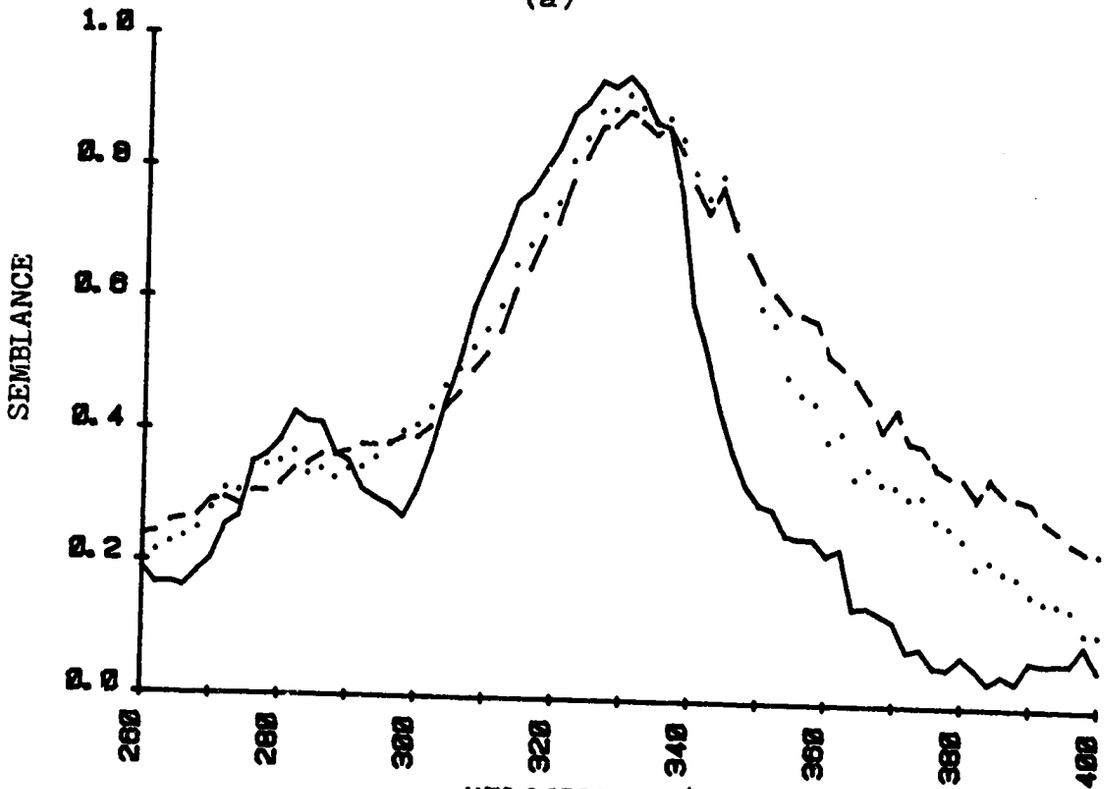

(b)

Figure 30. (a) The arrival signal which is one and half cycles of a sinc function with a duration of approximately 57 msec. (b) The velocity spectrum of the direct waves for the synthetic profile. The solid, dot and dash curves represent the semblances for time windows with durations of approximately 19, 38, and 57 msec, respectively.

semblance values at the peaks on the velocity spectra. This would explain the low semblance values and the spurious peaks on the velocity spectra of the Apollo ASE data.

Figure 31 shows a representative velocity spectrum of the direct waves for the ASE data which is from the second geophones profile of Apollo 14 ASE. Since the semblance is very sensitive to the interference and noise, only clear traces can be used; that is, thumper shots 12 through 21 are delayed and stacked (also see Figure 23, page 57). The solid, dot, and dash curves, again, represent the semblance curves for the time windows with durations of approximately 19, 38, and 57 msec, respectively. The semblance peaks near 370 m/sec are believe to be spurious because the peak of 19 msec time window is not stationary for the other two time windows and the semblances drop almost by a factor of 2 in that region. However, the semblance curves at the neighborhoods of approximately 320 and 282 m/sec show similar character to that found in the synthetic velocity spectrum; that is, the curves shift to the right and left at the neighborhoods of the velocities of the primary direct waves and the surface-reflected waves, respectively, when the duration of the time window increases (Figure 30(b)). This similar character suggests that the values of 320 and 282 m/sec may correspond to the velocities of the primary direct and the first sur-

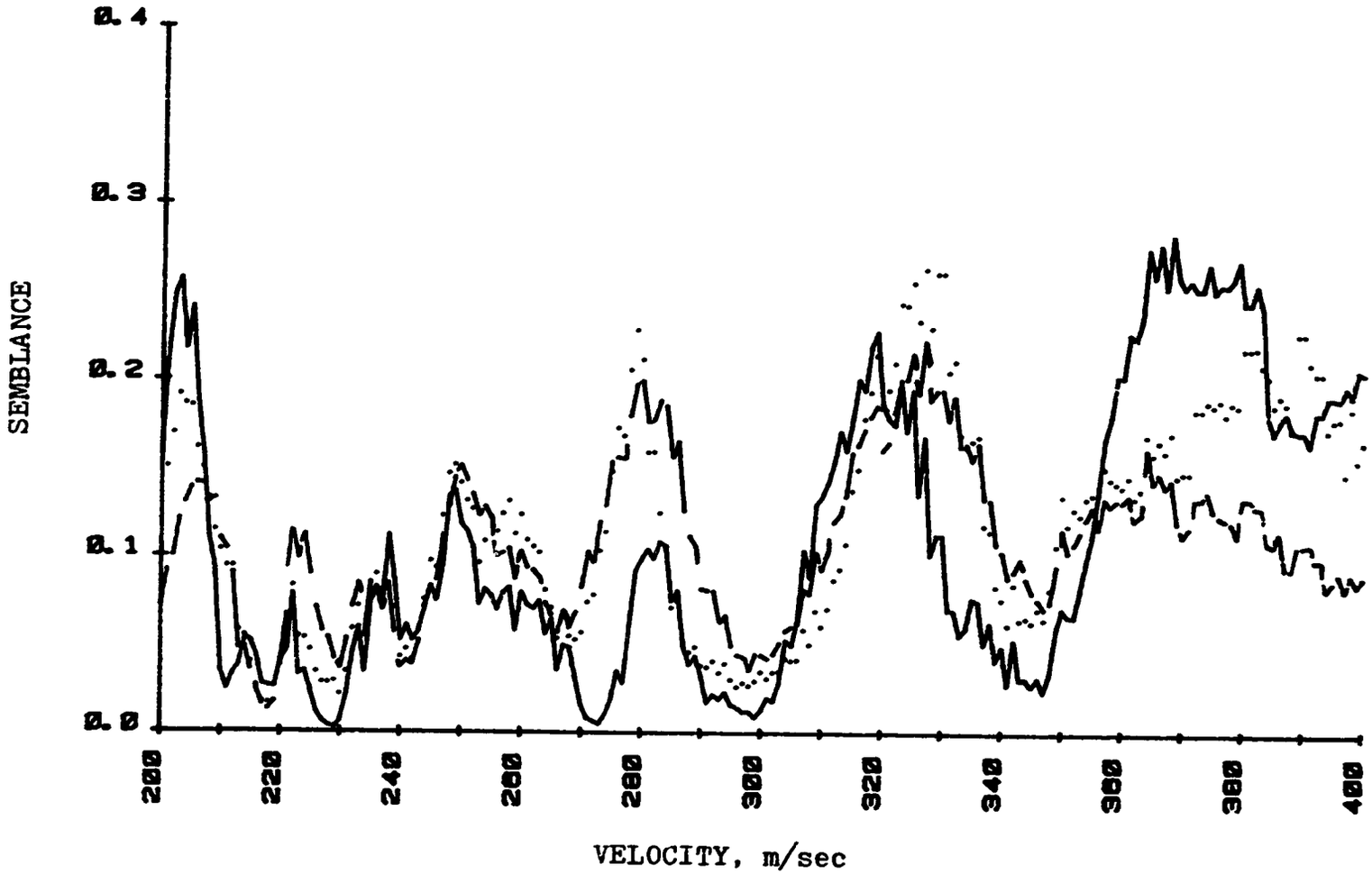

Figure 31. Velocity spectrum of the direct waves for the second geophone profile of Apollo 14 ASE. The solid, dot, and dash curves represent the semblances of the time windows with durations of approximately 19, 38, and 57 msec, respectively.

face-reflected waves, respectively. Furthermore, if the value of 320 m/sec is the velocity of the primary direct waves, the velocity deviation between the theoretically expected value for the first surface-reflected waves and 282 m/sec is only about 1%. However, the determination of the velocities for higher orders other than that of the first surface-reflected waves is difficult because their apparent velocities are so close to each other that the determination from the velocity spectrum is impossible.

Figure 32(a) and 32(b) show the synthetic velocity spectra, using a 19 msec time window, for the reflection and refraction, respectively. The expected values of the intercept times and the RMS velocities for the synthetic reflected and refracted waves are 157 msec and 130 m/sec, 134 msec and 250 m/sec, respectively. There are offsets between the locations of the expected peaks, marked "o", and the measured peaks, marked ".", found in the synthetic velocity spectra. The offsets of peak locations are caused either by the interfering of the seismic signals or the noise. However, the centers of the semblance contour are not far away from the expected ones; therefore, the semblance-contour centers for the reflected and refracted waves of Apollo ASE data will be used to evaluate the parameters of the assumed velocity model.

Figure 33 shows a representative velocity spectra

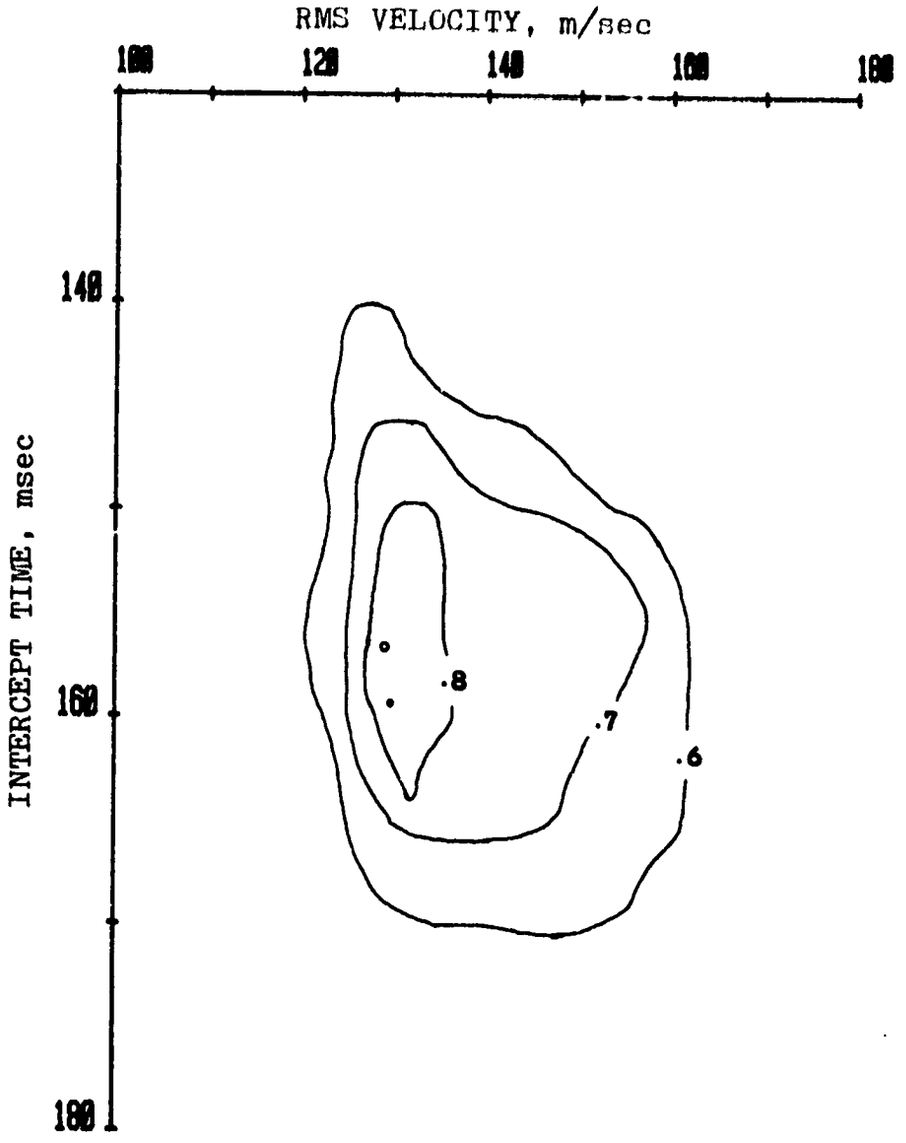

Figure 32(a). Synthetic velocity spectrum for the reflected waves using a 19 msec time window. The S/N ratio is 2.6. The dot represents the measured semblance peak and o represents the expected semblance peak.

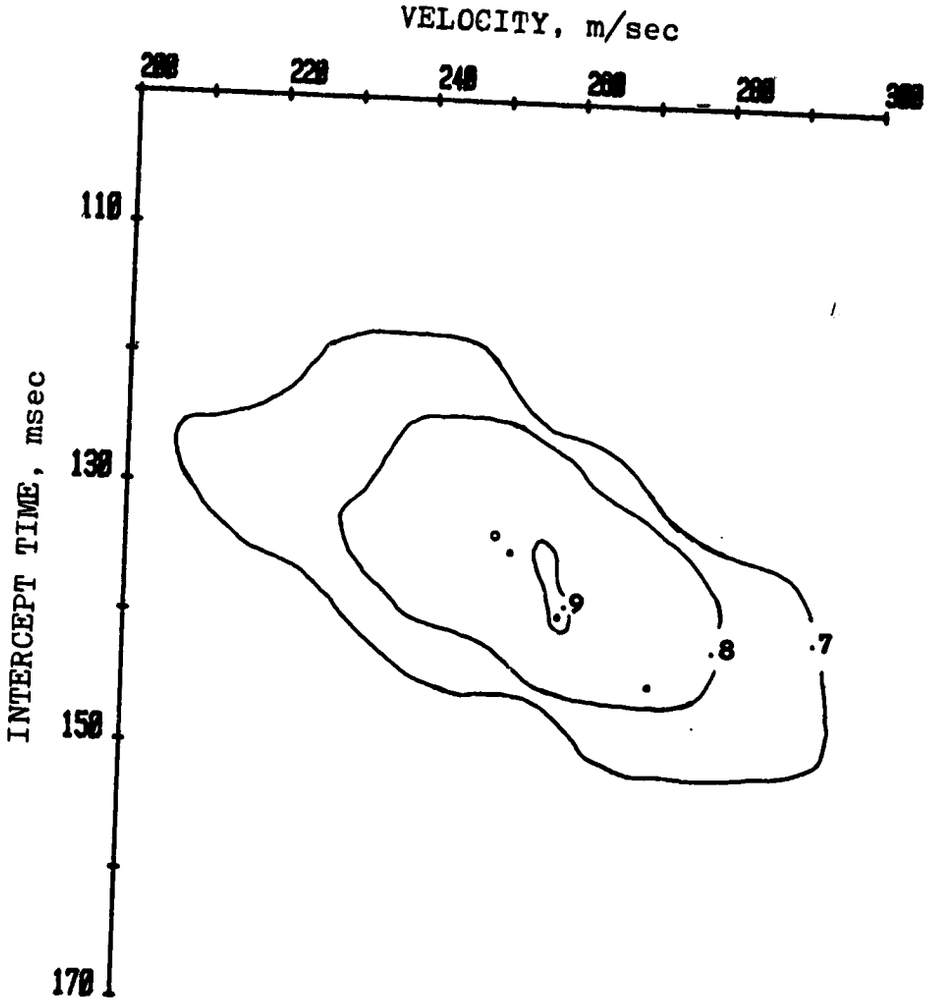

Figure 32(b). Synthetic velocity spectrum for the refracted waves using a 19 msec time window.

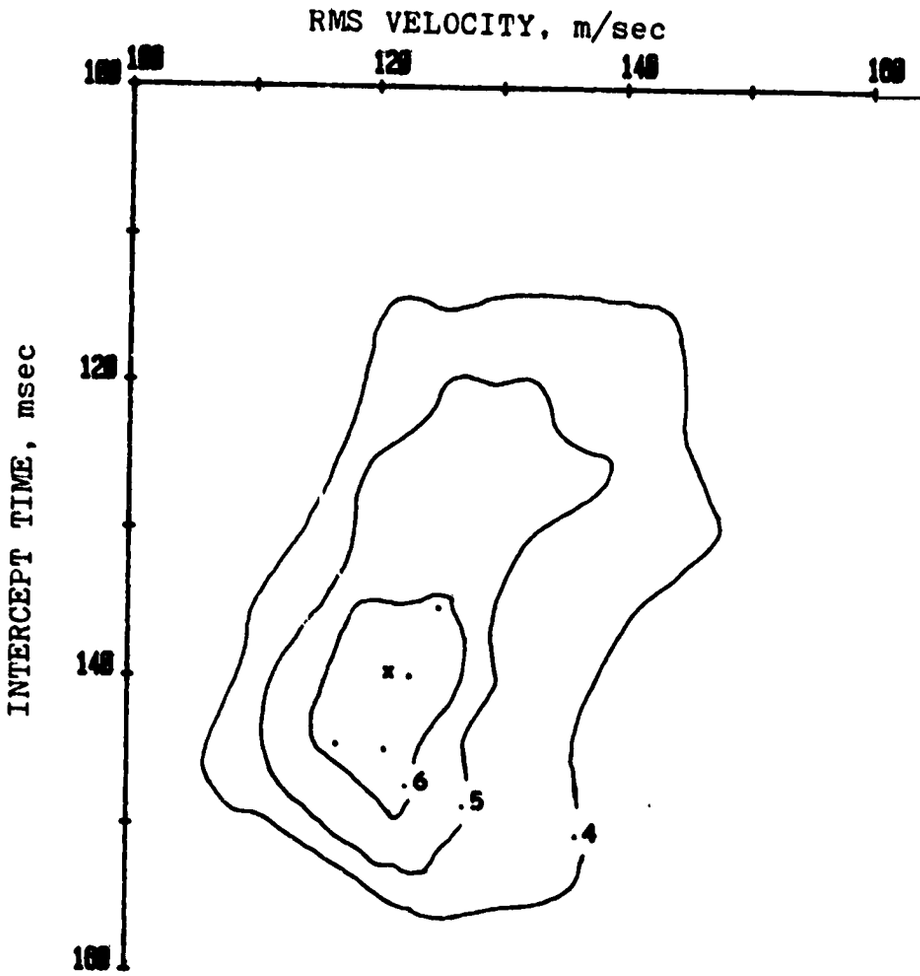

Figure 33. The velocity spectrum for the reflected waves is from the first geophone profile of Apollo 14 ASE using a 19 msec time window. The dots indicate the semblance peaks and x represents the center of the semblance contour.

for the reflected waves of the Apollo ASE data. The velocity spectrum is from the first geophone profile of Apollo 14 ASE using a time window of 19 msec duration. The dots indicate the semblance peaks and x indicates the center of the semblance contour. The contour shows a similar character to that of the synthetic profile. The time windows of longer duration will only broaden the contour of the semblance peak but have similar character. The intercept time and the RMS velocity at the contour center of the velocity spectrum are at approximately 140 msec and 121 m/sec, respectively, which gives for the thickness, H, and the velocity, V_o, 8.4 m and 318 m/sec, respectively. This independent evaluation verifies the reference velocity of the surface powder layer, V_o, is approximately 320 m/sec.

Figure 34 shows the velocity spectrum for the refracted waves which is from the second geophone profile of Apollo 14 ASE using a time window of 19 msec duration. The dots and x, again, represent the semblance peaks and the center of the semblance contour, respectively. There are only seven clear seismic traces on the second geophone profile of Apollo 14 ASE (also see Figure 23, page 57). However, those traces with geophone/source distances less than the critical distance can not be used for the velocity spectrum analysis of the refracted waves because refracted waves do not exist before the

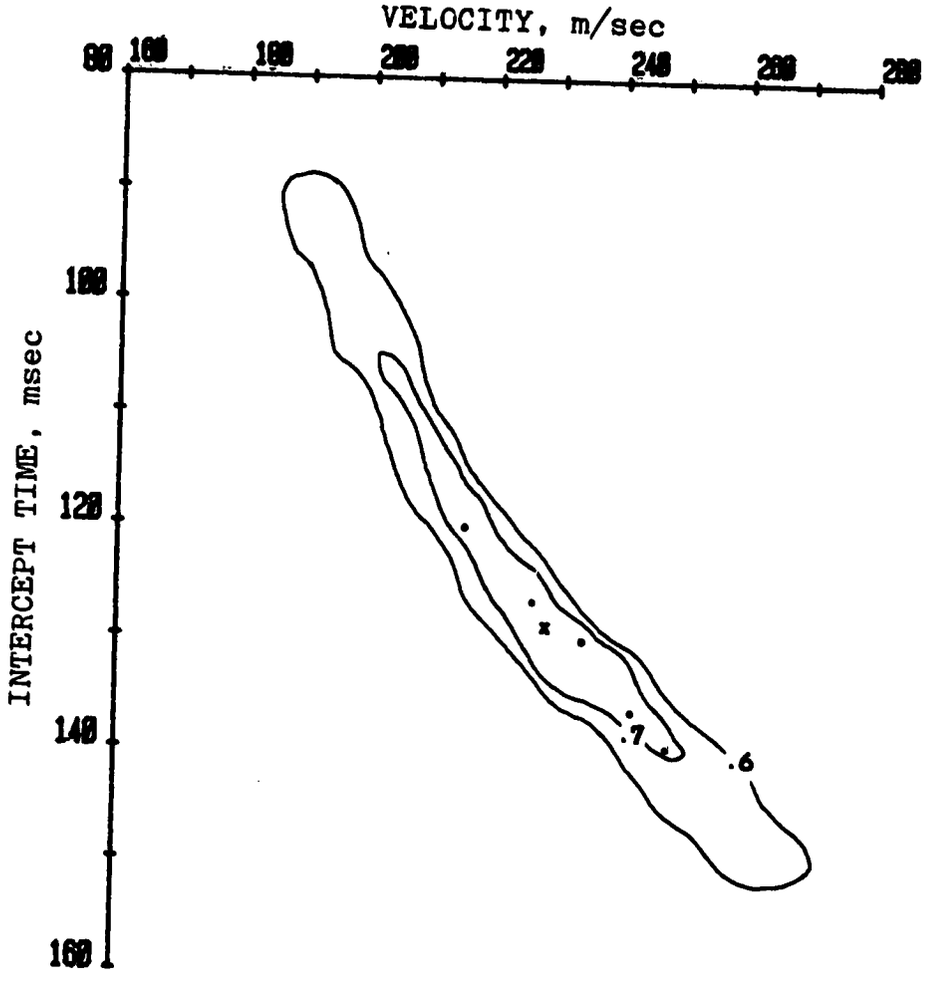

Figure 34. The velocity spectrum for the refracted waves is from the second geophone profile of Apollo 14 ASE using a 19 msec time window. The dots indicate the semblance peaks and x represents the center of the semblance contour.

critical distance. The critical distance is assumed to be less than 13.71 m. That is, there are only five available traces for this analysis of the refracted waves. The semblance peak is distributed in a very narrow belt area. The region for the intercept time and refraction velocity is from 120 msec and 213 m/sec to 135 msec and 246 m/sec, respectively. If we assume the reference velocity of the powder layer be 320 m/sec, then the corresponding thickness of the surface powder layer vary from 9.0 to 9.7 m, respectively. Furthermore, the center of the semblance contour for the refracted waves is approximately at 128 msec and 230 m/sec which corresponds to a thickness of the surface powder layer be 9.3 m.

The previous investigation in the section of "Traveltime Variations" show that the reference velocity of the surface powder layer is approximately 350 m/sec. The thickness of the powder layer is approximately 11 m. The constant velocity of the homogeneous medium is 250 m/sec. The results of the velocity-spectrum analysis are consistent with those values found in the previous investigations. The differences of the reference velocity, the thickness of the powder layer, and the constant velocity of the homogeneous medium are 9.6%, 15.5%, and 8.0%, respectively. These percentages of the differences are reasonable and possible.

Geophone-Coupling and Shot-Strength Variabilities:

An analysis of the amplitude data is made to investigate the exponent of the amplitude variation and the variabilities of the geophone sensitivities (in place) and the thumper-shot strengths, if there are sufficient redundancy in the data. The amplitude variation of the direct waves can be written in a general form both for the constant velocity medium and for a powder-layer medium as follows (Gangi and Yen, 1979)

$$A_{ij} = G_i S_j \left| X_i - X_j \right|^m$$

where G_i : the sensitivity of the i-th geophone at X_i

S_j : the strength of the j-th thumper shot at X_j

m : the exponent of the amplitude variation

The above equation is normalized and linearized in terms of the relative geophone sensitivities ($g_i = G_i/G_I$), relative thumper-shot strength ($s_j = S_j/S_J$), the exponent, m, of the amplitude variation, and an arbitrary constant by taking the logarithm. The arbitrary constant is the product of the reference geophone sensitivity and the reference thumper-shot strength ($a_o = G_I S_J$). Minimizing the summed, weighted, and squared error function as a function of those parameters (g_i's, s_j's, a_o, and m), the above equation results in a matrix form (for details, see Gangi and Yen, 1979)

$$\bar{a} = \bar{\bar{A}} \cdot \bar{p} \qquad (8)$$

where $\bar{a}$ is a vector, whose components depend on the measured amplitudes, the weights, and the geophone/source distances; $\bar{\bar{A}}$ is a squared and symmetric matrix whose components depend on the weights and distances while p is a vector whose components are the unknown parameters: g_1 ..., s_j ..., a_o, and m. We assume that the distances are measured with high accuracy and we establish the weights which depend on the qualities of the data. Consequently, the stability of the inverse matrix $\bar{\bar{A}}^{-1}$ and the errors of the vector $\bar{a}$ are established only on the accuracy of the amplitude measurements.

The weights for the Apollo 16 ASE thumper shots are tabulated in Table 17 (from Gangi and Yen, 1979). Table 17 (from Gangi and Yen, 1979) shows that 14 of 19 thumper shots give useful amplitude data and only 3 (Thumper-shots 6, 7, and 17) of these 14 thumper-shots give first-arrival amplitude data on more than one geophone (also see Table 16, page 71; from Gangi and Yen, 1979). Geophone 2 and Thumper-shot 7 are used as the reference geophone and the reference thumper-shot, respectively. Consequently, we have six amplitude measurements (two for each thumper-shot) to solve six unknowns a_o, g_1, g_3, s_6, s_{17}, and m. The matrix equation (Equation (8)) - in terms of the weights, distances, and correlated and measured amplitudes - becomes

Table 17. Weights applied to the measured amplitude data of Apollo 16 ASE. (From Gangi and Yen, 1979)

Weights: w_{ij}

Shot No., j	Geophone No., i		
	1	2	3
1	0	0	0
2	0	0	1
3	0	0	1
4	0	0	1
5	0	0	1
6	0	½	½
7	0	1	¼
8	0	1	0
9	0	1	0
10	0	1	0
11	0	0	0
12	0	1	0
13	0	0	0
14	¼	0	0
15	0	0	0
16	1	0	0
17	1	¼	0
18	1	0	0
19	0	0	0

$$\begin{bmatrix} -3.734 \\ -0.211 \\ -1.164 \\ -1.592 \\ -0.914 \\ -11.710 \end{bmatrix} = \begin{bmatrix} 3.50 & 1.00 & .75 & 1.00 & 1.25 & 10.35 \\ - & 1.00 & 0 & 0 & 1.00 & 2.62 \\ - & - & .75 & .50 & 0 & 2.39 \\ - & - & - & 1.00 & 0 & 3.13 \\ - & - & - & - & 1.25 & 3.48 \\ - & - & - & - & - & 30.84 \end{bmatrix} \cdot \begin{bmatrix} a_o \\ g_1 \\ g_3 \\ s_6 \\ s_{17} \\ m \end{bmatrix}$$

Solving this matrix equation, we find that the relative geophone sensitivities and thumper-shot strengths are

$$G_1/G_2 = .724$$
$$G_3/G_2 = 1.40$$
$$S_6/S_7 = .803$$
$$S_{17}/S_7 = .848$$
$$m = -3.57$$

Unfortunately, those values seem to be unreliable. The reason for the unreliability of the values is because of the lack of redundancy and the quality of the data. The 30 to 40% differences in the relative geophone sensitivities are higher than that expected, but are not too unreasonable. The 15 to 20% variations of the relative thumper-shot strengths are possible but larger than expected. The values of the exponent, m, is almost doubled compared to that of the single geophone profiles and stacked profiles (also see Table 16, page 71; from Gangi and Yen, 1979).

A similar treatment can not be made on the

amplitude data of Apollo 14 ASE thumper shots because there are no correlated amplitude data for Geophones 2 and 3 of Apollo 14 ASE due to the misfires and poor S/N ratio. Neither can it be performed on the grenade or grenade launching data of Apollo 16 ASE due to the difficulties in measuring their amplitudes.

CHAPTER V. SUMMARY AND CONCLUSIONS

The seismic data used to determine the velocity structure of the very shallow lunar crust are from thirty-two thumper shots (thirteen from the Apollo 14 ASE and nineteen from Apollo 16's) and three grenade launchings of Apollo 16 ASE. The data are used to compare two velocity models; namely, the homogeneous and layered model (Kovach et al, 1971, 1972, 1974) and the self-compacting-powder layer model (Gangi, 1972).

To cover the maximum dynamic range, the seismic data are log compressed into thirty-two binary levels for the ASE's which gives a coarseness to the amplitude sampling. Furthermore, severe glitches are found in the lunar seismograms (Figure 16, page 39). They are recognized by the fact that they are of short duration and have values which are inconsistent with the preceding and/or following sampling values.

To improve the quality of the data, they are "deglitched" to remove the extraneous values and filtered by four-pole, anti-aliased Butterworth bandpass filters with -3 dB frequencies at 3 and 66 Hz, and 20 and 40 Hz (Figure 21, page 47). In addition, the Apollo 14 and 16 stacked profile, the Apollo 14 stacked and Apollo 16 stacked profiles, and the single geophone profiles of Apollo 14 and 16 ASE's are used to examine the velocity variation on the lunar crust at these two landing sites.

If there are any significant difference in the velocity structures at these two sites, the results of these profiles will show the differences. Little difference is found.

For the traveltime variation, Gangi and Yen (1979) indicate that the traveltime data plotted on the log/log graph will give the exponent of the velocity function. That is, the traveltime/separation function, in general, has the form

$$t(x) = cx^m/V_o$$

where c is a constant, V_o is the reference velocity at 1 km, and m=0.833 predicted by the self-compacting powder layer or $c/V_o=V'$, where V' is the constant velocity on the surface layer, and m=1 predicted by the homogeneous and layered medium.

The traveltimes of the first arrivals (Table 11, page 54; modified from Gangi and Yen, 1979) can be determined accurately only up to separations of 32.0 m for the stacked profiles. While the reference velocities vary between 430 m/sec and 630 m/sec for the stacked profiles, the values of the exponent, m, vary between 0.74 and 0.80. The values of the exponent are all consistently lower than that predicted by the homogeneous and layered model and tend to that predicted by the powder-layered model.

However, there are some good first arrivals found in the single geophone profiles at larger separations.

The traveltime data of the single geophone profiles of Apollo 14 ASE (Figure 24, page 60) show a smooth curve up to approximately 30 m; no straight line can be fitted to these data points which will pass through the origin at the same time. Furthermore, the value of the exponent, m=0.82, for those data points is close to that proposed by Gangi (1972). These strongly suggest that the continuous velocity model might be a more proper representative for the velocity variation on the lunar surface. We find the reference velocity at a depth of 1 km for the sixth-root velocity variation to be 345 m/sec with a thickness of 11 m. Beyond 32 m, a straight line is observed and those data points are assumed to be refracted waves from the (second) homogeneous layer with a constant velocity of 254 m/sec (Figure 26, page 64).

Unfortunately, the first arrivals for the Apollo 16 single geophone profiles can not be determined with any accuracy for separations greater than 30 m because of the quality of the data. The values of the reference velocities vary from 1059 m/sec to 773 m/sec for separations less than 30 m, while the values of the exponent, m, vary from 0.65 to 0.71 (Table 13, page 65). The exponent, again, is closer to that predicted by the self-compacting powder layer (Gangi, 1972) than that predicted by the homogeneous and layered model (Kovach et al, 1971, 1972, 1974). If we assume that the velocity of the

surface layer at the Apollo 16 landing site has a one-sixth power variation and we correlate the grenade launching data with the thumper-shot data of Apollo 16 ASE, we find a reference velocity of 357 m/sec at 1 km with a thickness of 12 m for the (surface) powder layer and a constant velocity of 302 m/sec for the (second) homogeneous layer. It is of some interest to notice that the deviations of the velocity structures between the Apollo 14 and 16 landing sites are within 16%; namely, 4% for the reference velocity, 8% for the thickness of the (surface) powder layer, and 16% for the constant velocity of the (second) homogeneous layer.

For the amplitude variation, Gangi and Yen (1979) indicate that the theoretical amplitude/separation function for the homogeneous and layered model is x^{-2} while the approximated amplitude/separation variation for the self-compacting powder layer is $x^{-(13-s)/12}$, where $s > 1$, if we assume that: 1) there is no energy loss either by conversion or by attenuation, 2) no scatterers in the lunar regolith, 3) all the thumper shots are of equal strengths, and 4) all the geophones are equally coupled and oriented. The amplitudes of the first arrivals (Table 16, page 71; from Gangi and Yen, 1979) are measured up to separations of 32.0 m for all the stacked and single geophone profiles. However, the measurements of the first-arrival amplitudes are more difficult than those of the traveltimes because of the

coarseness of the amplitude sampling and the poor S/N ratio at larger separations. The values of the exponent from the measured data (Table 16, page 71; from Gangi and Yen, 1979) all lie between -1.5 and -2.5. They tend to the value predicted by the homogeneous and layered model, not that predicted by the powder layered model. However, the two predicted values of the exponent should be treated as the upper limits for the measured data.

We also find the value of the coefficient of attenuation, 0.047 m^{-1}, which dominates the amplitude variation at larger separations. The investigation of the variabilities of the geophone sensitivities and thumper-shot strengths (Gangi and Yen, 1979) indicates that there are 30 to 40% differences in the relative geophone sensitivities and 15 to 20% variations of the thumper-shot strengths for the Apollo 16 ASE. These variabilities seem high but are not too unreasonable. This analysis requires accurate amplitude measurements and correlative amplitude data at two or more geophones. The same analysis can not be performed on the amplitude data of Apollo 14 ASE thumper shots because of the misfires and the poor S/N ratio.

The semblances are calculated by delaying and summing the traces along a profile over a spectrum of the velocity, $\bar{V}$, and the intercept time, t_o. The maximum value of the semblance will occur at the values of t_o and $\bar{V}$ which are associated with the traveltime curve of the

event for the assumed velocity structure. The semblance is also related to the S/N ratio in the data. The maximum semblance is 1 when there are only signals. The semblance is 0, if the S/N ratio is zero.

The semblances of the Apollo ASE data vary between approximately 0.2 and 0.7 which suggests that the S/N ratio is between approximately 0.5 and 1.5. However, spurious peaks are distributed over the velocity spectra. Tests of the velocity spectra of the synthetic seismogram indicate that the narrower the duration of the window, the higher the semblance value. Furthermore, the semblances of the velocity spectra are sensitive to interference of the signals and to noise; also, the semblance peaks shift to the right and left at the neighborhoods of the velocities of the direct and multiply direct waves, respectively. There are offsets between the locations of the expected and measured peaks of the velocity spectra of the reflected and refracted waves. The centers of the semblance contours for the reflected and refracted waves are used to evaluate the parameters of the assumed velocity model.

The assumed velocity model is that there is a powder layer whose velocity function is $V(z)=V_o(z/z_o)^{1/6}$, where V_o is a reference velocity at a depth of z_o, overlying a homogeneous layer with a constant velocity. The reference velocity at a depth of 1 km is approximately

320 m/sec which is verified by: 1) comparing the velocity spectra of the direct waves with that of the synthetic velocity spectra, 2) the velocity, 282 m/sec, of the first multiply direct waves which should be $2^{-1/6}$ times the reference velocity, and 3) the independent determination of the reference velocity, 318 m/sec, from the velocity spectra of the reflected waves. The thickness of the surface powder layer evaluated from the velocity spectra of the reflected and refracted waves are 8.4 and 9.3 m, respectively. The constant velocity of the lower layer is 230 m/sec. These parameters of the velocity model are consistent with those found in the previous investigation. All of them are within 10%.

An uneven powder-layer surface may explain some of the unusual characteristics found on the Passive Seismic Experiment seismograms (summarized by Gangi, 1972). The one-sixth power velocity variation of the powder layer predicts that the velocity at the near lunar surface is zero and the seismic rays return back to the surface at (or near to) 0° from the vertical. This will explain the lack of correlation between the vertical and horizontal components of the Passive Seismic Experiment seismograms. The uneven lunar surface of the powder layer will cause the "random walking" of the seismic rays which, in turn, has a long duration of the signal (Gangi, 1972; Gold and Soter, 1970).

REFERENCES

Carrier, D., 1971, Private communication to Gangi, A.F.

Conte, S.D. and Boor, C., 1972, Elementary numerical analysis: New York, McGraw-Hill Book Co., p.44.

Cooper, M.R., Kovach, R.L., and Watkins, J.S., 1974, Lunar near-surface structure: Rev. of Geophysics and Space Physics, v.12, p.291-308.

Cooper, A.M. and Kovach, R.L., 1975, Energy, frequency, and distance of moonquakes at the Apollo 17 site: 6th Proc. Lunar Sci. Conf., p.2863-2879.

Dainty, A.M., Toksoz, M.N., Anderson, K.R., Pines, P.J., Nakamura, Y., and Latham, G., 1974, Seismic scattering and shallow structure of the moon in Oceanus Procellarum: Moon. v.9, p.11-29.

Dix, C.H., 1955, Seismic velocity from surface measurement: Geophysics, v.20, p.68-86.

Dobrin, M.B., 1976, Introduction to geophysical prospecting: 3rd Edition, New York, McGraw-Hill Book Co., p.39.

Gangi, A.F., 1972, The lunar seismogram: Moon, v.4, p.40-48.

Gangi, A.F. and Yen, T.E., 1979, Velocity structure of the shallow lunar crust: The Moon and the Planets (To be published).

Gassmann, F., 1951, Elastic waves through a packing of spheres: Geophysics, v.16, p.673-685.

Gold, T. and Soter, S., 1970, Apollo 12 seismic signal: Indication of a deep layer of powder: Science, v.169, p.1071-1075.

Kanamori, H., Nur, A., Chung, D., Wones, D., and Simmons, G., 1970, Elastic wave velocity of lunar samples at high pressures and their geophysical implications: Science, v.167, p.726-728.

Kanamori, H., Mizutani, H., and Hamano, Y., 1971, Informal Conference, Jan. 11-14, 1974, v.II, National Aeronautics and Space Administration, Manned Spacecraft Center, Houston, Texas.

Kaufman, H., 1953, Velocity functions in seismic prospecting: Geophysics, v.18, p.289-297.

Kovach, R.L., Watkins, J.S., and Landers, T., 1971, Active seismic experiment: Sec. 7 of Apollo 14 Preliminary Science Report, NASA SP-272.

Kovach, R.L. and Watkins, J.S., 1973, The velocity structure of the lunar crust: Moon, v.7, p.63-75.

Kovach, R.L., Watkins, J.S., and Talwani, P., 1972, Active seismic experiment: Sec. 10 of Apollo 16 Preliminary Science Report, NASA SP-315.

_____ 1974, Active seismic experiment: Sec. 10 of Apollo 17 Preliminary Science Report, NASA SP-330.

Kovach, R.L., 1978, Private communication.

Latham, G.V., Ewing, M., Press, F., Sutton, G., Dorman, J., Nakamura, Y., Toksoz, N., Wiggins, R., and Kovach, R., 1970, Passive seismic experiment: Sec. 3 of Apollo 12 Preliminary Science Report, NASA SP-235.

Lauderdale, W. and Eichelman, W., Tech. Eds., 1976a, Active seismic experiment (NASA Experiment S-033): Sec. 5 of Apollo Scientific Experiment Data Handbook, NASA TMX-58131.

_____ 1976b, Lunar seismic profiling experiment (NASA Experiment S-203): Sec. 23 of Apollo Scientific Experiment Data Handbook, NASA TMX-58131.

_____ 1976c, Lunar geology (NASA Experiment S-059): Sec. 13 of Apollo Scientific Experiment Data Handbook, NASA TMX-58131.

Oppenheim, A. and Schafer, R., 1975, Digital signal processing: Englewood Cliffs, New Jersy, Prentice-Hall, p.211.

Taner, M.T. and Koehler, F., 1969, Velocity spectra - Digital computer derivation and applications of velocity functions: Geophysics, v.34, p.859-881.

Toksoz, M.N., Dainty, A.M., Solomon, S.C., and Anderson, K.R., 1974, Structure of the moon: Rev. of Geophysics and Space Physics, v.12, p.539-567.

White, J.E., 1965, Seismic waves: New York, McGraw-Hill Book Co., p.215.

VITA

Tzuhua Edward Yen, son of Li-Hsia Pan and Hsiao-Pen Yen, was born on May 25, 1951 at Taipei, Taiwan, the Republic of China. He graduated from National Central University in Taiwan with a B.S. degree in geophysics in 1974. He entered the Graduate School of Texas A&M University in September, 1975, to work toward a Master of Science degree in geophysics.

Permanent mailing address: 8-3, Alley 325, Lane 150, Sec. 5, Hsin-Yi Rd., Taipei, Taiwan, R.O.C.